

## REVIEW ARTICLE

### Plasma etching: Yesterday, today, and tomorrow

Vincent M. Donnelly<sup>a)</sup> and Avinoam Kornblit<sup>b)</sup>

*Department of Chemical and Biomolecular Engineering, University of Houston, Houston, Texas 77204*

(Received 19 July 2013; accepted 13 August 2013; published 5 September 2013)

The field of plasma etching is reviewed. Plasma etching, a revolutionary extension of the technique of physical sputtering, was introduced to integrated circuit manufacturing as early as the mid 1960s and more widely in the early 1970s, in an effort to reduce liquid waste disposal in manufacturing and achieve selectivities that were difficult to obtain with wet chemistry. Quickly, the ability to anisotropically etch silicon, aluminum, and silicon dioxide in plasmas became the breakthrough that allowed the features in integrated circuits to continue to shrink over the next 40 years. Some of this early history is reviewed, and a discussion of the evolution in plasma reactor design is included. Some basic principles related to plasma etching such as evaporation rates and Langmuir–Hinshelwood adsorption are introduced. Etching mechanisms of selected materials, silicon, silicon dioxide, and low dielectric-constant materials are discussed in detail. A detailed treatment is presented of applications in current silicon integrated circuit fabrication. Finally, some predictions are offered for future needs and advances in plasma etching for silicon and nonsilicon-based devices. © 2013 American Vacuum Society. [<http://dx.doi.org/10.1116/1.4819316>]

#### I. INTRODUCTION

Plasmas have been used to etch fine features in Si integrated circuits for nearly 40 years. Without this technology, we would be stuck in the 1970s listening through tinny headphones to disco music on our “small” portable cassette tape player. Carrying laptops around would be more for fitness than for convenience and mobile “smart” phones would require wheels. Today, instead we take these marvelous devices for granted. Among the many important breakthroughs that were required to make this all possible, plasma etching plays a major role in allowing complex circuit patterns printed in a photolithographically defined polymer to be transferred to the silicon, silicon dioxide, and metals that make up the integrated circuits at the heart of these devices.

The first commercially available microprocessor, the Intel 4004, was launched in 1971. It was a 4 bit processor, contained 2300 transistors, operated at 1.08 MHz clock-frequency, and a minimum feature size of 10  $\mu\text{m}$ .<sup>1</sup> Intel’s third generation multicore processors, launched in late 2012, are 64 bit processors, containing  $1.4 \times 10^9$  transistors, operating at roughly 3 GHz clock-frequency and a minimum feature size of 22 nm.<sup>2</sup> Although many factors contributed to the advances in microprocessors’ performance, a key element has been the ability to fabricate smaller transistors. This is attributed to advancements in lithography and pattern-transfer methods. The purpose of this review is to cover the advancements in the latter. In the early days of integrated circuit fabrication, pattern-transfer was accomplished by wet etching. However, with time, plasma etching became the preferred method.

Here we attempt to provide a modern review of this field in a comprehensive as possible manner. Given the scope of this undertaking, this is a nearly impossible task. Many important studies will be left out. We also note that there are several earlier books on plasma etching<sup>3,4</sup> as well as more detailed treatments of important aspects such as plasma physics and electrical engineering.<sup>5–7</sup> Instead, the attempt here is to cover in some detail the applications of plasma etching in integrated circuits and to a lesser extent, in microelectromechanical systems (MEMS) devices. The subject is placed in historical perspective and is accompanied by a discussion of mechanisms of plasma etching and selected diagnostics that provide both fundamental insights into plasma etching processes and are in widespread use in manufacturing. An attempt is also made to predict the future needs for plasma etching, looming problems, and possible solutions.

#### II. BRIEF HISTORY

The use of glow discharges dates back to the late 19th century where sputtering, first discovered by Grove<sup>8</sup> and also observed near the electrodes in vacuum tubes, was used for the production of mirror surfaces.<sup>9</sup> The term “plasma” to designate partially ionized gas is attributed to Irving Langmuir who studied glow-discharges, and according to his colleague and collaborator, Lewi Tonks,<sup>10</sup> coined the term during a discussion between them. The first known use of the term in the literature is dated 1928.<sup>11</sup>

In the early days of integrated-circuit processing, wet-etching was used for pattern transfer. With time, however, plasma-based pattern transfer replaced wet chemistry for most if not all the steps. The development of modern plasma-etching equipment for pattern-transfer evolved along

<sup>a)</sup>Electronic mail: [vmdonnelly@uh.edu](mailto:vmdonnelly@uh.edu)

<sup>b)</sup>Electronic mail: [avtek0@gmail.com](mailto:avtek0@gmail.com)

two paths that eventually merged into the current configuration, where the substrate to be etched is placed on a radio frequency (RF)-powered electrode, with or without an additional plasma-generation source. The two approaches, physical (i.e., sputtering) and chemical, had different goals. The former was needed for pattern transfer that could not be accomplished by wet-chemical means, while the latter was intended to replace wet chemicals in IC fabrication.

The first path, sputtering, was used in the early 1960s for the fabrication of beam-lead devices (beam-leads were an alternate technology to wire-bonding, where gold semirigid cantilevered leads were used to connect the device to the outside world). In the process, developed by Martin Lepselter from Bell Laboratories,<sup>12–14</sup> gold leads, 12.5  $\mu\text{m}$  in thickness, were electroplated onto a metal stack consisting of an adhesion-promoting layer or a “glue-layer” (titanium or zirconium) and platinum (needed to prevent a chemical reaction between the gold and the glue-layer). The etching of the metal stack below the gold could not be easily accomplished by wet etching. For instance, aqua regia (one part concentrated HCl plus three parts concentrated  $\text{HNO}_3$ ), one of the few chemicals that will etch platinum,<sup>15</sup> will etch gold about 190 times faster,<sup>16</sup> leading to severe undercutting of the gold. Back-sputtering of the platinum solved the problem, sometimes with the downstream addition of oxygen<sup>17</sup> to increase the selectivity to the glue-layer. In a further development, an RF sputtering method (using an argon plasma) was implemented by Davide<sup>18,19</sup> from IBM, utilizing a “blocking” capacitor<sup>20</sup> to couple the RF generator to the electrode on which the substrate had been placed. The resulting negative bias led to ion acceleration toward the biased electrode and was used to pattern cermet-film resistors.

The chemical approach for plasma etching in the semiconductor industry started in the late-1960s when Stephen Irving from Signetics demonstrated the ability to strip photoresist in oxygen plasma.<sup>21–23</sup> The reactor, that had been used to remove organic residues from various substrates by “burning” or “ashing” them, was manufactured by Tracer Labs, a division of LFE Corporation.<sup>24</sup> It consisted of a reaction vessel, where an external coil was used to generate the plasma by an electrodeless discharge [the concept was not new and was used first by Thomson in 1891 (Ref. 25)]. However other issues, such as residues and device damage<sup>23</sup> [associated with ultraviolet (UV) radiation] had to be addressed before plasma-ashing became a viable alternative to wet stripping. Irving recognized the wider implication for etching other materials as well by using either fluorine or chlorine-based compounds to etch  $\text{SiO}_2$  or aluminum, respectively.<sup>26</sup> The motivation for use of plasma to clean or pattern semiconductor devices was driven primarily by the need to reduce chemical waste associated with the use of wet etchants,<sup>23,27</sup> but other advantages became apparent as well. As silicon-nitride became the material of choice for the encapsulating layer, there was no wet etchant that could be used to pattern it to form the contact to the aluminum metal layer below.<sup>27</sup> Fluorine based plasmas became the obvious choice to pattern the nitride without eroding the aluminum metal in the contact-pads.

While etching  $\text{SiO}_2$  with fluorine-compound based plasma looked attractive, it would not be practical if the selectivity (i.e., the etch-rate ratio of  $\text{SiO}_2$  to the underlying substrate) were low. For instance,  $\text{CF}_4$  plasmas can etch silicon faster than  $\text{SiO}_2$ . The issue of additives (e.g.,  $\text{H}_2$ ) or alternative gases ( $\text{C}_2\text{F}_6$ ,  $\text{C}_3\text{F}_8$ ,  $\text{CHF}_3$ ) to increase selectivity with respect to silicon was discussed extensively by Heinecke.<sup>28,29</sup>

The early plasma reactors were barrel type, where wafers were placed in a quartz chamber with external electrodes<sup>30</sup> (or a coil—Fig. 1). The appropriate gas was introduced into the chamber while RF was applied across the electrodes to generate the plasma. These etchers, while adequate for resist stripping, lacked wafer temperature control and, at least initially, suffered from poor etch uniformity, required for device processing. It was not until the radial-flow reactor was introduced that plasma etching became a viable production alternative to wet etching for patterning. In this reactor (known also as the Reinberg reactor<sup>31</sup>), wafers were placed on the grounded electrode, while RF is applied to the opposite electrode (Fig. 2).

The convergence of the two approaches for plasma etching took place when Hosokawa *et al.*<sup>32</sup> introduced fluorine and chlorine-containing gases (e.g.,  $\text{CF}_4$ ,  $\text{CCl}_3\text{F}$ ,  $\text{CCl}_2\text{F}_2$ , etc.) instead of Ar to a RF sputtering apparatus. The motivation was to increase the etch rate of various materials, such as silicon, glass, aluminum, molybdenum, stainless steel, and photoresist. However, there was no discussion of the applicability of the technique to pattern transfer. The technique, now called reactive ion etching (RIE),<sup>33–35</sup> reactive sputter etching (RSE),<sup>36,37</sup> or ion-assisted plasma etching,<sup>38</sup> became the method of choice (with some enhancements that will be discussed in the next section) for patterning devices.

The first all dry-etched device was processed in 1975 by Texas Instruments.<sup>27</sup> The motivation was to reduce the amount of solvents in the processing line as well as the ability to pattern the silicon nitride passivation-layer to access the bond-pads. However, as critical dimensions (CD) became smaller and smaller, vertical dimensions approached and exceeded horizontal dimensions, mask undercutting became intolerable, and anisotropic etching became the primary motivation for using plasmas for pattern-transfer.

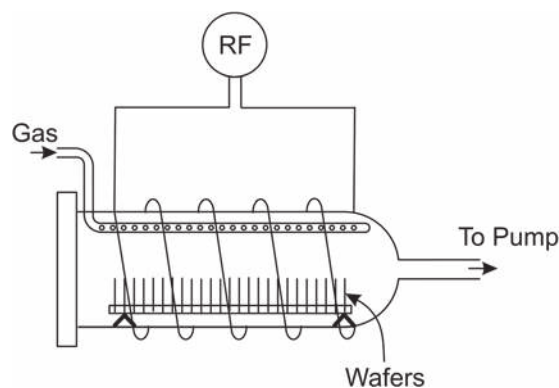


Fig. 1. Barrel reactor. Wafers are mounted on a quartz boat inserted through a door (on left) into a quartz tube. After pumpdown, gas flow is initiated followed by RF power applied to a coil wrapping around the quartz tube.

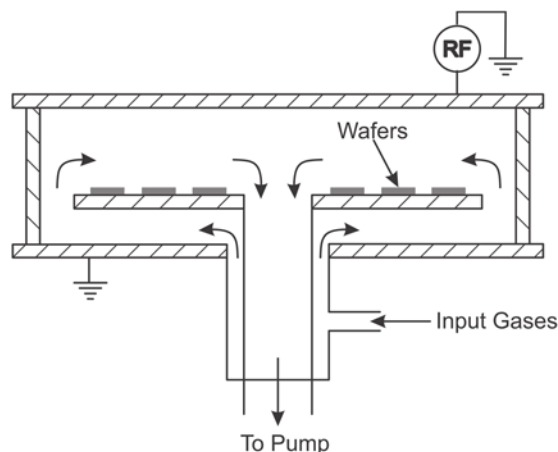


FIG. 2. Reinberg reactor. Wafers are placed on a platen at ground potential. After pumpdown, gases are flowed over the wafers from edge to center, while RF power is applied to the upper electrode.

### III. EQUIPMENT EVOLUTION

The etching tools used in the early days for pattern transfer were diode reactors with the wafers placed either on the grounded or RF-powered electrode that was capacitively coupled to the plasma with an excitation frequency of 13.56 MHz. Tools with the former configuration were referred to “plasma reactors” while those with the latter configuration were dubbed “reactive-ion-etchers” (RIE) or “reactive-sputter etchers” (RSE). The plasma reactors operated at relatively high pressures (hundreds of mTorr) with the two electrodes roughly equal in area [Fig. 3(a)], while reactive-ion-etchers operated at lower pressures, with the powered electrode smaller than the grounded electrode [Fig. 3(b)]. The asymmetry of the two electrodes, coupled with the use of a blocking capacitor, yielded a negative dc self-bias voltage on the smaller (usually powered) electrode. The ratio of voltages across the sheaths near the powered and grounded electrodes was originally thought to vary as the ratio of areas of the grounded and powered electrodes to the forth power.<sup>39</sup> While the area ratio dependence was later shown to be much less severe,<sup>40</sup> the smaller electrode was nonetheless found to

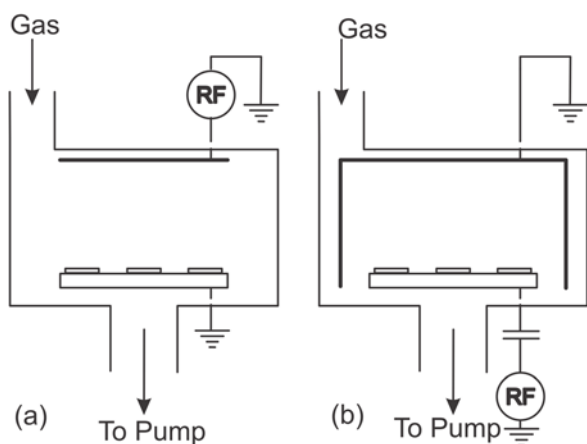


FIG. 3. Parallel plate reactors: (a) “Plasma mode”—wafer on grounded electrode; (b) “RIE mode”—Wafer on RF-powered electrode.

obtain a much larger sheath potential than the larger electrode. This causes more energetic ion bombardment of substrates placed on the smaller electrode, enabling anisotropic etching.

As the industry migrated toward plasma etching processes and replaced wet etching as the preferred method for pattern-transfer, throughput became an important issue. Reactive ion etchers that could process large batches of wafers were the early solution for the problem.<sup>38,41,42</sup> An example is shown in Fig. 4. Although these etchers could handle up to eighteen 150 mm diameter wafers, the challenges were the control of etching uniformity (within a wafer as well as wafer-to-wafer) and wafer handling (automatic loading and unloading). As the industry migrated to 200 mm wafers, with the need to achieve better etching uniformity (both within-wafer as well as wafer-to-wafer), batch reactors became less attractive, and enhanced etching-rate single-wafer-etchers took their place.

The key to high-throughput single-wafer etchers is enhanced etching-rate and the ability to integrate multiple etching chambers on a single platform. Depending on the application, the higher etching rate can be achieved by increased pressure ( $>100$  mTorr), the use of magnetic fields to confine the electrons, referred to as magnetically enhanced RIE (MERIE), or by using inductive coupling or microwave frequencies to achieve high-density plasmas ( $>10^{11}$  positive ions/cm<sup>2</sup>). In this case, the source is decoupled from power delivered to the stage to allow ion-energy control independent of plasma density.<sup>43</sup>

#### A. Magnetic enhanced reactive ion etching

In this method, electrons spiral around imposed magnetic field lines, increasing their trajectory toward the chamber walls. The end result is higher number of collisions per electron, leading to a higher ionization rate. Early MERIE tools utilized either permanent magnets<sup>44</sup> (e.g., MRC MIE-710) or moving magnets behind the wafers<sup>45</sup> (e.g., Tylan/Tokuda HiRIE 500). The more common designs, however,

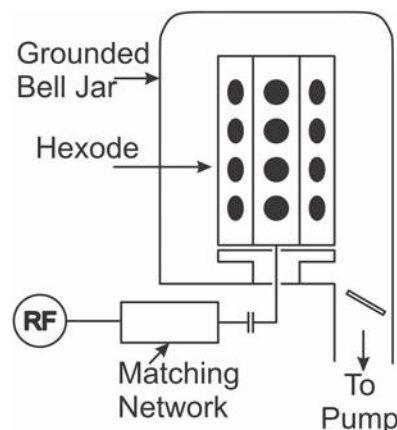


FIG. 4. Batch RIE reactor where wafers are mounted on a multifacet cathode. With a six facet cathode (hexode), twenty-four 100 mm wafers could be etched simultaneously (or eighteen 125 and 150 mm wafers). The 200 mm version (pentode configuration) could accommodate ten 200 mm wafers. The electrode ratio for this configuration is greater than 2.

involved magnetic fields generated outside the chamber walls either by rotating magnets (TEL DRM) or rotating magnetic-field generated by varying currents in two sets of perpendicular coils<sup>45</sup> (Applied Materials—a number of models). In the latter case (Fig. 5), the magnetic field could be turned on and off as needed with the additional control of rotation frequency. At low pressures, the magnetic field enhances etching rates—the electrons' path to the chamber wall is longer, leading to higher ionization due to increased collision rate with neutrals. At higher pressures ( $\geq \sim 100$  mTorr), its effects are smaller, as the inelastic mean free path becomes much smaller than the reactor dimensions. Above 200 mTorr, contributions of the magnetic-field to etch rate are negligible.

## B. Multiple-frequency capacitively coupled plasma etchers

The need to decouple plasma generation from ion-energy control was realized as early as 1979.<sup>46</sup> Etchers with dual RF powered electrodes were introduced in the mid-1980s (e.g., Drytek 384T and Tegal 1500). The former had two opposing electrodes powered with the same frequency (13.56 MHz), with a grounded chamber wall and a grid,<sup>47</sup> while in the latter, the two electrodes were powered with different frequencies, with a grounded third electrode.<sup>48</sup> Later generations of the Tegal triode etchers included magnetic confinement<sup>49,50</sup> as well.

In current dual-frequency capacitively coupled plasma (CCP) reactors, marketed by TEL and Lam Research, high-frequency ( $\geq 13.56$  MHz) is applied to the upper electrode, and the lower electrode that holds the substrate is powered by the lower frequency. In newer configurations, there is the option to couple both frequencies to the lower electrode, with additional hardware to confine the plasma.<sup>51,52</sup> This minimizes interaction with the chamber wall and facilitates more efficient chamber cleans that can be carried out after every wafer. The exact frequencies will vary by application, manufacturer, and equipment-generation. A schematic of a

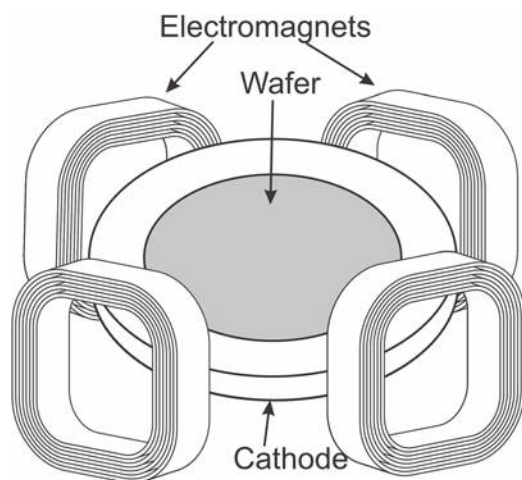


FIG. 5. Applied Materials MERIE chamber. The current in the four coils could be varied to generate a rotating magnetic field. The coils are placed outside the chamber walls.

dual-frequency reactor is shown in Fig. 6(a). These reactors normally operate at higher pressures than the high-density reactors discussed below and are usually used for dielectric-etch applications.

More recently, Lam Research has introduced a CCP etcher where three frequencies, 2, 27, and 60 MHz, are utilized.<sup>53,54</sup> In this configuration, the upper electrode is either RF powered with one frequency or grounded. In the former, two frequencies are applied to the lower electrode, while in the latter all frequencies are coupled to the lower electrode.<sup>55</sup>

In another twist, introduced by TEL, the top electrode, in addition or instead of being RF-powered, may be DC-biased, while the lower electrode is RF biased [DC/Rf hybrid reactor,<sup>56–60</sup> Fig. 6(b)]. The reason for DC biasing is to generate high-energy ballistic electrons<sup>59</sup> that will accelerate toward the opposite RF powered electrode, with some reported benefits of reduced electron-shading and improved resist integrity.<sup>61</sup>

## C. High density etchers

Numerous plasma etchers have been introduced where the plasma is generated by a source that is not capacitively coupled to the plasma. The ion-density in these etchers is generally about an order of magnitude or more higher than in the CCP etchers described above. The wafer is placed on an RF-biased lower electrode, and plasma is generated by a source placed a short distance above the wafer. Common high-density sources are inductive, electron-cyclotron-resonance (ECR), surface-wave-plasma (SWP), and helicon. These and other sources are discussed extensively elsewhere.<sup>43</sup>

### 1. Inductively coupled source

In these systems, a coil (or multiple coils to control uniformity) outside the chamber is used for plasma generation. The coil could be planar<sup>62</sup> [Fig. 7(a)] placed on a dielectric window (Lam Research transformer-coupled plasma, or TCP®), three-dimensional bowl shaped (Applied Materials DPS®), or simply a cylindrical coil. The walls are at ground

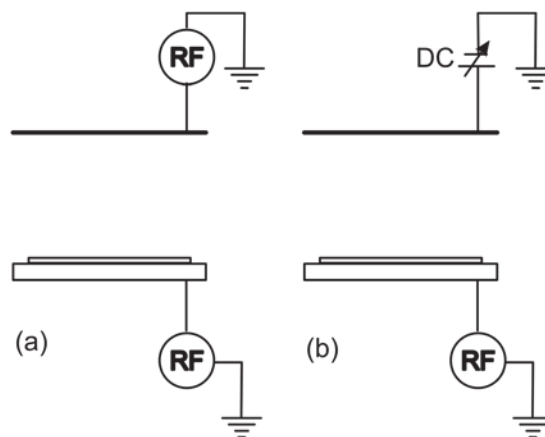


FIG. 6. Capacitively coupled plasma etcher with the two electrodes powered. In another version, the top electrode is grounded and the two RF generators are coupled to the lower electrode. (a) Both electrodes are RF powered (b) a RF/DC hybrid reactor with the top electrode DC powered.



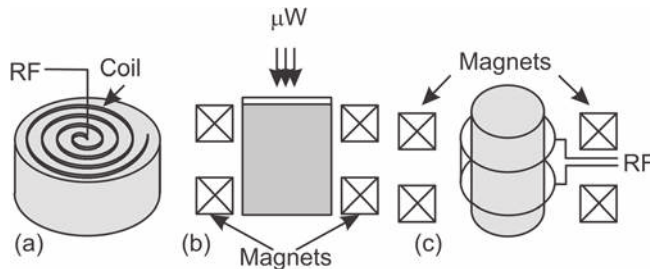


FIG. 7. Various high-density plasma sources: (a) Inductive-planar coil; (b) ECR; (c) helicon.

potential, but they are usually coated with an insulating, ceramic layer and are often behind an insulating liner. The substrate is placed on the stage that is capacitively coupled to a RF source. As in CCP systems, the small electrode holding the wafer develops a negative dc self bias when RF power is imposed; hence, it can be thought of as a cathode. In some etchers, the plasma is confined by a magnetic field generated by fixed magnets.

Inductively coupled etchers generally operate at pressures of a few mTorr to tens of mTorr and are used for the etching of trenches, gate-electrodes, high- $\kappa$  dielectrics, aluminum and its alloys. There are also special configurations to etch materials that do not form volatile compounds (Hitachi offers such a system), including alloys of nickel and iron, noble metals, lead zirconate titanate (PZT), barium strontium titanate (BST), and others. In these cases, where sputtering is the mechanism for pattern transfer, the by-products accumulate on the chamber walls, which then have to be physically cleaned from time to time. If the etch by-products are conductive, however, they may coat the dielectric window; a capacitively coupled plasma reactor is preferred in these instances.<sup>63</sup>

## 2. Electron-cyclotron-resonance source

In an ECR plasma,<sup>64</sup> radiation is launched through a dielectric window into a low-pressure volume containing the gas to be ionized [Fig. 7(b)]. The frequency of the radiation in commercial etchers is typically in the microwave regime (2.45 GHz), but UHF (450 GHz) was used in some etchers as well mainly for dielectric etch applications.<sup>65</sup> The electrons generated are confined by a magnetic field generated by a few magnets and are forced to move in a circular motion. The frequency of rotation (cyclotron frequency) is given by  $\nu = (1/2\pi)(eB/m)$ , where  $e$  and  $m$  are the electron charge and mass, respectively, and  $B$  is the magnetic flux density. At resonance, the right-hand side equals the excitation frequency, and therefore  $B = 0.0875$  T (875 G) and 0.0161 T (161 G) for  $\nu = 2.45$  GHz and 450 MHz, respectively. The chamber below the resonance cavity is typically surrounded by magnets for improved uniformity. Currently, the main applications of ECR etchers are silicon or aluminum etching.

## 3. Helicon source

Helicon sources<sup>66</sup> are not currently used in mainstream commercial etchers. The source utilizes a specially designed

antenna and operates at frequencies in the megahertz range in the presence of an axial magnetic field, producing bounded whistler waves.<sup>67</sup> Depending on the antenna design, different modes of excitation are possible. Early helicon sources for plasma etching operated in the  $m = 1$  mode,<sup>68–70</sup> but the one that eventually gained presence in the commercial market operated at the  $m = 0$  mode<sup>71</sup> (MORI source, first marketed by PMT and subsequently by Trikon). The former is characterized by electrical field lines that do not change their pattern with position but the pattern rotates along the direction of the  $B$  field, while the latter exhibits field lines that change direction from radial to azimuthal, depending on position. The etch chamber is often magnetically confined. The MORI source has been used for etching silicon, metal, as well as dielectrics.

## 4. Surface wave plasma source

This source uses microwaves to generate a high density discharge without the presence of a DC magnetic field.<sup>72</sup> These type of etchers were first commercialized in the early 1990s (e.g., Sumitomo SW4010), but never became widely used. However, recently TEL has introduced a SWP etch chamber with a radial-line slot antenna, utilizing a 2.45 GHz microwave source. It has been reported that the electron energy distribution function (EEDF) in the plasma-generation zone is non-Maxwellian,<sup>73,74</sup> and therefore no unique electron temperature,  $T_e$ , can be assigned.<sup>74</sup> Away from the plasma generation zone the bulk of the EEDF approaches a Maxwellian distribution with  $T_e$  around 1 eV. The intensity of vacuum ultraviolet (VUV) radiation near the wafer, linked to device damage,<sup>75,76</sup> is reported to be considerably lower than the radiation associated with inductive sources.<sup>74</sup>

## D. Downstream etchers

In these systems, plasma is generated in a remote chamber (either by a microwave or an inductive source), in a manner that does not expose the wafer to UV radiation, which can lead to device damage (e.g., threshold shift).<sup>23</sup> In addition, due to the long length of tubing between the source and the substrate, no charged particles reach the etching chamber and the substrate is exposed only to neutrals. These etchers are used for isotropic etching processes. The main application is for resist-stripping (ashing) with O atoms at elevated temperature (200–300 °C). The formation of nonreactive, ground state  $O_2$  is suppressed by the addition of other gases such as  $N_2$ .<sup>77</sup>  $N_2/H_2$  mixtures can also be used for resist stripping, albeit at a lower rate.<sup>78</sup> This mixture is useful when oxidation of the exposed substrate (e.g., TiN film, or low- $\kappa$  dielectrics) is to be avoided.<sup>78,79</sup> Another application is the soft etch of silicon by atomic fluorine resulting from the dissociation of gases such as  $NF_3$  or  $CF_4$  at room temperature. Substrate heating, when necessary, is accomplished either by a heated chuck or lamp. Depending on the tool, wafers can be etched either by resting on the chuck, or on the lift-pins. In the latter configuration, both front and back-sides of the wafer can be etched simultaneously. The chuck can often be RF powered to initiate the etch by removing a hard-to-etch film on top of

the layer to be removed, such as the crust formed on top of photoresist during ion implantation.

### E. Temperature control

In all applications where photoresist is used as the mask, there is a need to keep the wafer temperature low enough to prevent the resist from flowing or reticulating. Both temperature and UV radiation generated by the plasma are the causes of the latter, and in fact act in synergy.<sup>80</sup> In other cases, temperature is a critical parameter in determining the rate of the etch process (e.g., aluminum etching) and it must be controlled. In earlier generations of etchers, this was accomplished by placing the wafer on the chuck, sometimes with force applied at the periphery of the wafer placed on a domed pedestal. Later generation etchers have utilized helium heat-exchange gas, pressurizing the gap between the wafer and the chuck. This pressure is typically between 4 and 30 Torr, and the gap is within or below the mean-free-path of helium at the operating pressure (roughly 0.01 mm at 10 Torr and 40 °C). Under these conditions, the heat transfer coefficient does not vary much with variations in the gap dimensions.<sup>81</sup> Although in principle other gases may be used for heat exchange, helium is preferred because of its high heat-transfer coefficient and high ionization potential (i.e., the He leaking into the plasma does not perturb it). With the introduction of electrostatic chucks (ESC), the He leak-up rate into the chamber is used to monitor wafer clamping and the health of the ESC. Warped wafers (especially ones that are bowed upwards as a result of a highly tensile film on the front of the wafer) can lead to high helium leak-up rate and inadequate clamping or “chucking.”

Both heated ( $T > 150\text{ °C}$ ) and cryogenically cooled chucks are used in some applications. The former is used in to increase the vapor pressure of the etch by-products (e.g., high- $\kappa$  etching), while the latter is used in limited applications to minimize lateral etching (e.g., silicon etching with  $\text{SF}_6$  in a non-Bosch process).

### F. Endpoint detection

At most etching levels, some endpoint detection is needed, first to ensure that etching is complete, and second to avoid excessive etching time that may erode the underlying layer. There are numerous methods that have been used over the years in research laboratories and production environment, such as interferometry,<sup>82</sup> ellipsometry,<sup>83–85</sup> and optical emission spectroscopy (OES).<sup>86–90</sup>

While ellipsometry is a useful research tool, it has not found much use in production. Interferometry was widely used in batch etchers, but with the transition to single wafer etchers, optical-emission monitoring became the preferred method for endpoint detection, due to its relative simplicity in terms of hardware and software implementation. Interferometry is still useful in some applications, where etching steps are to be changed based on depth of material etched (see discussion below and example in Fig. 8).

The interferometric method relies on interference between light beams reflected from the top and the bottom

surface being etched. If the imaginary component,  $k$  of the refractive index,  $n + ik$ , is small, a periodic reflected signal will be observed, with periodicity corresponding to  $\Delta d = \lambda / (2\sqrt{n^2 - \sin^2\theta_i})$ , where  $\Delta d$  is the thickness associated with a period,  $\theta_i$  is the angle of incidence with respect to the surface normal, and  $\lambda$  is the wavelength of the light-source being used. The light source could be external [laser or UV (Ref. 91)] or even internal, i.e., the plasma glow itself.<sup>92,93</sup> In the latter case, it could be used to monitor the etching process over the entire wafer. From the periodicity of the reflected light, etch rates can be determined, and endpoint is realized when the reflected signal becomes flat (Fig. 8, end of trace I).

The monitoring of reflectance can also be used to detect endpoint of an absorbing layer (high imaginary refractive index,  $k$ ) on top of another by monitoring the change in reflectance. For example, this method was used to monitor the etching of aluminum in a batch reactor, using a He-Ne laser as the light source.<sup>94</sup> A large change in reflectance occurs when the metal is cleared.<sup>94</sup> A similar approach was used in the fabrication of x-ray masks to monitor the etching of tungsten sandwiched between two layers of Cr on top of a polysilicon membrane.<sup>95</sup>

In a slight modification of the method, it can be used for endpoint prediction.<sup>78,96–98</sup> For example, reflectivity changes have been used in etching of polysilicon gates to stop on less than 1 nm of thermal oxide, by initiating a selective overetch step before the polysilicon cleared. In this case, the wavelength of the external light source was chosen to yield a change in reflectance 10–20 nm before endpoint, which triggered the overetch step.<sup>96</sup>

The technique most commonly used for endpoint determination is OES (Sec. IV A), where a particular wavelength in the plasma is monitored throughout the etch process for any change associated with the removal of the film being etched. It can be associated with an etch by-product, like CO emission in oxide etching (which leads to the signal decline at endpoint), or reactant, such as Cl or  $\text{Cl}_2$  in polysilicon etching (which leads to a signal rise at endpoint). The

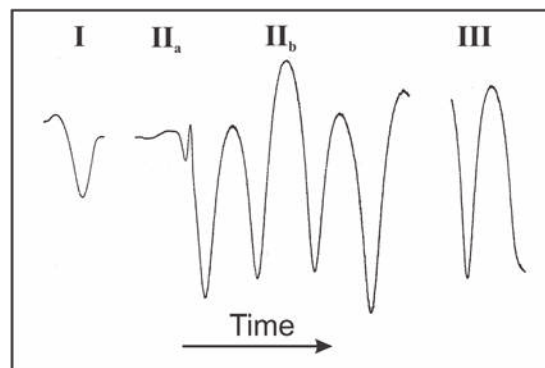


FIG. 8. Reflected light recorded during etching of a  $\text{TaSi}_x$ /polysilicon gate stack with an antireflecting coating (ARC), showing periodicity associated with interference. **I**: ARC etch (with  $\text{Cl}_2$ ). **II**:  $\text{TaSi}_x$  and the bulk of the polysilicon (with  $\text{CFCl}_3/\text{O}_2$ ); steps **IIa** and **IIb** correspond to the etching of  $\text{TaSi}_x$  and polysilicon, respectively. **III**: Etching of the remainder of the polysilicon with  $\text{Cl}_2/\text{O}_2$ . A long overetch step (not shown) with a low-bias  $\text{Cl}_2/\text{O}_2$  plasma was carried out to clear residual polysilicon resulting from the topography associated with these device.

appropriate monitoring wavelength is either selected by a filter, photomultiplier tube, or an optical multichannel array. In the latter case, it is possible to monitor multiple wavelengths simultaneously. In cases where a rotating magnetic-field is used, some averaging of the signal over one or more rotation-periods is required to produce a meaningful signal. An example of an emission trace used to monitor WSi<sub>x</sub>/polysilicon gate etching is shown in Fig. 9. While OES is a powerful technique for endpoint detection, it is not sensitive enough in cases where the exposed area is very small, such as in contact and via etching.

Both reflectivity and OES techniques require an access windows on the chamber that must remain clean to obtain stable signals of sufficient intensity. Typically, a heated quartz window is used to prevent polymer buildup.

Other endpoint detection methods, such as pressure change, bias change, and mass spectrometry are discussed elsewhere.<sup>94</sup> These are not used in production due to their complexity and/or lack of sensitivity.

## IV. DIAGNOSTICS AND MECHANISMS

### A. Some basic considerations in ion-assisted etching

Anisotropic plasma etching is made possible by the perpendicular bombardment of the surface by positive ions that are accelerated by a sheath potential that develops on surfaces exposed to the plasma. Within this simple classification of ion-assisted etching, many types of reactions can occur. Anisotropic etching requires a combination of energetic ions and reactive neutral species. The flux of neutral species should preferably be much larger than the positive ion flux, so that the etching rate is mainly limited by the ion flux. This

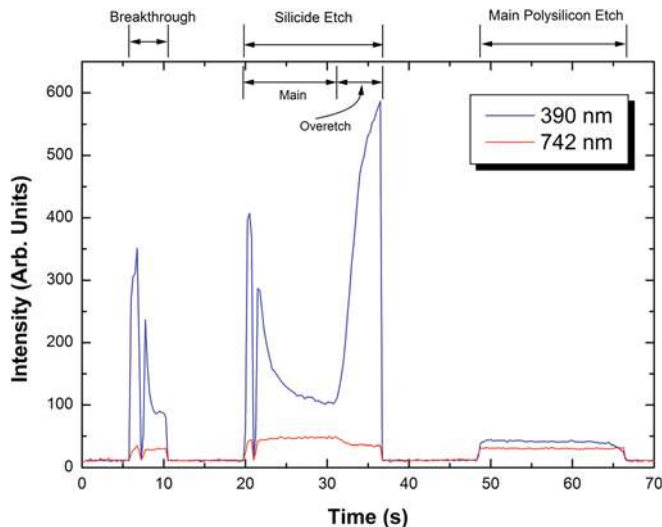


FIG. 9. (Color online) Emission signals associated with a multistep WSi<sub>x</sub>/polysilicon gate etching process. Two wavelengths, 390 and 742 nm were used to monitor the process in a Lam 9400 etcher. **Breakthrough:** High-bias Cl<sub>2</sub>. **Silicide etch:** Cl<sub>2</sub>/O<sub>2</sub>. **Polysilicon etch:** Cl<sub>2</sub>/HBr/O<sub>2</sub>. **Overetch (not shown):** HBr/O<sub>2</sub>. The intensity fluctuations at the beginning of the breakthrough and the silicide etch reflect instability of the RF power associated with the matching network of the source. The 390 nm trace rises at endpoint of the WSi<sub>x</sub> etch step while the 742 nm trace falls. The 390 nm emission line is used to determine endpoint of the main polysilicon etch (the fall of the 742 nm trace is associated with RF power being turned off).

allows the fastest etching rates to be obtained with minimum dependence on the feature aspect ratio and the area of exposed material.

### 1. Vaporization of products

It is advantageous if the etching gas is able to form a volatile compound with the film or silicon substrate that is being etched. Although it is possible to obtain useable etching rates with some sputtering processes, including with reactive gases that aid in breaking substrate bonds but generate nonvolatile products, these products will redeposit on the wafer and coat the reactor surfaces, causing many feature-scale and reactor scale problems. Also such processes are not very selective.

For a compound to be sufficiently volatile, its evaporation rate should be much higher than the desired etching rate. The maximum evaporation rate is computed by the principle of detailed balance: at equilibrium, the forward and reverse rates of every elementary process are equal. Consequently, for a gaseous species at a number density,  $n$ , in equilibrium with its liquid or solid state in a closed system, its evaporation rate equals its impingement rate on the solid or liquid. The impingement rate or flux (molecules-cm<sup>2</sup>s<sup>-1</sup>) of species onto a surface is

$$f_i = \frac{nv}{4}. \quad (1)$$

The thermal speed,  $v$  (in cm/s), is given by

$$v = \left( \frac{8kT}{\pi m} \right)^{1/2}, \quad (2)$$

where  $k$  is the Boltzman constant ( $8.314 \times 10^7$  erg K<sup>-1</sup> mole<sup>-1</sup>),  $T$  is the temperature in Kelvin, and  $m$  is the mass in grams/mole. For an ideal gas at pressure  $p$  (expressed as dyne-cm<sup>-2</sup> [1 dyne-cm<sup>-2</sup> = 0.1 Pa =  $7.502 \times 10^{-5}$  Torr]), the impingement rate can be expressed as

$$f_i = \frac{p}{\sqrt{2\pi mkT}}. \quad (3)$$

The equilibrium vapor pressure,  $p_v$ , is described by the Clausius–Clapeyron equation:

$$p_v = p_0 \exp\left(\frac{-\Delta H}{RT}\right), \quad (4)$$

where  $\Delta H$  is the heat of vaporization and  $p_0$  is a constant of integration. Consequently, at equilibrium, the evaporation rate (equals the impingement rate) is given by

$$f_e = f_i = \frac{p_v}{\sqrt{2\pi mkT}}. \quad (5)$$

The evaporation rate is given by the right side of Eq. (5), regardless if the system is closed or open and far from equilibrium.

For the most common materials used in silicon microelectronics devices, the etching products in halogen, carbon, hydrogen, and oxygen-containing plasmas are SiF<sub>4</sub>, SiF<sub>2</sub>, SiCl<sub>4</sub>, SiCl<sub>2</sub>, SiBr<sub>4</sub>, SiBr<sub>x</sub>H<sub>y</sub>, SiCl<sub>x</sub>Br<sub>y</sub>H<sub>z</sub>, SiOF<sub>2</sub>, CO, CO<sub>2</sub>,



O<sub>2</sub>, COF<sub>2</sub>, metal halides, and metal oxy-halides. These are not necessarily the primary etching products leaving the surface, but are nonetheless the predominant stable products that are pumped away. With the exception of some refractory metal compounds and Si-dihalides, the evaporation rates for these products are many orders of magnitude larger than typical etching rates, hence these stable products will never reach an appreciable coverage on surfaces and etching of these materials is *never* limited by the evaporation rate, even in the case of Si etching in an HBr plasma, where SiBr<sub>4</sub> is the *least* volatile product possible. Hence, even though it is true that SiBr<sub>4</sub> is less volatile than SiCl<sub>4</sub>, Si etching in a HBr plasma is not slower than that in a Cl<sub>2</sub> plasma because the product is less volatile.

For a species to be present on the surface during etching, it must be strongly adsorbed. The rate of thermal desorption is given by

$$k_d = \nu_0 \exp(-E_a/RT), \quad (6)$$

where  $\nu_0$  is the pre-exponential or so-called attempt frequency and  $E_a$  is the activation energy for desorption, or binding energy for the adsorbate. The pre-exponential factor is often simply assumed to be equal to a typical vibrational frequency of  $\sim 10^{13} \text{ s}^{-1}$ , although it is in fact equal to  $kT/h$  times the ratio of partition functions of the transition state for desorption to that of the reactant state and can vary from typically  $10^8$  to  $10^{15} \text{ s}^{-1}$ . Like  $\nu_0$ , the binding energy can also span a wide range of values, reflecting the complex nature of the surface layer and the multitude of bonding configurations. Using a value of  $10^{13} \text{ s}^{-1}$  for  $\nu_0$ , it can be seen from Eq. (6) that a species must have a binding energy of 16 kcal/mol (0.69 eV) at room temperature to have a  $\sim 0.1 \text{ s}$  lifetime on the surface, comparable to the time required to etch 1 monolayer. This binding energy exceeds physisorption energies for most adsorbate–substrate combinations, but is less than most chemical bonds; consequently, any chemisorbed species will likely live indefinitely on the surface, while products like SiBr<sub>4</sub> will desorb nearly instantaneously after being formed.

Therefore, surfaces are covered with chemisorbed species during and after etching. It is mostly plasma radicals that will adsorb and form this chemisorbed layer, but feed gases can sometimes also react (e.g., Cl<sub>2</sub> with Si and Al). Once this chemisorbed layer forms, containing atoms from the etching gas and (usually) the substrate, it must be removed (after perhaps being further “activated”) for etching to proceed. This is usually accomplished by ion bombardment. In one notable exception, Al etching at higher pressures, ion bombardment is not necessary, and the chemisorbed layer formed by reactions of Cl<sub>2</sub> and Cl spontaneously converts to a physisorbed AlCl<sub>3</sub> layer that rapidly desorbs. In most cases, however, it is the ion-stimulated removal of the chemisorbed layer that makes anisotropic etching possible.

## 2. Adsorption and etching by neutrals

A few reactions of neutrals with materials used in microelectronics devices have been studied. These experiments measure sticking coefficients, the reaction coefficients, and

recombination coefficients. In an oversimplified treatment, the sticking coefficient can be defined by the Langmuir–Hinshelwood adsorption model, which, using Cl adsorption on Si as an example, can be described as



where Si $\cdot$  is an adsorption site. The relative density of such adsorption sites is defined as  $\theta$ , which can range from 0 to 1. The probability for adsorption is given by

$$k_{\text{ads}} = S(1 - \theta), \quad (8)$$

where  $S$  is the sticking coefficient (or probability) at Si $\cdot$ . When all sites are occupied, the probability for adsorption is zero. Most etching processes operate near this limit.

Even on clean, perfect crystalline surfaces, adsorption is more complicated and often occurs by a precursor-mediated mechanism in which an adsorbate has a high sticking coefficient, even on an adsorbate-covered surface. The weakly bound adsorbate diffuses along the surface until it either finds a vacant site for adsorption (Si $\cdot$  in the example above), reacts, or desorbs. On rough surfaces that are present during etching, the adsorption and diffusion processes are more complicated, with a range of differing adsorption sites and rates.

Although sticking coefficients are often treated as adjustable parameters in models, some measured values have been reported. These parameters usually do not correspond to the Langmuir–Hinshelwood sticking coefficient at a vacant site, as defined above, and instead are either reaction coefficients that lead to generation of products that desorb or incorporate into a growing film.

A reaction coefficient for etching,  $\varepsilon_{X(S)}$ , can be defined as the probability that an impinging neutral will react with an atomic or molecular material,  $S$ , in the absence of ion bombardment or other sources of energetic particles, to generate a volatile product that promptly desorbs.<sup>99</sup> It is given by

$$\varepsilon_{X(S)} = \frac{(x/y) N_A \rho_S R_{X(S)}}{M_S (n_X v_X/4)}, \quad (9)$$

where  $R_{X(S)}$  is the etching rate,  $N_A$  is Avogadro’s number,  $\rho_S$  and  $M_S$  are the density and mass of the substrate, and  $x/y$  is the average stoichiometry of the SX<sub>x</sub> etching products that desorb, divided by the X<sub>y</sub> stoichiometry of the etchant (e.g.,  $y = 2$  for Cl<sub>2</sub>).

Reaction coefficients have been measured for some relevant etchants and materials and are important for determining isotropic etching rates and so degree of undercutting. The etching rate of substrate  $S$  by species  $X$  is often given in the form of an Arrhenius expression

$$R_{X(S)} = A T_g^n n_X \exp(-E_a/RT_S), \quad (10)$$

where  $A$  and  $E_a$  are the Arrhenius pre-exponential factor and activation energy, respectively,  $n_X$  is the number density of  $X$  at gas temperature  $T_g$ , and  $T_S$  is substrate temperature, and



$n$  is either 0.5 or 0, depending on whether the dependence of the impingement rate on  $T_g$  is separated from or included in the activation energy. For  $n$ -type Si etching, the dopant level affects the pre-exponential. In these cases,  $A$  can be expressed as<sup>100</sup>

$$A = A_0 N_e^\gamma, \quad (11)$$

where  $N_e$  is the  $n$ -type carrier concentration and  $\gamma$  is an empirical factor.

### 3. Ion induced etching reactions

The etching rate for many materials during simultaneous exposure to ion and neutral fluxes is much faster than the sum of the sputtering and chemical etching rates (plasma etching's version of the "whole is greater than the sum of its parts"<sup>101</sup>). The details of this process are extremely complicated. Several distinct mechanisms have been identified. Although ion bombardment sometimes aids in removing a passivating species from horizontal surfaces that would otherwise slow or stop etching, in virtually all cases ion bombardment enhances the reaction between the neutrals and substrate that leads to the formation of a volatile product. This is true even in the case of etching of Si in fluorine-atom-generating plasmas such as  $\text{SF}_6/\text{O}_2$ , where the etching rate by F atoms is quite high.

The details of ion-assisted etching reactions have been reviewed previously.<sup>5,102,103</sup> Coburn, Winters, and co-workers have shown that for  $\text{Ar}^+$ -assisted etching of a fluorinated Si surface, the process occurs by a "chemical sputtering" process in which ion bombardment causes chemical reactions to occur that lead to the formation of products that then desorb. These reactions are generally assumed to happen on a very short time scale ( $\sim 1$  ps)<sup>104</sup> in the collision cascade created by the transfer of momentum from the impacting, neutralized ion to the substrate and reactant atoms in the near-surface region. Product desorption can take much longer, but is usually not rate-limiting.

### 4. Other plasma-surface reactions

Plasma interactions with surfaces other than those being etched also affect the plasma etching process, though indirectly. Species in the plasma stick on the walls and masked portions of the substrate and can lead to the growth of a film, or the formation of a product that desorbs. These processes modify the plasma species concentrations and can lead to changes in etching rates, profile shapes, selectivities, and other figures of merit. Therefore, surface reaction coefficients are of interest for conditions as close as possible to real etching plasmas.

Fisher and co-workers have measured sticking coefficients and reaction coefficients of selected radicals under conditions close to those in the plasma.<sup>105–107</sup> Beams of  $\text{SiH}$ ,  $\text{OH}$ ,  $\text{NH}$ ,  $\text{NH}_2$ ,  $\text{CF}$ , and  $\text{CF}_2$  radicals generated in various plasmas were directed at substrates such as  $\text{SiO}_2$  and fluorocarbon films in a differentially pumped chamber, and detected by laser-induced fluorescence (LIF) as they impinge on a surface and reflect

from the surface. An image of the path of the incoming and outgoing radicals is captured, hence the technique is called "imaging of radicals interacting with surfaces." Sticking and/or reaction coefficients can be obtained with this method. For  $\text{CF}_2$  scattering off  $\text{SiO}_2$ ,  $\text{Si}_3\text{N}_4$ , Si, stainless steel, and photoresist substrates, the flux of scattered  $\text{CF}_2$  exceeds its incident flux, indicating that this product is formed by a surface reaction of other impinging species (e.g.,  $\text{CF}$  and/or  $\text{CF}_3$ ) that are also present in the plasma beam source.<sup>108</sup>

### B. Selected diagnostic techniques for etching plasmas

It is beyond the scope of this article to review the many diagnostic methods that are available to characterize processing plasmas, including electrical probe methods to determine ion and electron number densities and electron energy distributions. Instead we will highlight a few selected techniques that are useful for understanding and monitoring etching processes. These can be divided into gas-phase and surface probes.

The gas phase plasma contains mostly neutrals. These are stable feed gas species, radicals formed by the decomposition of the feed gas, stable etching products, and radicals that can be primary products or product fragments that are formed by electron impact. In some cases, a complete determination of the plasma neutral composition is desired for a deeper understanding of plasma chemistry. In other cases, one or several species are monitored to sense endpoints when thin films have been etched away.

There is also an important need to monitor the chemical and physical nature of surfaces immersed in plasmas. This includes not only the surfaces of wafers being etched, but also the plasma chamber wall surfaces. Controlling the latter is essential for maintaining stable processing conditions, since the composition of radicals in the plasma is greatly affected by heterogeneous reactions that are in turn dependent on the nature of the chamber wall surface. Ellipsometry and infrared absorption spectroscopy are *in situ* methods that have been used to monitor species on surfaces in real time. The chemical composition of surfaces immersed in plasmas can also be investigated by electron spectroscopy methods [mostly x-ray photoelectron spectroscopy (XPS)] that require the sample to be transferred from the plasma chamber to the analysis chamber without exposure to air. Recently advances have been made in a "spinning wall" technique in which a small portion of the chamber wall is rapidly rotated such that the surface can be analyzed by Auger electron spectroscopy and desorption mass spectrometry.<sup>109,110</sup>

#### 1. Mass spectrometry

Mass spectrometry is the broadest gas-phase diagnostic method, capable of detecting any neutral or charged species in the plasma. In practice, however, this is anything but straightforward. In a "residual gas analysis" mode, mass spectrometry can be used to routinely monitor stable species that leave the plasma, and/or form in downstream regions on the way to the mass spectrometer. This can be used to infer

which radicals may be present in the plasma (e.g.,  $C_2F_6$  formation downstream from a  $CF_4$  plasma is likely a result of  $CF_3$  recombination). Etching products can also be detected by mass spectrometry, and can be used in end-point detection, although such an approach is almost never used because optical emission spectroscopy is simpler and more sensitive.

To detect reactive neutrals, a small aperture needs to be installed in the wall of the plasma chamber. Line-of-sight detection of species passing through the aperture and entering the input of the mass spectrometer ionizer is of course essential but not sufficient. Two stages of differential pumping are required and the product beam must be chopped to distinguish the beam signal from the background gas in the mass spectrometer chamber. Only when the neutral mean free path,  $\lambda_n$ , is comparable to the reactor radius,  $R$  (almost never the case), does mass spectrometry monitor species with similar efficiency at the center and edge of the plasma. Under typical conditions of  $R > 15$  cm diameter chambers, and  $\lambda_n < 1$  cm (for gas pressures of  $> 5$  mTorr), the method is highly biased toward species near the walls.

Another shortcoming with mass spectrometry is that it is difficult to assign peaks to a particular species. Occasionally, this is due to a coincidence in mass (e.g., Si and CO), but more commonly, the issue is distinguishing parents from daughter ions that are formed in the ionizer of the mass spectrometer. Cracking patterns for stable species such as  $SiCl_4$  can be measured to help unravel the connection between the detection of daughter fragments and the number densities of the parent and daughter neutral species. Signal intensities can also be recorded as a function of the mass spectrometer electron impact ionizer energy. Such appearance potential measurements can help to separate the signals originating in daughter fragments from those corresponding to the parent ion of radicals.<sup>111–113</sup>

Ions can also be directly detected with a mass spectrometer, with the ionizer switched off.<sup>113</sup> An energy analyzer between the ion input region and the detector can energy-select the ions and by sweeping the pass energy, an ion energy distribution (IED) can be obtained with respect to ground potential (assuming the mass spectrometer is grounded). In CCPs and inductively coupled plasmas (ICPs) with no Faraday shield, the IED is governed by the electron temperature and the product of the ion transit time across the sheath and the frequency of oscillations in the sheath potential (i.e., the applied RF).<sup>5</sup> When it takes many RF cycles for the ion to cross the sheath, and no collisions occur, ions will impinge on grounded surfaces with a nearly monoenergetic IED and an energy of the mean sheath potential. Knowing the composition of impinging ions and taking into account the influence of substrate bias, mass spectrometer measurements of ions impacting grounded surfaces at the edge of the plasma can be used to infer what happens at the RF-biased substrate.

## 2. Optical, gas phase techniques

Practical diagnostic methods for plasma etching must be nonintrusive. Optical techniques satisfy this requirement.

Plasma-phase (as opposed to surface) optical diagnostics techniques include (in roughly decreasing order of usage) optical emission spectroscopy, LIF, UV absorption, infrared (IR) absorption, and laser-Raman scattering. Application of these spectroscopic techniques for thin film materials processing has been reviewed.<sup>114</sup>

*a. Optical emission spectroscopy.* OES is the most widely used diagnostic technique in plasma etching. It was first used in an etching application by Harshbarger *et al.* in 1977 to study a  $CF_4/O_2$  plasma during Si etching in parallel plate plasma.<sup>87</sup> They identified F, O, Si, and CO emissions and showed that F and Si emission exhibited a maximum as a function of  $O_2$  addition to  $CF_4$ .

The vast majority of optical emission in etching plasmas is a result of electron-impact excitation. Most atomic and diatomic species can be monitored by OES. Some triatomic molecules such as  $CF_2$ ,  $SiCl_2$ ,  $NH_2$ , and  $CO_2^+$  can also give rise to optical emission, but emission from larger molecules is either lacking because of low-lying, nonradiative bound and dissociative states or is broad and featureless because of the large density of vibrational states. Because of the complexity of the excitation mechanism, OES is usually a qualitative technique. This does not hamper the main application for OES: endpoint detection. It does, however, make it difficult (but not impossible) to determine quantitative, relative, and absolute species number densities by this method (see below).

Typical optical emission spectra of a chlorine plasma during fast etching of Si and slow etching of  $SiO_2$  are shown in Fig. 10. The spectra are dominated by emission from Cl, and, when large areas of Si are present and the substrate stage is RF-biased, from Si,  $SiCl$ ,  $SiCl_2$ , and  $SiCl_3$  (and/or  $SiCl_3^+$ ).<sup>115</sup> The Si and  $SiCl$  emissions are typically used to sense the endpoint of the etching of a thin film of Si in chlorine-containing plasmas.  $SiBr$  emission can also be used in  $HBr$ -containing plasmas. Emission from  $Cl_2$  is also apparent in the spectrum recorded during etching of  $SiO_2$ .  $Cl_2$  emission near 305 nm is

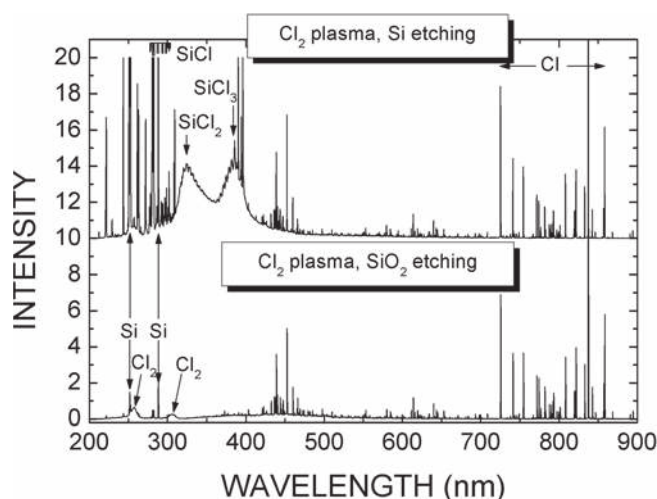
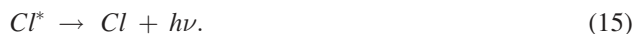


FIG. 10. Plasma induced emission spectra of a  $Cl_2$  ICP system described elsewhere (Ref. 456) during etching of Si (top) and  $SiO_2$  (bottom, intensities multiplied by 4.33 before being plotted).

attributed to electron impact excitation of an ion pair state of  $\text{Cl}_2$  at 8.4 eV, or possibly to one at 9.2 eV.<sup>116</sup>

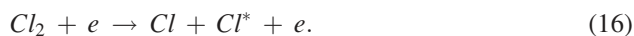


where the superscript “\*” indicates the electronically excited state(s) and  $h\nu$  is a photon of frequency  $\nu$  ( $= 9.84 \times 10^{14} \text{ s}^{-1}$  for a wavelength of 305 nm). It has been shown that the Cl emissions are mostly a result of electron impact excitation of Cl atoms<sup>116–118</sup>



This makes detection of Cl emission useful for measuring endpoints as well; as a material that consumes Cl is etched away, Cl emission increases.

For more quantitative determination of even relative Cl number densities, it is necessary to consider that  $\text{Cl}^*$  is also excited to a smaller extent from dissociation of  $\text{Cl}_2$ .<sup>118</sup>



Hence, Cl emission intensity depends on both Cl and  $\text{Cl}_2$  number density. O emission behaves similarly, originating from both O and  $\text{O}_2$  in oxygen plasmas. The dissociative excitation of O emission is relatively much more important in  $\text{O}_2$  plasmas compared to Cl in  $\text{Cl}_2$  plasmas because of the stronger  $\text{O}_2$  bond relative to  $\text{Cl}_2$ , and generally higher electron temperatures in  $\text{O}_2$  plasmas.<sup>119</sup> If the plasma contains large fractions of  $\text{SiCl}_x$  etching products and not much Cl, then production of Cl emission from dissociative excitation of  $\text{SiCl}_x$  may also need to be included, but the strong  $\text{SiCl}_x$  bond should make this a minor process, except for extreme conditions.

Emission from  $\text{SiCl}_x$  indicates that these species are present in the plasma. Of course, some of these emissions could be the result of dissociative excitation of higher Si-chlorides, such as  $\text{SiCl}_3 + e \rightarrow \text{SiCl}_2^* + \text{Cl} + e$ . This does not matter for endpoint detection but does prevent OES from providing anything more than a qualitative indicator of ground state number densities of these species. It is much better to detect these species directly by UV absorption spectroscopy<sup>120</sup> or mass spectrometry.<sup>121,122</sup>

Weak emission from  $\text{Cl}^+$  in the UV and visible regions is also observed in high-density  $\text{Cl}_2$  plasma emission spectra, as shown in the expanded spectrum in Fig. 11 (blue, upper trace). Emission from  $\text{Cl}_2^+$  between 400 and 550 nm can also be found in the spectrum at high power and low pressure in Fig. 11 (blue, upper trace), but it is relatively much more prominent in lower density plasmas, as shown in the example in Fig. 11 (black, bottom trace). Electronically excited ions such as  $\text{Cl}_2^+$  can be produced by a one-step electron impact excitation from the ground state of neutral  $\text{Cl}_2$

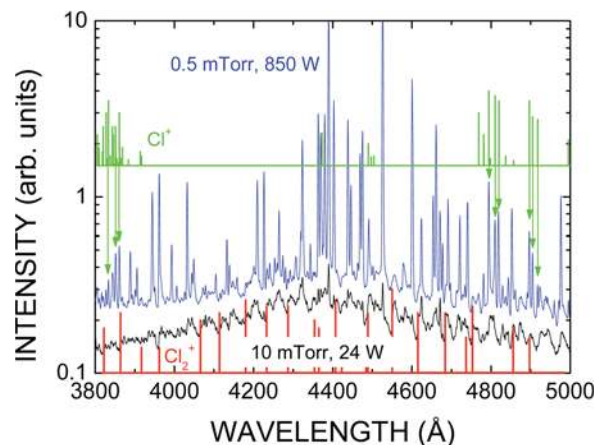
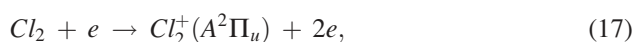
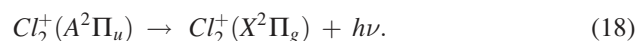


FIG. 11. (Color online) Low power (24 W)–high pressure (10 mTorr), and high power (850 W)–low pressure (0.5 mTorr)  $\text{Cl}_2$  ICPs.  $\text{Cl}_2^+$  bandhead and  $\text{Cl}^+$  line positions and intensities are represented by the “stick spectra” at the top and bottom.



If little emission is detected from  $\text{Cl}_2^+$  and strong emission is observed from  $\text{Cl}^+$ , then  $\text{Cl}^+$  is likely the dominant ion, as it was at 0.5 mTorr and 850 W. When the converse is true, then  $\text{Cl}_2^+$  is the dominant positive ion, as it is in the example of 10 mTorr and 24 W. This is also consistent with direct measurements of  $\text{Cl}_2^+$  by LIF in a  $\text{Cl}_2$  plasma: when the reactor was operated in a low-power CCP mode,  $\text{Cl}_2^+$  emission was relatively strong,  $\text{Cl}^+$  emission was weak and LIF measurements taken together with Langmuir probe measurements showed that  $\text{Cl}_2^+$  was the dominant ion, while in the high-power ICP mode,  $\text{Cl}^+$  emission was strong and  $\text{Cl}_2^+$  was barely detectable in either emission or by LIF, hence the dominant ion was  $\text{Cl}^+$ .<sup>123,124</sup>

A sample emission spectrum of a fluorocarbon plasma ( $\text{C}_2\text{F}_6$ ) during etching of  $\text{SiO}_2$  and Si is shown in Fig. 12. The spectrum contains features that can be assigned to  $\text{C}_2$ , Si, SiF, and C. In addition, emission from F was found in the

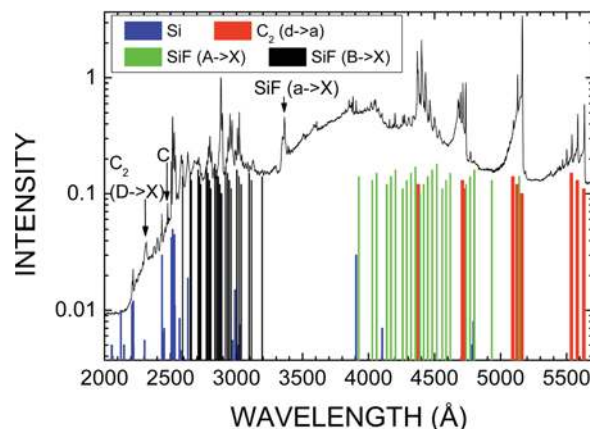


FIG. 12. (Color online) Emission spectrum of a  $\text{C}_2\text{F}_6$  inductively coupled plasma during etching of  $\text{SiO}_2$  and Si. The “stick” spectra indicate the positions of known emissions from Si, SiF, C, and  $\text{C}_2$ . The heights of the “sticks” are of no significance.



red/near-infrared region (not shown). Because of the presence of a heated “silicon roof” in the reactor used to obtain this spectrum, the plasma was depleted of F atoms, hence fluorine is contained in  $\text{SiF}_x$  species and not as much is available to form  $\text{CF}_2$  and  $\text{CF}_3$ . Emission from these species tends to dominate lower density plasmas. In high density fluorocarbon plasmas depleted of fluorine, the radical  $\text{C}_2$  appears to be a dominant species. The polymer layer that deposits under these conditions is depleted in fluorine.

**b. Actinometry.** If an excited state ( $k$ ) of species  $X$  is populated solely by electron impact excitation from its ground state ( $i$ ) then its absolute ground state number density ( $n_X$ ) can, in principle, be obtained from the intensity ( $I_{X,i,j,k}$ ) of emission at wavelength  $\lambda_{X,j,k}$  accompanying the transition  $X_k \rightarrow X_j$ , and the relationship<sup>5</sup>

$$I_{X,i,j,k} = 4\pi\alpha(\lambda_{X,j,k}) n_X Q_{X,k} b_{X,j,k} \int_0^\infty \sigma_{X,i,k}(v) v^3 f_e(v) dv, \quad (19)$$

where  $\alpha(\lambda_{X,j,k})$  is the spectrometer sensitivity at  $\lambda_{X,j,k}$ ,  $\sigma_{X,i,k}(v)$  is the cross section at electron speed  $v$  for electron impact excitation of  $X_k$  from  $X_i$ ,  $f_e(v)$  is the electron speed distribution function  $4\pi v^2 f_e(v) dv$  (the number of electrons with speeds between  $v$  and  $v + dv$ ),  $Q_{X,k} = \tau^{-1}/(\tau^{-1} + k_q P)$  is the quantum yield for emission by  $X_k$ , where  $\tau$  and  $k_q$  are the radiative lifetime and quenching rate constant for  $X_k$  by all species at total pressure  $P$ , and  $b_{X,j,k}$  is the branching ratio for the transition  $X_k \rightarrow X_j$ .

The electron speed distribution and the proportionality constant are difficult to determine. Consequently rare gas actinometry is often used to convert emission intensities into quantitative, relative number densities. This technique was first applied in plasmas by Coburn and Chen.<sup>125</sup> In this approach, a small amount of a rare gas,  $A$ , with an excited state  $A_k$  that has an energy close to that of  $X_k$  is added to the discharge. The energy levels of the rare gases span the range from 9.7 eV for Xe to 23 eV for He. Assuming that rare gas emissions are caused solely by electron impact excitation of the ground state, an expression analogous to Eq. (19) relates emission from the rare gas to its known number density

$$I_{A,i,j,k} = 4\pi\alpha(\lambda_{A,j,k}) n_A Q_{A,k} b_{A,j,k} \int_0^\infty \sigma_{A,i,k}(v) v^3 f_e(v) dv. \quad (20)$$

It is usually assumed that the relative energy dependence of the cross section for electron impact excitation of the species of interest is the same as that of the rare gas, i.e.,  $\sigma_{A,i,k}(v) \propto \sigma_{X,i,k}(v)$  at any  $v$ . Consequently, the  $n_X$  can be simply expressed as

$$n_X = a_{X,A} n_A (I_{X,i,j,k}/I_{A,i,j,k}), \quad (21)$$

where  $a_{X,A}$  is a proportionality constant. Relative densities of atoms (F, Cl, H, and O), and small molecules ( $\text{Cl}_2$ , CF,  $\text{CF}_2$ ,

$\text{BCl}$ ) have been determined in a wide variety of plasmas by this method. In a few cases, absolute number densities have also been measured through several calibration methods.

Actinometry is a simple method that, when carefully applied, can provide valuable quantitative measurements of species concentrations in commercial plasmas with limited optical access. Perhaps the most common and most reliable use of actinometry is for measurement of F atom densities in fluorine-containing plasmas. Fluorine atom actinometry, using the 750.4 nm line of Ar, was first reported by Coburn and Chen for  $\text{CF}_4/\text{O}_2$  plasmas<sup>125</sup> and was later used by many researchers, including d'Agostino *et al.*<sup>126,127</sup> in  $\text{CF}_4/\text{O}_2$  and  $\text{SF}_6/\text{O}_2$  plasmas, Donnelly *et al.*<sup>128</sup> in  $\text{CF}_4/\text{O}_2$  and  $\text{NF}_3/\text{Ar}$  plasmas, Schabel *et al.*<sup>129</sup> in  $\text{C}_2\text{F}_6/\text{Ar}$  ICPs, and Karakas *et al.*<sup>130</sup> in  $\text{CH}_3\text{F}/\text{O}_2$  plasmas.

Atomic oxygen emission actinometry has also been reported,<sup>131,132</sup> with verification by LIF.<sup>132</sup> When divided by Ar emission at 750.4 nm, it was found that O emission at 844.6 nm ( $3p^3P \rightarrow 3s^3S$ ), tracked  $n_O$  reasonably well, while O emission at 777.4 nm ( $3p^5P \rightarrow 3s^5S$ ) did not. The latter was attributed to dissociative excitation of  $\text{O}_2$ , as verified by linewidth measurements. As mentioned above, the O 844.6 nm line also suffers from dissociative excitation of  $\text{O}_2$ , even in a high density ICP.<sup>119</sup> This is because O atom densities are usually less than those of  $\text{O}_2$  (if oxygen is not being largely consumed by reactions with materials or feed gas components), a result of the large  $\text{O}_2$  bond strength (5.11 eV).

Actinometry has also been widely used for measurement of relative number densities of Cl-atoms. Often the Ar 750.4 nm line is used, even though it is not such a good energy match for the Cl emitting levels. Using the Xe 828.0 or 834.7 nm line provides a much better energy match to the Cl emitting levels, and more consistent tracking of Cl number density.<sup>118</sup> In addition, dissociative excitation of  $\text{Cl}_2$  [reaction (16)] is a source of Cl emission at low  $n_{\text{Cl}}$ . Direct evidence for this was observed in  $\text{Cl}_2$  plasmas.<sup>118</sup>

### 3. Surface techniques

Analysis of plasma-exposed surfaces can be carried out in a number of ways. It is far easier to perform the analysis by moving the sample (usually under vacuum) to a chamber equipped with a standard analysis method such as XPS. This method is discussed in some detail in the next section. In some cases, it is of interest to analyze surfaces while they are immersed in the plasma. Several approaches have been demonstrated. Aydil and co-workers have used total internal reflection, Fourier-transform infrared absorption to monitor adsorbates on a GaAs sample mounted near the reactor wall.<sup>133,134</sup> This technique provides quantitative analysis for many species with monolayer detection, but requires IR-transparent substrates and relatively long times. In the laser desorption-laser induced fluorescence (LD-LIF) technique, a pulsed laser heats the surface, causing desorption of adsorbates that are detected by LIF, excited by the tail of the same laser pulse.<sup>135–139</sup> This method has very high sensitivity for some species (e.g., <1% of a monolayer of SiCl and SiBr) and fast (ns) time response, but the interpretation is more

difficult and it is limited to a relatively few species, and thermally robust surfaces. Another approach, called the “spinning wall” method inserts a cylindrical substrate into the reactor wall.<sup>109,121,122,140–146</sup> Part of the cylinder is in the plasma while another section is in a differentially pumped chamber with a mass spectrometer and Auger electron spectrometer (AES) facing the surface. By rapidly rotating the substrate, portions of the surface that were in the plasma as little as 1 ms ago can be diagnosed. Weakly bound species and heterogeneous reaction products can be observed with the mass spectrometer and strongly bound species can be detected by AES.

*a. Vacuum-transfer XPS.* Electron spectroscopy techniques such as XPS and Auger electron spectroscopy are extremely useful for quantitative identification of species on surfaces, and especially for XPS, chemical bonding, and structural information. The plasma environment does not allow these techniques to be used in real time; therefore, analysis of plasma-etched materials is carried out after etching by transferring the sample to a separate analysis chamber. If this is done by bringing the sample out into the air, then the surface layer will be oxidized in most cases. Of course, characterization of air-exposed wafers is often of interest for long-term reliability reasons, but if studying the plasma-surface interaction is the prime motivation, then air exposure must be avoided.

Several research groups have constructed integrated plasma etching/surface analysis machines that allow samples to be moved under vacuum from the etching chamber to the analysis chamber.<sup>147–154</sup> This is usually done by moving the sample through a loadlock chamber with linear transfer devices. One such system is shown in Fig. 13. One obvious question is how does the surface change between the instant when the plasma is extinguished and when analysis begins, a delay of at least several minutes after etching? Chemisorbed

species will not desorb, but physisorbed species present at low coverages during etching will react and/or desorb before analysis can be carried out. Weakly adsorbed species, though often important for etching reactions, are not expected to be present at high concentrations. The chemisorbed layer is also very important, since ion bombardment causes reactions in this layer that lead to etching. The vacuum transfer surface analysis method provides valuable insights into the nature of this layer, which is stable and long lived in the absence of air or ion bombardment.

Si etching in F and Cl-containing plasmas has been studied in some detail. Low resolution spectra of unpatterned Si after etching in a chlorine ICP are shown in Fig. 14. Si(2p), Si(2s), Cl(2p), and Cl(2s) peaks are readily identified, along with O(1s) and C(1s) contamination in some cases. Loss features at multiples of the bulk Si plasmon resonance are also observed. The plasmon features to the high binding energy side of the Cl(2p) and Cl(2s) peaks indicate that some Cl has penetrated rather deep into the Si. When the “take-off” angle is small (the angle between the electron collection direction and the surface), XPS is more surface sensitive. The Cl peaks become more intense relative to Si, indicating that Cl is near the surface. From further analysis of the take-off angle dependence of the intensities in the spectra in Fig. 14, the thickness of the chlorinated layer can be derived ( $\sim 2$  nm). This subject is expanded upon below in the section on the nature of the Si surface layer.

### C. Mechanistic studies of etching of selected materials

All anisotropic etching processes involve one (or both) of the above mechanisms. In most cases, no reaction takes place between the neutrals and the material to be etched, despite the fact that a volatile product can form and the reaction between the atomic etchants (e.g., Cl atoms) and the substrate (e.g., Si) is exothermic to produce the gaseous product ( $\text{SiCl}_4$ ). In this case, energetic ion bombardment speeds up the rate of reactions that generate gaseous products and anisotropic etching occurs. In a few cases, such as

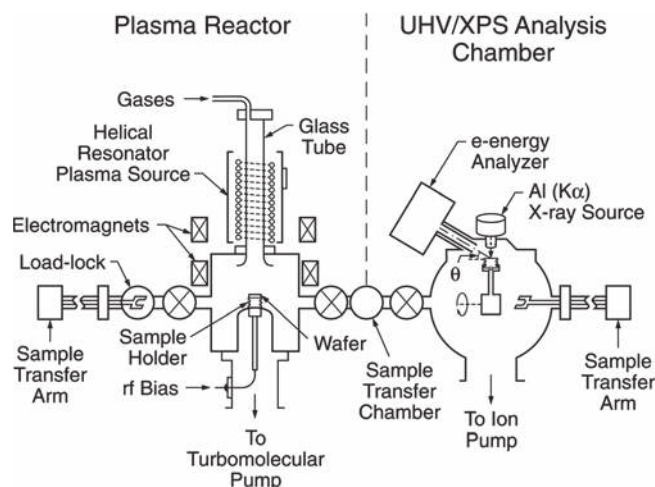


FIG. 13. Schematic of an inductively coupled (helical resonator) plasma reactor attached to a sample transfer chamber that is connected to an ultrahigh vacuum (UHV) chamber equipped with XPS. The take-off angle  $\theta$  is the angle between the axis of the photoelectron collection lens and the wafer plane (Ref. 115).

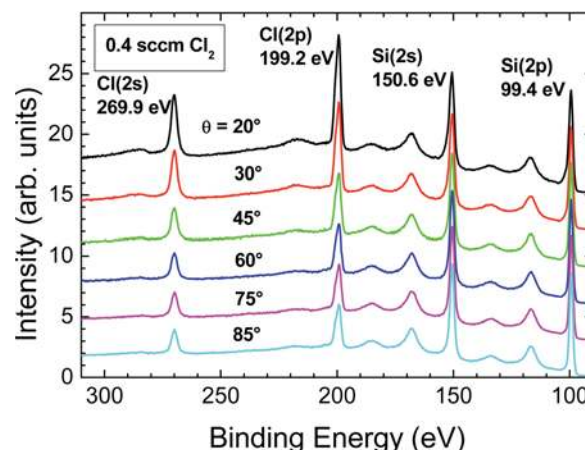


FIG. 14. (Color online) Low resolution XPS spectra as a function of takeoff angle for blanket Si etched in a high density  $\text{Cl}_2$  ICP, under conditions described in a previous publication (Ref. 115).

in etching of Al in a chlorine-containing plasma, spontaneous fast etching occurs in the absence of ion bombardment and this process is stopped by depositing a very thin layer on the sidewalls. This protective layer is sputtered away faster than it can deposit on horizontal surfaces, allowing anisotropic etching to be obtained. Selected examples are now presented in some detail.

### 1. Si etching in halogen-containing plasmas

Coburn and Winters were the first to show conclusively that the etching rate of a material (Si), normally slow when exposed to either neutral etchants ( $\text{XeF}_2$ ) or ion bombardment ( $\text{Ar}^+$ ), was greatly accelerated in the simultaneous exposure to both.<sup>155</sup> This classic experiment was carried out with beams of  $\text{XeF}_2$  and  $\text{Ar}^+$  in a high-vacuum chamber, thus avoiding the complex plasma environment. Many variations on this experiment have contributed to our understanding of ion-assisted etching processes. A summary of some of this work is presented in Table I of Vitale *et al.*<sup>156</sup>

Early work by the IBM group focused on ion-enhanced etching of Si by  $\text{XeF}_2$ , partly because etching of Si in  $\text{CF}_4$ -containing plasmas was one of the first plasma etching processes developed. F-atoms are the active etchant for Si in this plasma, as well as in  $\text{SF}_6$  plasmas that are used to etch Si at faster rates. Most anisotropic etching of silicon is carried out in Cl and/or Br-containing plasmas, however, because isotropic chemical etching by Cl and Br is much slower than etching by F-atoms. Most, but not all of the technologically relevant combinations of ions ( $\text{Cl}_2^+$ ,  $\text{Cl}^+$ , and  $\text{Ar}^+$ ) and neutrals ( $\text{Cl}_2$  and Cl) have been investigated.

Isotropic etching of Si can also occur as a result of chemical reactions with F, Cl, or Br atoms to form volatile products. These processes are described by the reaction probabilities,  $\epsilon_{X(S)}$ , defined above. Etching rates and reaction probabilities for Si by F atoms have been reported by Flamm *et al.*<sup>99</sup> Values for Cl atoms have been given by Ogrzylo *et al.*<sup>100</sup> and Walker and Ogrzylo.<sup>157</sup> These researchers also measured reaction coefficients for Br atoms with Si.<sup>158</sup> Using a density of 2.33 for Si, and assuming that the etching products are  $\text{SiF}_4$  for F, and an equal mixture of the di-halide and tetra-halide (so  $x=3$ ) for Cl and Br, reaction probabilities from these studies are reproduced in Fig. 15 as a function of substrate temperature.

Several general conclusions can be drawn from the data in Fig. 15. At room temperature, chemical etching of Si by halogen atoms follows the trend  $\text{F} > \text{Cl} > \text{Br}$ , expected from the Si-halogen bond strengths (140, 90, and 80 kcal/mol, respectively). The dopant type and level strongly affects the Cl and Br reactivity. Highly doped n-type Si ( $\text{n}^+\text{-Si}$ ) etches much faster than lightly doped n-type or p-type Si. This dopant dependence has been attributed to the shift in the Fermi level, making formation of  $\text{Cl}^-$  favored.<sup>100</sup>  $\text{Cl}^-$  is drawn through the  $\text{SiCl}_x$  surface layer by the resulting electric field. The formation of  $\text{F}^-$  has also been invoked to explain the smaller enhancement in the etching of  $\text{n}^+\text{-Si}$  by F-atoms.<sup>159</sup> Isotropic etching of Si by F is fast enough to be a concern for anisotropic etching in high density plasmas that generate

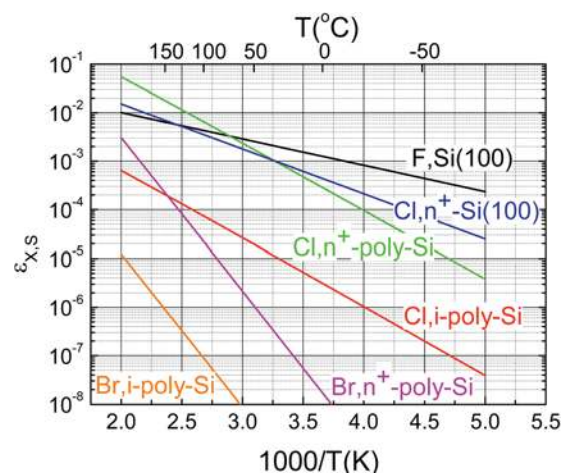


FIG. 15. (Color online) Reactions coefficients for F, Cl, and Br atoms with Si, generated from data and expressions given in published studies (Refs. 99, 100, 157, and 158).

large percentages of F atoms (e.g.,  $\text{CF}_4/\text{O}_2$ ,  $\text{SF}_6/\text{O}_2$ , or  $\text{NF}_3$ ). To slow isotropic etching by F atoms, it is often necessary to add a species that coats the sidewall and slows lateral etching. Thermally activated isotropic etching can also be slowed, relative to ion assisted etching, by cooling the substrate. At low partial pressures of Cl atoms ( $< 10$  mTorr), isotropic etching by Cl and Br atoms is very slow for all levels of p-type, intrinsic, and lightly to moderately doped n-type Si. Highly doped n-type Si will exhibit a large degree of undercutting at Cl partial pressures of only a few mTorr. Under these cases, some sidewall protection scheme is necessary.

For anisotropic etching, the ion-assisted etching rate must greatly exceed the etching rate by neutral species. The fundamental parameter of interest is the ion-assisted etching yield, defined as the number of substrate atoms or molecules removed per incident ion. Figure 16 presents measurements by Levinson *et al.*<sup>160</sup> of Si yields as a function of the square root of ion energy for  $\text{Cl}_2$  and either  $\text{Ar}^+$  or  $\text{Cl}_2^+$ , carried out in the limit of a high neutral-to-ion flux ratio. A simple linear square root relationship was found, with a threshold energy below which ion assisted etching ceases, as has been observed in many etching investigations.<sup>161</sup> At higher energies, the nature of the ion (reactive  $\text{Cl}_2^+$  versus unreactive  $\text{Ar}^+$ ) plays only a small role in determining the yield. For example, near 500 eV, the yields are only  $\sim 5\%$  higher for  $\text{Cl}_2^+/\text{Cl}_2$  than for  $\text{Ar}^+/\text{Cl}_2$ , while at 60 eV, the yields for  $\text{Cl}_2^+/\text{Cl}_2$  are  $\sim 50\%$  higher than for  $\text{Ar}^+/\text{Cl}_2$ .<sup>160</sup> Yields extrapolate to 0 at about 25 and 35 eV for  $\text{Cl}_2^+/\text{Cl}_2$  and  $\text{Ar}^+/\text{Cl}_2$ , respectively; hence, near threshold, the nature of the ion becomes important. The  $\text{Ar}^+/\text{Cl}_2$  yield at 100 eV is in good agreement with the value of 0.7 reported by Chang *et al.*<sup>162</sup> for the same conditions.

Yields have been measured as a function of the  $\text{Ar}^+$ -to- $\text{Cl}_2$  flux ratio (Fig. 17) and have been found to saturate at a low ratio, indicating ion-flux-limited etching and a small sticking coefficient by  $\text{Cl}_2$  on the ion-bombarded/chlorinated surface. At high ion-to-neutral flux ratios (not usually obtainable in plasma etching processes unless the halogen fraction in the feed gas is very low), the surface is mostly free of



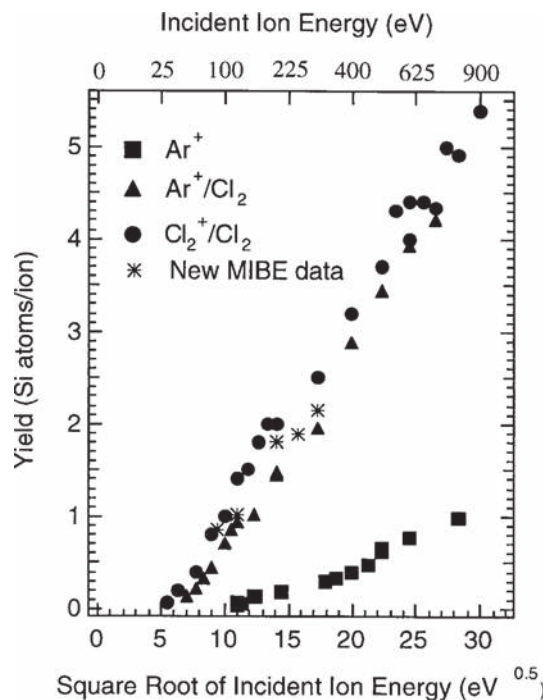


FIG. 16. Si ion-assisted etching yields as a function of the square root of ion energy, measured with high neutral-to-ion beam flux ratios. Reproduced with permission from Levinson *et al.*, J. Vac. Sci. Technol. A **15**, 1902 (1997). Copyright 1997, American Vacuum Society.

adsorbed Cl and the sticking coefficient is much higher [0.5 (Ref. 163)].

Argon ion-assisted etching by Cl-atoms has also been reported. Two to five times higher ion yields are found when the surface is chlorinated with Cl instead of Cl<sub>2</sub>.<sup>162</sup> The enhancement for Cl vs Cl<sub>2</sub> is smaller (about two-fold) with Cl<sup>+</sup>, compared to Ar<sup>+</sup>.<sup>164</sup> These results indicate that when ion-bombarded Si is exposed to Cl, it forms a more heavily chlorinated surface layer than when it is instead exposed to Cl<sub>2</sub>, but that some of the Cl comes from Cl<sup>+</sup> (and presumably Cl<sub>2</sub><sup>+</sup>) in a chlorine plasma. This results agrees with LD-LIF studies (see Fig. 18), where the Cl areal density on Si exposed to a chlorine ICP was about twice that on Si exposed to Cl<sub>2</sub> gas with the plasma off.

Vitale *et al.*<sup>156</sup> and Jin *et al.*<sup>165</sup> have also carried out measurements in a plasma beam system. This system does not produce single reactive neutral or ion species, but instead provides a mix of species that would be similar to that in a plasma. Their etching yields as a function of the square root of ion energy for F<sub>2</sub>, Cl<sub>2</sub>, Br<sub>2</sub>, and HBr plasmas are reproduced in Fig. 19. They find that the number of Si atoms removed per ion has a similar dependence on ion energy above a threshold energy,  $E_{th}$ . F atoms from the F<sub>2</sub> plasma will rapidly etch Si in the absence of ion bombardment;<sup>99</sup> hence,  $E_{th}$  for the F<sub>2</sub> plasma beam is near zero. They find threshold energies for Cl<sub>2</sub> and HBr plasma beams are ~5–10 eV, while  $E_{th}$  for Br<sub>2</sub> appears to be much higher (44 eV).  $E_{th}$  for the Cl<sub>2</sub> plasma beam is lower than that reported for dual Cl/Cl<sup>+</sup> beams (~16 eV),<sup>164</sup> as well as for Cl<sub>2</sub>/Cl<sub>2</sub><sup>+</sup> beams.<sup>166</sup>

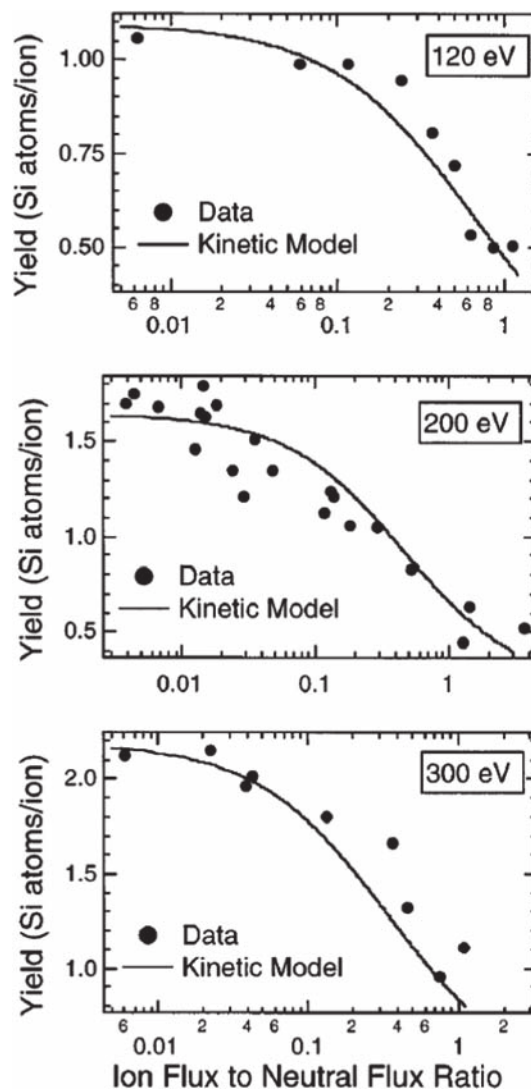


FIG. 17. Si ion-assisted etching yields as a function of ion-to-neutral flux ratio, measured at three ion energies. Reproduced with permission from Levinson *et al.*, J. Vac. Sci. Technol. A **15**, 1902 (1997). Copyright 1997, American Vacuum Society.

The apparently low  $E_{th}$  values for the Cl<sub>2</sub> beam in the experiments by Vitale *et al.*,<sup>156</sup> derived by extrapolating from ion energies at which appreciable etching is observed to zero etching rate, could be a result of etching at ion energies below  $E_{th}$ , caused by low energy ions, electrons, photons, and/or Cl atoms. Recently, Shin *et al.*<sup>167</sup> reported a similar ion energy dependence for p-type single crystal Si(100) etching in a Cl<sub>2</sub> plasma at ion energies above  $E_{th}$ . These measurements are reproduced in Fig. 20. The substantial etching rate below the energy threshold for ion-assisted etching was unexpected, since it has been reported that p-type Si(100) is not etched by Cl atoms.<sup>100,157</sup> Indeed, the lack of undercutting of masked samples also indicates that Cl atoms are not responsible for etching below  $E_{th}$ . Instead, it was concluded in that work that this subthreshold etching was induced by vacuum ultraviolet illumination of the surface in the presence of gaseous Cl and Cl<sub>2</sub>.<sup>167</sup>

Above the photo-assisted etching component (the dashed line in Fig. 20), an ion-assisted etching threshold of 18 eV is

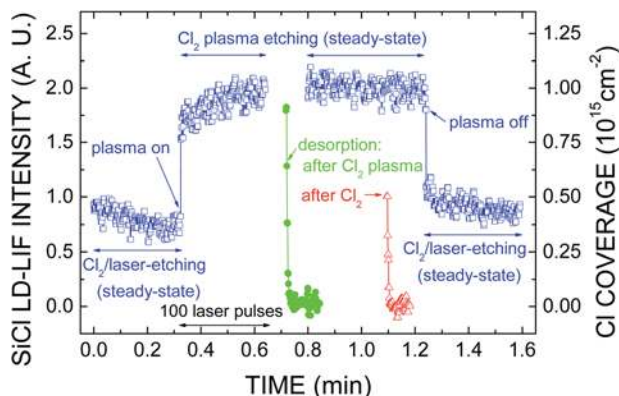


FIG. 18. (Color online) LD-LIF measurements of intensity of laser-desorbed SiCl (2924 Å) as a function of time during etching of Si(100) in a chlorine helical resonator plasma (Ref. 135). The signal is proportional to Cl coverage. The open squares show steady-state laser-induced etching of Si by Cl<sub>2</sub>, followed by etching as the plasma suddenly turns on (at 0.33 min) and off (at 1.25 min). Pressure = 2.2 mTorr, flow rate = 5.5 sccm, power = 280 W, substrate bias voltage = -34 V dc, laser repetition rate = 10 Hz, and laser fluence = 0.50 J/cm<sup>2</sup>. The solid symbols show the time dependence of desorbed SiCl (and Cl coverage) after chlorination with the plasma off (Δ) and on (•), and subsequent pumpdown. The times for these last two traces were offset so that they were near the respective steady-state traces.

found, with a second threshold at about 26 eV. The lower value is very close to  $E_{th} = 16$  eV for etching with co-impinging Cl and Cl<sup>+</sup> beams,<sup>164</sup> while the upper value matches  $E_{th} = 16$  eV reported for Cl<sub>2</sub> and Cl<sub>2</sub><sup>+</sup> beams.<sup>160</sup> Since the plasma is a mixture of Cl, Cl<sub>2</sub>, Cl<sub>2</sub><sup>+</sup>, and Cl<sub>2</sub><sup>+</sup>, the dual thresholds seem reasonable. If one were to extrapolate to zero etching rate, then apparent thresholds of 2.8 and 18 eV are obtained. Depending on the amount of VUV light reaching the sample in the experiments by Vitale *et al.*<sup>156</sup> and Jin *et al.*,<sup>165</sup> the low  $E_{th}$  values could easily be explained by this effect.

As discussed above, Si etching processes are rarely carried out in pure Cl<sub>2</sub> or Cl<sub>2</sub>/Ar plasmas because of the formation of microtrenches.<sup>168</sup> It has been found that adding HBr to Cl<sub>2</sub> plasmas converts sharp microtrenches into very broad, shallow ones.<sup>168</sup> This is believed to be due to a change from specular reflection of positive ions from a chlorinated sidewall in a chlorine plasma to a broad-angle reflection of ions from sidewalls exposed to an HBr-containing plasma.<sup>169</sup> It

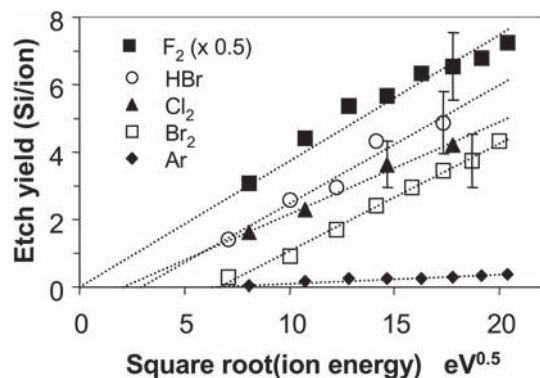


FIG. 19. Si etching rate vs the square root of ion energy for a plasma beam that contained a mix of ions and radicals, from Sawin and co-workers (Refs. 156 and 165).

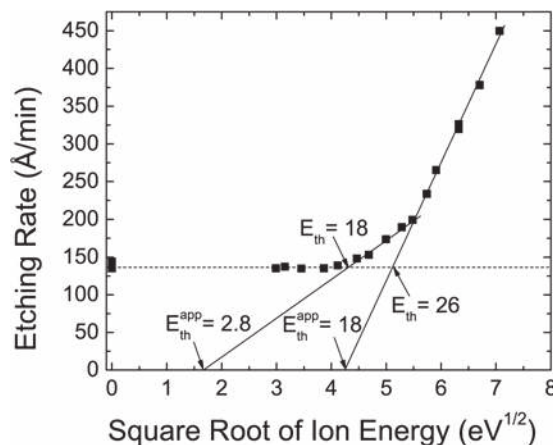


FIG. 20. Si(100) etching rates in a 50 mTorr 1%Cl<sub>2</sub>/Ar pulsed plasma, at 110 W average power, 10 kHz and 20% duty cycle [adapted from Shin *et al.* (Ref. 167)]. Synchronous bias in the afterglow from 70–98 μs produced a controlled, monoenergetic ion flux for etching. Etching below the apparent ion-assisted threshold at 18 or 26 eV was attributed to photon-assisted etching (Ref. 167).

was further proposed that the sidewalls may be rougher in HBr plasmas than in Cl<sub>2</sub> plasmas. The enhanced roughness of HBr plasma-exposed surfaces could be due to etching by H atoms. It could also be that surfaces become contaminated with small amounts of carbon in HBr-containing plasmas, while surfaces exposed to chlorine-containing plasmas are carbon-free. This carbon could mask small regions, causing uneven etching. While sidewall etching is hardly detectable in anisotropic etching processes, the roughness need not be substantial to cause glancing angle of incidence ions to be scattered over a wide angle, as is found in HBr-containing plasmas. Simulations by Helmer and Graves<sup>169,170</sup> indicate that 2 nm roughness is sufficient.

*a. Nature of the Si surface layer.* The surface layer that forms during Si etching in halogen-containing plasmas has been studied by the many experimental techniques discussed above and below, as well as in beam experiments designed to simulate the plasma environment, and by simulations, including molecular dynamics methods.<sup>171</sup> Of the experimental methods, the vacuum-transfer XPS method described above provides many important details. XPS with vacuum sample transfer has been used to determine Cl coverages and SiCl<sub>x</sub> stoichiometry on blanket, as well as patterned surfaces. From low resolution spectra such as those in Fig. 14, Si and Cl 2s and 2p core level features and plasmon losses associated with both the Si and Cl can be identified, and it can be concluded that the surface layer contains the equivalent of a couple of monolayers of chlorine.

The stoichiometry of the halogenated layer can be determined from high resolution Si(2p) spectra. An example of a Si(2p) spectrum, with background and the J = 1/2 spin-orbit component removed, is shown in Fig. 21.<sup>115</sup> SiCl, SiCl<sub>2</sub>, and SiCl<sub>3</sub> were identified at 100.2, 101.2, and 102.3 eV, respectively, in good agreement with binding energies reported by Durban *et al.*<sup>172</sup> in synchrotron photoemission studies of the chlorination of Si(111) with Cl<sub>2</sub>. The SiCl<sub>x</sub> peaks were much

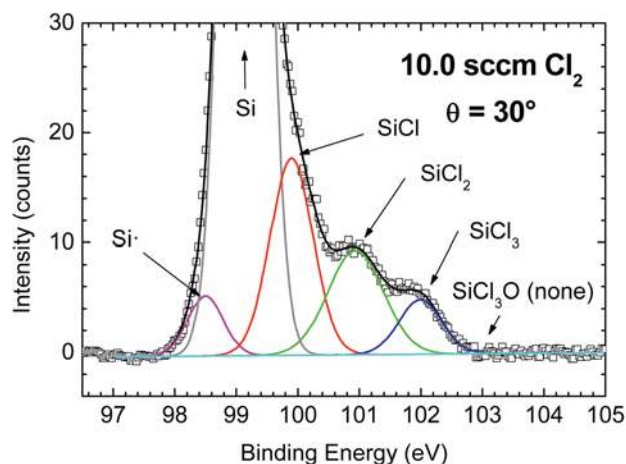


FIG. 21. (Color online) High-resolution Si ( $2p_{3/2}$ ) XPS spectrum acquired at  $\theta = 30^\circ$  for Si etched in a 10.0 sccm  $\text{Cl}_2$  plasma. The best fit from a nonlinear least squares model (solid line) includes five peaks (broken lines) assigned to: Si- (98.50 eV, 0.70 eV FWHM), Si bulk (99.14 eV, 0.70 eV FWHM), SiCl (99.90 eV, 0.84 eV FWHM),  $\text{SiCl}_2$  (100.94 eV, 1.10 eV FWHM), and  $\text{SiCl}_3$  (101.99 eV, 0.84 eV FWHM) components present in the chlorinated layer that is formed during etching (Ref. 115).

broader than the 0.6 eV resolution of the XPS instrument (especially for  $\text{SiCl}_2$ ), and hence cannot be attributed to resolution but are instead an indication of the high degree of disorder in the  $\text{SiCl}_x$  layer formed during plasma etching.

An additional, weak peak appearing as a shoulder on the low binding energy side of the at Si- (Si bound to 3 Si and one dangling bond) peak was attributed to Si. Its binding energy was found to be the same (98.8 eV) as that measured for Si after  $\text{Ar}^+$  sputtering, providing supports for the assignment. From an analysis of spectra at various take-off angles for different plasma conditions, the relative coverages Si, SiCl,  $\text{SiCl}_2$ , and  $\text{SiCl}_3$  were deduced, as well as the overall thickness of the chlorinated silicon layer.<sup>115,173</sup>

Measurements of Cl coverage as a function of ion energy ( $\text{Cl}_2^+$  and/or  $\text{Cl}^+$  or  $\text{Ar}^+$ ) from both plasma and beam experiments by several groups are summarized in Fig. 22, where the areal density of Cl determined by XPS (Ref. 173) and LD-LIF are plotted as a function of the square root of ion energy. Increasing ion energy increases the Cl coverage during Si etching, for ion energies less than 300 eV. Coburn<sup>174</sup> also found that ion bombardment increases chlorine coverage on Si (two “+” points in Fig. 22). The chlorine uptake on Si exposed to simultaneous  $\text{Ar}^+$  (1 keV) and  $\text{Cl}_2$  beams is  $\sim 3$  times larger than with just the  $\text{Cl}_2$  beam alone, whether the Si surface was an ordered, annealed surface, or one amorphized by ion bombardment prior to exposure to the  $\text{Cl}_2$  beam. The factor of 3 is less than expected from an extrapolation of the XPS and LD-LIF data in Fig. 22, perhaps because of the added Cl supplied by  $\text{Cl}^+$  and  $\text{Cl}_2^+$ . It could also indicate that the increase in Cl coverage saturates with increasing  $\text{Ar}^+$  energy. Such a saturation was observed in the  $\text{Cl}_2/\text{Ar}^+$  beam studies of Barker *et al.*<sup>175</sup> when the  $\text{Ar}^+$  energy was varied between 400 and 900 eV (solid circles included in Fig. 22).

Since the beam experiments by Coburn showed that simultaneous  $\text{Ar}^+$  and  $\text{Cl}_2$  exposure creates a more highly

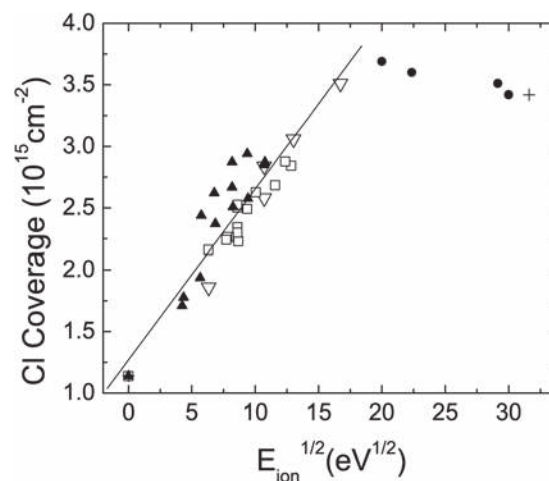


FIG. 22. Cl coverage on Si(100), during and after etching in high density  $\text{Cl}_2$  plasmas ( $\nabla$ ,  $\square$ ,  $\blacktriangle$ ), and for etching with simultaneous  $\text{Cl}_2$  and  $\text{Ar}^+$  beams ( $\bullet$ ,  $+$ ), expressed as areal density vs the square root of ion energy. Included are XPS (Ref. 173) ( $\nabla$ ) and LD-LIF measurements in a helical resonator plasma (Ref. 135) ( $\square$ ), as well as LD-LIF measurements in a flat coil ICP reactor (Ref. 138) ( $\blacktriangle$ ). XPS measurements are absolute. LD-LIF measurements and the beam measurements by Coburn (Ref. 174) ( $+$ ) are normalized to the XPS values. The beam measurements by Barker *et al.* (Ref. 175) ( $\bullet$ ) are normalized to Coburn's beam result at 1 keV. The points at zero ion energy correspond to uptake by laser-annealed Si(100) with the plasma off. The line is a linear least squares fit to all of the  $\text{Cl}_2$  plasma data.

chlorinated layer than sequential  $\text{Ar}^+$  followed by  $\text{Cl}_2$  exposures, the enhanced chlorination was attributed to a knock-on process, rather than an increase in binding sights by ion bombardment. In a knock-on process, short range ion impact on adsorbates causes the adsorbates to be implanted into the subsurface region. This mechanism was also proposed by Barrish *et al.*<sup>176</sup> for Si etching with  $\text{Cl}_2$  and  $\text{Ar}^+$  beams. While knock-on is a well known effect that no doubt plays some role in subsurface chlorination, ion-induced creation of added adsorption sites is not necessarily ruled out by the  $\text{Cl}_2/\text{Ar}^+$  beam experiments. Consider the differences in the types of amorphous layers created by  $\text{Ar}^+$  versus  $\text{Cl}_2^+$  bombardment.  $\text{Ar}^+$  bombardment breaks bonds during the collision cascade, but most of these broken bonds reform. The result is a fairly dense lattice with few voids.  $\text{Cl}^+$  and  $\text{Cl}_2^+$  bombardment also breaks bonds, but in addition prevents some of the Si-Si bonds from reforming through formation of mainly SiCl. This favors formation of a much more open surface structure than  $\text{Ar}^+$  amorphized Si.

The strongest evidence for this comes from molecular dynamics simulations by Graves and co-workers.<sup>104,177</sup> Some of these calculations are reproduced in Fig. 23.<sup>104</sup> Starting with a Si(100) surface, they found that bombardment with 50 eV  $\text{Ar}^+$  created a disordered but dense damaged layer, while bombardment with  $\text{Cl}^+$  at the same energy resulted in a highly disordered, roughened layer with small subsurface voids. Such a layer contains more binding sites for adsorption by neutral Cl and  $\text{Cl}_2$ .

Si etching mechanisms in HBr-containing and HBr/ $\text{Cl}_2$ -containing plasmas have also been investigated. Horizontal surfaces take up Br and Cl roughly in proportion to the HBr: $\text{Cl}_2$  feed gas ratio, as shown by the XPS and LD-LIF



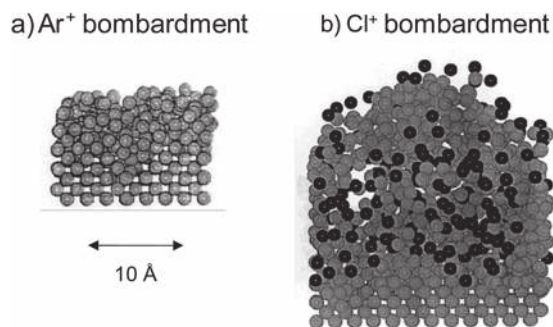


FIG. 23. Molecular dynamics simulations by Barone and Graves (Ref. 104) of 50 eV  $\text{Ar}^+$  or  $\text{Cl}^+$  bombardment of Si(100). The light and dark circles represent Si and Cl atoms, respectively.

measurements in Fig. 24.<sup>136</sup> Neither of these methods were capable of detecting hydrogen, so part of the falloff in total halogen coverage as a function of HBr addition could be due to adsorbed H that blocks sites for adsorption by Cl or Br. The etching rate has been found to fall as HBr is added to  $\text{Cl}_2$  feed gas. This was attributed to a combination of reduced halogen content in the layer and to a lesser degree, lower ion flux in HBr plasmas compared to  $\text{Cl}_2$  plasmas.<sup>136</sup>

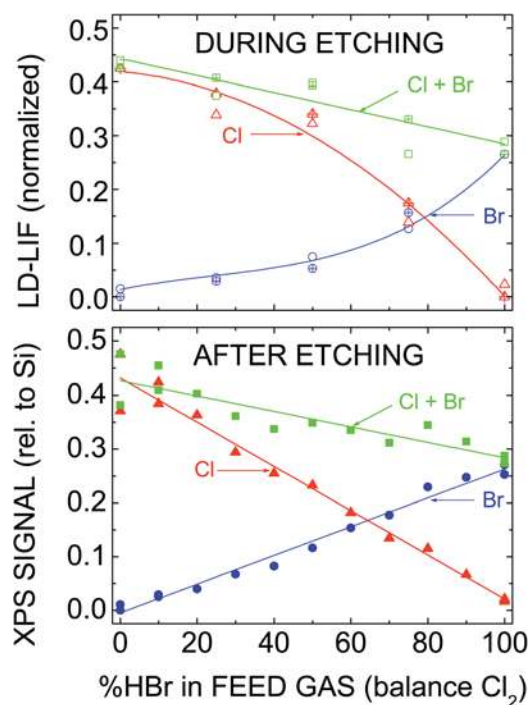


FIG. 24. (Color online) Cl and Br coverages as a function of HBr addition to a  $\text{Cl}_2$  plasma during and after Si(100) etching (Ref. 136). Bottom: Cl(2p) ( $\blacktriangle$ ), Br(3d) ( $\bullet$ ), and Cl(2p) + Br(3d) ( $\blacksquare$ ) XPS integrated peak intensities [normalized to Si(2p) and corrected for sensitivity differences], recorded after etching in HBr/ $\text{Cl}_2$  plasmas, as a function of % HBr. The solid lines are linear least square fits. Top: SiCl ( $\Delta$ ), SiBr ( $\circ$ ), and SiCl + SiBr ( $\triangle$ ) LIF intensities [normalized to the corrected Cl(2p) and Br(3d) XPS intensities at 100%  $\text{Cl}_2$  and HBr, respectively] vs. % HBr. The open symbols refer to intensities derived from single peaks  $\sim 2989$  Å for SiCl and 3009 Å for SiBr, and the open, crossed symbols refer to signals derived from a least squares fit to a combination of spectra for pure  $\text{Cl}_2$  and HBr plasmas. The curves, which are second- and third-order polynomial fits, are to guide the eye.

Sawin and co-workers have also studied etching of Si in HBr/ $\text{Cl}_2$  plasmas.<sup>156,165</sup> Their XPS measurements<sup>165</sup> of halogen coverage measured as a function of HBr fraction are virtually identical to those of Cheng *et al.*<sup>136</sup> in Fig. 24. They also found that the etching rate decreases with HBr addition to  $\text{Cl}_2$ , but ascribe it mainly to the lower ion flux and not to the reduced halogen coverage on the Si surface. This was based on the observation that if Si was etched in either a  $\text{Cl}_2$  or HBr plasma and then subjected to  $\text{Ar}^+$  bombardment, the initial enhanced sputtering rate was the same. They invoke adsorbed H in HBr plasmas as playing a role similar to Br or Cl in enhancing the rate.

Sawin and co-workers also studied the angle-of-incidence dependence of the etching rate for beams extracted from HBr and  $\text{Cl}_2$  plasmas.<sup>156,165</sup> They found that both yields peaked at normal incidence ( $=0^\circ$ ), but the yield in  $\text{Cl}_2$  plasmas was nearly constant between  $0^\circ$  and  $45^\circ$  while HBr plasma yields fell significantly between  $0^\circ$  and  $45^\circ$ . They carried out simulations of feature profile evolutions and attribute the straighter sidewalls in HBr plasmas versus  $\text{Cl}_2$  plasmas to this difference in dependence of the ion-assisted etching yield on angle of incidence.

As can be seen from Fig. 15, the chemical (i.e., isotropic) etching rates by Cl and Br atoms is very slow for all but heavily doped *n*-type Si. Consequently, no undercutting is expected and none is found.<sup>178</sup> No sidewall protection is needed, whether intentional (e.g., oxygen or fluorocarbon addition) or serendipitous (as a benefit of mask erosion). In fact, vacuum-transfer XPS analysis of photoresist-masked *p*-type Si in a HBr plasma showed that there is no carbon or oxygen on the sidewall.<sup>178</sup> When some undercutting does occur, either from wide-angle ion bombardment, from possible attack by H atoms, from photo-assisted etching, or in the case of etching of heavily *n*-doped Si, the deposition of a thin film on the Si etched feature sidewalls can be beneficial in obtaining near-ideal profile shapes. Sidewall films can be formed by adding oxygen to HBr-containing plasmas.<sup>179</sup> An  $\text{SiO}_2$  layer has been shown to form under these conditions, with little carbon, even when photoresist masks were used.<sup>154</sup> The presence of this thin layer suppresses bowing and notching.<sup>154</sup> Oxygen addition to HBr-containing plasmas also improves selectivity to underlying oxygen-containing layers such as  $\text{SiO}_2$ .

## 2. $\text{SiO}_2$ etching in fluorocarbon plasmas

F atoms react slowly with  $\text{SiO}_2$  in the absence of ion bombardment (1/40th the rate of  $\text{F} + \text{Si}$  at room temperature).<sup>99</sup> This rate is too slow to cause much undercutting in most  $\text{SiO}_2$  etching processes. Cl, Br, and H do not react with  $\text{SiO}_2$  at room temperature. Ion bombardment greatly accelerates the etching of  $\text{SiO}_2$  by F atoms<sup>128</sup> (and also of Cl and Br), but because Si also etches rapidly under these conditions, this approach is not commonly used for silicon microelectronics applications. Instead, fluorocarbon plasmas are used for selective etching of  $\text{SiO}_2$  over Si. Although the bulk of dielectric etching in IC fabrication is of lower dielectric constant insulators, etching of  $\text{SiO}_2$  is still important. In

addition, the process has been studied more than any other with perhaps the exception of Si etching. Much of what has been learned in these studies also relates to etching of other materials such as SiN.<sup>180</sup>

Fluorocarbon plasmas etch SiO<sub>2</sub> in reactions that can form stable products SiF<sub>4</sub>, CO, CO<sub>2</sub>, and perhaps COF<sub>2</sub>, or even SiOF<sub>2</sub>. CF<sub>2</sub> and CF<sub>3</sub> radicals, generated by electron impact dissociation and detachment of the feed gas, do not spontaneously etch SiO<sub>2</sub> in the absence of ion bombardment.<sup>181</sup> Neutral CF<sub>x</sub> radicals and ions bombard surfaces and lead to the formation of a fluorocarbon film. The deposition of this thin film on *horizontal* surfaces is the most important aspect of the etching of SiO<sub>2</sub> in fluorocarbon-containing plasmas. Coburn used *in-situ* Auger electron spectroscopy to investigate the formation of fluorocarbon films on Si and SiO<sub>2</sub> in CF<sub>4</sub>/H<sub>2</sub> plasmas.<sup>182</sup> He found that a thicker film formed on Si than on SiO<sub>2</sub>. The high selectivity of etching SiO<sub>2</sub> over Si was attributed to this difference in film thickness.

Unlike processes that rely on a sidewall film to suppress etching, the fluorocarbon film supplies reactants that are activated by ion bombardment. The film also improves selectivity toward etching of Si. The composition of the film and its deposition rate on SiO<sub>2</sub> depend on which fluorocarbon feed gas is used, the addition of other gases, the reactor materials, and other processing conditions. If the deposition rate is too fast, then the film continues to thicken and no etching occurs. Under useful condition, a constant steady-state film thickness and composition is maintained while the underlying SiO<sub>2</sub> layer is etched at a constant rate.

Butterbaugh *et al.*<sup>181</sup> studied the etching of SiO<sub>2</sub> in the presence of beams of Ar<sup>+</sup>, F, and CF<sub>2</sub>. They found that either F or CF<sub>2</sub> enhanced the yield of Ar<sup>+</sup> etching and that the enhancement was larger for F. They also found that supplying a flux of CF<sub>2</sub> had no additional enhancement of the etching with simultaneous Ar<sup>+</sup> and F beams impinging. As pointed out by Butterbaugh *et al.*,<sup>181</sup> this is consistent with the prior observation that the etching rate of SiO<sub>2</sub> in CF<sub>4</sub>/O<sub>2</sub> plasmas and NF<sub>3</sub>/Ar plasmas are the same at the same fluorine atom number density.<sup>128</sup> The yields for 500 eV Ar<sup>+</sup> can approach unity for high F/Ar<sup>+</sup> flux ratios.<sup>183</sup>

Oehrlein and co-workers have extensively studied etching mechanisms for SiO<sub>2</sub> in fluorocarbon plasmas.<sup>184–186</sup> They found that the deposition rate of the fluorocarbon film depends on gas composition and self bias voltage (Fig. 25). Lower ion energies favored faster deposition rates, displayed as negative values in Fig. 25. If a fluorocarbon film was deposited at low ion energy and then, under the same plasma conditions, subjected to high ion energies it etched. These net etching rates are given by the positive values in Fig. 25. Under conditions when the etching rate for the fluorocarbon film is much slower than the deposition rate, a thick film continuously grows and no etching of the underlying SiO<sub>2</sub> or Si occurs. If conditions are such that the film etching rate is much greater than the deposition rate, then little if any film will form on Si or SiO<sub>2</sub>. When the film etching and deposition rates are nearly equal, then the nature of the underlying material determines the steady-state film thickness. If it

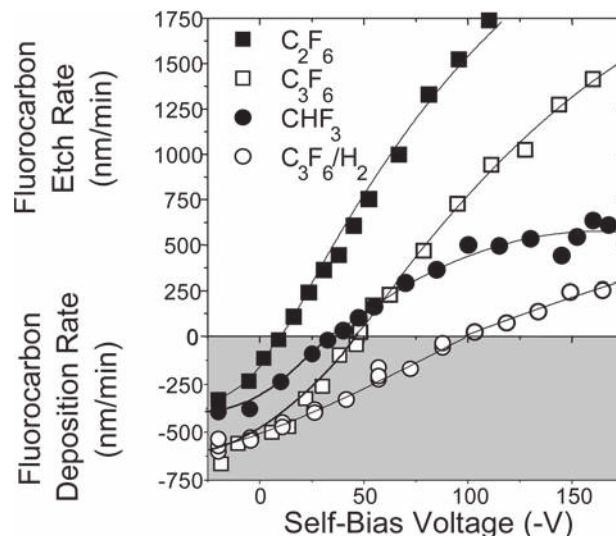


FIG. 25. Deposition and etching rates of the film deposited in fluorocarbon plasmas for different feed gases as a function of the dc self-bias voltage (and hence ion bombardment energy) (Ref. 186).

etches fast, as it does for SiO<sub>2</sub>, then the film is relatively thin, while if it etches slower as for Si, then a thicker film is present.

Some of the processes that occur during etching of SiO<sub>2</sub> in fluorocarbon-containing plasmas are summarized in the model put forth by Sankaran and Kushner; their schematic mechanism is reproduced in Fig. 26.<sup>187</sup> The film affects etching in two ways. First, it attenuates the energy of impacting ions that penetrate the film and reach the underlying layer. Ion-assisted etching rates typically decrease with the square root of ion energy above a threshold energy, hence, the thicker the film, the slower the etching rate. This inverse dependence of etching rate as a function of film thickness is illustrated by the measurements by Schaepekens and Oehrlein, reproduced in Fig. 27.<sup>186</sup> Somewhat surprisingly, SiO<sub>2</sub>, Si, and Si-nitride all fall on the same curve.

More recently, it was shown that the etching rate of Si, SiO<sub>2</sub>, and Si-nitride scales inversely with the amount of fluorine in the film.<sup>184</sup> The explanation for this is that this fluorine is liberated by ion bombardment. Some of it diffuses to

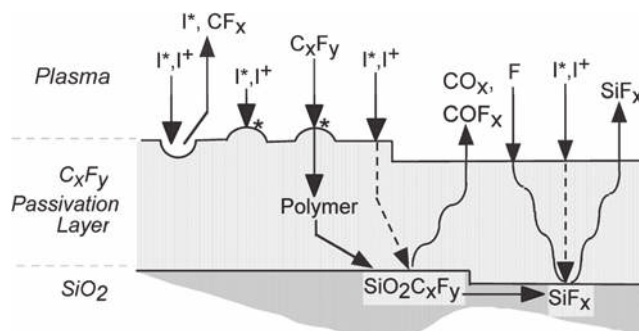


FIG. 26. Surface reaction mechanism during etching of SiO<sub>2</sub> in fluorocarbon-containing plasmas (Ref. 187). I<sup>+</sup> and I\* refer to positive ions and energetic neutrals, respectively. The dashed lines indicate that the particle loses energy during traversal through the polymer film. The curved lines represent species that diffuse through the polymer.

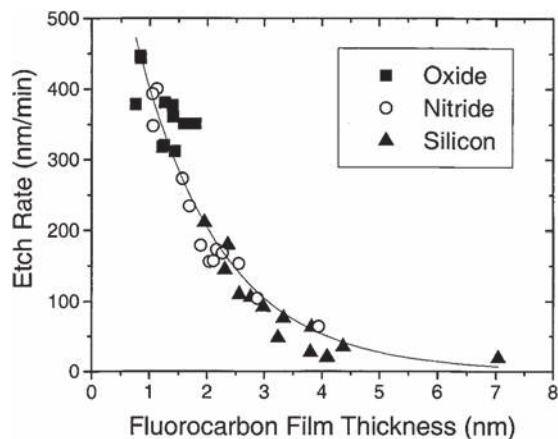


FIG. 27. Etching rate vs thickness of the fluorocarbon film for Si, SiO<sub>2</sub> ("oxide") and SiN ("nitride") with different fluorocarbon gases. The C<sub>3</sub>F<sub>6</sub>/H<sub>2</sub> mixture contained 27% H<sub>2</sub> (Ref. 186).

the underlying surface and participates in etching. Fluorine-containing products are liberated from the film; hence, fluorine content in the fluorocarbon film is reduced.

Charging in high aspect ratio features is believed to be responsible for "etch stop" that is often observed for dielectric materials.<sup>188–201</sup> Etch stop can also be caused by deposition of fluorocarbon polymer at the bottoms of high aspect holes in insulating films.<sup>153</sup> The combination of charging and polymer deposition can cause other interesting phenomena. When high aspect ratio holes are etched into an insulating film, a twisting is sometimes observed, as shown in Fig. 28.<sup>202</sup> It appears to be random; the origin is believed to be due to statistical variation in the amount of polymer and the

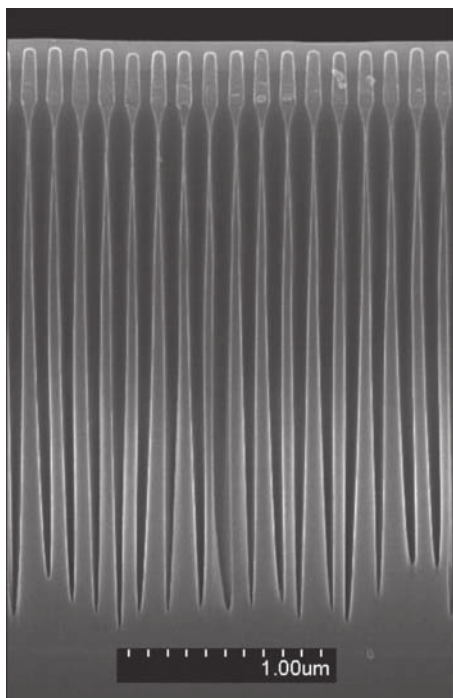


FIG. 28. Scanning electron micrograph of high aspect ratio holes etched into SiO<sub>2</sub> in a fluorocarbon-containing plasma. Reproduced with permission from Wang and Kushner, J. Appl. Phys. **107**, 023309 (2010). Copyright 2010, The American Institute of Physics.

amount of charge deposited on one side, causing the ions to be deflected off normal incidence, producing asymmetric profiles. Wang and Kushner simulated this twisting effect during etching of SiO<sub>2</sub>.<sup>202</sup> An example from that study is reproduced in Fig. 29. The different panels represent different random seeds in the Monte-Carlo simulations. They find that once twisting begins in a feature, it propagates. This has to do with the fact that ions are neutralized on glancing collisions with the sidewalls. These neutrals then perpetuate the twisted trench or hole. They also found that injecting high energy electrons into the trench helped to neutralize charge and reduce the severity of the twisted features.

### 3. Low- $k$ dielectrics

Low dielectric constant materials usually contain carbon and silica, as in for example methylsilsequioxane (MSQ), or SiOC(H). Fluorocarbon containing plasmas are used to etch these materials, and the fluorocarbon layer that forms on surfaces during etching plays a similar role in controlling etching rates of the film, as well as allowing etching to be selective to other materials such as SiC(H) etch stop layers.<sup>203,204</sup> The thickness and C/F ratio of the steady-state fluorocarbon layer is greater on MSQ than on SiO<sub>2</sub> [see, for example, Fig. 30 (Ref. 205)], suggesting that carbon in the etching film is the main source of C in the layer. For both MSQ and hydrogen silsequioxane (HSQ), the hydrogen in the film leads to a reduction of fluorine in the film through the formation of HF.<sup>203,205</sup> The fluorocarbon layer is also thicker on SiC(H) films than on SiOC(H) films<sup>204</sup> [Fig. 30 (Ref. 205)], indicating that the oxygen in the film helps to remove the fluorocarbon layer.<sup>203</sup>

To further reduce the dielectric constant of insulating layers in interconnects, pores are introduced into the film. The etching of porous silica and other porous low- $\kappa$  films is usually faster than of the same materials without pores. The factor by which the etching rate is enhanced might be expected to scale simply with the reduction of mass of the film. In fact, the rate can be enhanced either more or less than this amount.<sup>206</sup> The introduction of pores can even lead to a suppression of etching rate under certain conditions.<sup>206</sup> The pore size and degree of fluorocarbon film deposition play key roles in determining the etching rate behavior of

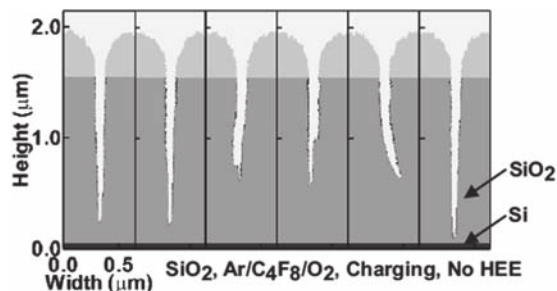


FIG. 29. Simulations by Wang and Kushner (Fig. 6, Ref. 202) of etching of high aspect ratio features in SiO<sub>2</sub> in a C<sub>4</sub>F<sub>8</sub>/O<sub>2</sub>/Ar plasma with charging included, but no high-energy electrons. Reproduced with permission from Wang and Kushner, J. Appl. Phys. **107**, 023309 (2010). Copyright 2010, The American Institute of Physics.



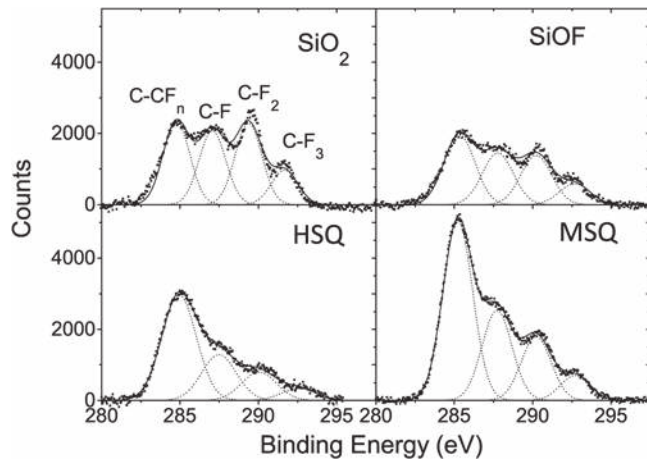


FIG. 30. C(1s) XPS spectra of fluorocarbon layers on SiO<sub>2</sub>, fluorinated oxide (SiOF), HSQ, and methyl silsesquioxane (MSQ) after partial etching in a C<sub>3</sub>F<sub>6</sub> plasma at 6 mTorr, 1400 W source power and a substrate self-bias of 2150 V<sub>DC</sub> (Ref. 205).

porous material relative to the nonporous material of the same chemical composition. As proposed by Standaert *et al.*<sup>206</sup> and simulated by Sankaran and Kushner,<sup>187</sup> filling of the pores with fluorocarbon deposits will slow the etching rate. When the deposition is severe and the pores are large, this can lead to a reduction in etching rate to below that for nonporous material. For small pores, the rate can be enhanced more than the amount expected by the reduction in density. Detailed simulations have been performed by Sankaran and Kushner<sup>207</sup> for etching of porous silica in C<sub>4</sub>F<sub>8</sub>-containing plasmas. Blanket etching rates and profile evolutions were generated, and in cases where experimental data are available, compared favorably.

## V. APPLICATIONS

### A. General concepts

Many issues must be considered in evaluating an etching process. These issues are often coupled, and sometimes trade-offs must be considered in optimizing a process.

Etch-rate **uniformity** is critical in most applications. In a batch reactor, both wafer-to-wafer and within-wafer uniformities must be considered. Two definitions for etching nonuniformity are commonly used. If  $\bar{E}$  is the average of etch rate  $E_i$  of  $N$  measurements across a wafer (or a batch of wafers), then three standard-deviations,  $\sigma$ , from  $\bar{E}$  will be

$$3\sigma = 3\sqrt{\frac{\sum_{i=1}^N (E_i - \bar{E})^2}{N-1}}, \quad (22)$$

hence, the etching nonuniformity is  $300\sigma/\bar{E}$ , expressed in %. This three-sigma nonuniformity means that 99.7% of the etch-rate measurements will fall within  $\bar{E} \pm 3\sigma$ . This is rarely the case, however, since etching nonuniformity is usually not random (center to edge, top to bottom, etc.). Another widely used expression for percent nonuniformity is defined as

$$\% \text{ nonuniformity} = 100 \times \frac{E_{\max} - E_{\min}}{2\bar{E}}, \quad (23)$$

where  $E_{\max}$  and  $E_{\min}$  are the highest and lowest measured etch rates.

Typically, 3% nonuniformity within a wafer is considered good. However, there are applications that are more forgiving, while others are more critical. If the process has good selectivity (to be defined below) to an underlying layer, uniformity is less critical, while in applications when etching creates a particular depth feature (e.g., trenches in silicon), uniformity of etching is extremely critical. Uniformity can be optimized by reactor design (electrode design, gas delivery system, magnetic confinement, and use of multiple coils for inductive sources), choice of chemistry and process parameters (e.g., gas flow, pressure, magnetic field and power, as well as the use of additives). Some etching processes are more chemical than ion-assisted (e.g., Al etching in Cl<sub>2</sub>-containing plasmas, or silicon etching with SF<sub>6</sub> or NF<sub>3</sub>) and therefore are more prone to nonuniformity when large open areas are etched and the feed gas is largely consumed (see “loading effect” below). In these cases, additional hardware (such as focus and shadow rings) can often improve uniformity.

A high **selectivity**, defined as the ratio between the rate of the layer being etched, relative to that of an underlying layer or masking material, is of critical importance. For example, when polysilicon gate electrodes are formed in field-effect transistors (FETs), the polysilicon (poly-Si) is etched until the underlying gate dielectric (e.g., SiO<sub>2</sub>) begins to be exposed in those regions where the film was slightly thinner and/or the etching rate was slightly faster. As the process is carried to completion and the remaining poly-Si is etched away or “clears” (the so-called “overetch” step), the exposed gate dielectric layer must remain, since its removal will result in attack of the Si substrate below. Consequently, a high selectivity of poly-Si etching over the gate dielectric is required. Similarly, the selectivity with respect to the mask must be high enough that the integrity of the mask is preserved during the main etch and overetch period.

The selectivity, however, is not always a well-defined quantity. In many instances, the etching rate changes during the process, and as a result, the selectivity varies as well. The etching rates and selectivity can also vary with the aspect ratio of the features being etched. (Aspect-ratio-dependent etching rates are discussed below.) In addition, while selectivity associated with a process may appear high on a macroscale, local effects such as feature “faceting” and “trenching” (discussed below) may make bulk high-selectivities meaningless.

The determination of selectivity is not always straightforward. For gate etching, post-etch measurements of the remaining gate-dielectric are often erroneously high (sometimes higher than the initial thickness) due to deposits that form during etching. In addition, when SiO<sub>2</sub> is exposed to the plasma after poly-Si etching in an oxygen-containing plasma such as HBr/O<sub>2</sub>, oxygen can penetrate the exposed SiO<sub>2</sub> layer and oxidation of the underlying Si substrate can occur, also making the remaining dielectric layer thicker and the selectivity appear artificially larger than it is.<sup>96,208</sup>

**Loading** is the decrease of etching rate with an increase in the amount of exposed material being etched. It can be global, where the spatially-averaged etch rate varies, or local, where the etching rates of regions of the chip depend on the density of the features. The loading effect is observed when the active species in the plasma are depleted rapidly by reaction with the material being etched.<sup>209,210</sup> It is affected by the lifetime of the active species as well as chamber volume (larger volume, which may be impractical, reduces the loading effect<sup>209–212</sup>) and feed gas flow rate (etching rates decrease with decreasing flow rate<sup>115</sup>). The loading effect is strong when the process is dominated by fast chemical etching by neutrals, where the etching rate is often observed to be first order in neutral etchant number density,<sup>99</sup> and weaker when etching is driven by ion-stimulated removal of a halogenated surface layer.<sup>212</sup> The former is observed, for instance, in  $\text{SF}_6$  or  $\text{NF}_3$ -containing plasmas when a large amount of Si is etched, and F-atoms become depleted. On the other hand, etching Si in  $\text{Cl}_2$  plasmas varies much less with the area of exposed Si because the composition of the halogenated surface layer is largely independent of loading,<sup>115</sup> and no chemical etching by Cl atoms occurs (except for  $n^+$ -Si). Etching is limited by ion stimulated desorption, and the ion flux is fairly insensitive to loading. In some applications, such as fabrication of silicon microlenses (where a pattern of spherically shaped polymer mask is transferred into the substrate below by polymer-erosion<sup>213,214</sup>), the loading effect needs to be addressed, since the area of exposed substrate changes as the polymer erodes, and maintaining constant etch rates of both polymer and substrate material is critical for obtaining the desired lens shape.

**Aspect Ratio Dependent Etch Rate (ARDE)** or “**RIE Lag**” refers to a phenomenon where etch rate slows down as the etching proceeds down a hole or a trench. A number of mechanisms have been proposed<sup>215–217</sup> and involve transport of neutrals and ions as well as charging and shadowing effects. Locally, this effect can take place when the aspect ratio (i.e., the ratio between the depth and width of the space between features) changes, either as a function of depth or as a function of position across the wafer. During contact etching, the aspect-ratio increases and the etching rate generally decreases or, in extreme cases, etching stops. This occurs sooner in smaller features, meaning that when contacts with different diameters are patterned on the same wafer, the smaller contacts etch slower. By adjusting the ion/neutrals ratio (e.g., by increasing the pressure), however, and moving toward a regime dominated by polymer deposition, the effect is reduced and even reversed.<sup>217</sup>

**Faceting** of the mask is the result of ion bombardment. Since the sputtering yield is a function of angle,<sup>218–220</sup> the sharp (or nearly sharp) corners may erode and attain an angle commensurate with the angle associated with the maximum sputtering rate.<sup>221</sup> Since the ion flux per unit area decreases with the angle of incidence,  $\theta$ , the maximum sputtering rate will take place at an angle larger than  $0^\circ$  if the sputtering-yield as a function of  $\theta$  rises faster than  $1/\cos \theta$ .<sup>221</sup> If the mask erodes significantly, then the bottom edge will move inward, away from the etched step and the feature will

develop a tapered profile.<sup>222</sup> In addition, deflection of ions from the sloped surface can cause a microtrench to develop at the feature base (see below) as well as affect the profile of a neighboring line [see Fig. 31(a)].<sup>222</sup>

Impinging ions are nearly perpendicular to the wafer surface, but there is a small lateral component that can affect the profile of the feature being defined. In some cases this can lead to a near-specular reflection off vertical sidewalls, increasing the ion flux near the base of the feature and causing **microtrenching** [Fig. 31(b)], an undesired effect.<sup>221</sup> In other instances, the off-normal-incidence ions cause a slope in the profile and may round the bottoms of trenches (depending on the application, this could be a desired or undesired effect). A good example of these two effects is the etching of trenches in silicon with  $\text{Cl}_2$  or  $\text{HBr}$ -containing plasmas (see also discussion above). The former causes the formation of sharp microtrenches while the latter leads to much wider trenches that have rounded corners.<sup>223–226</sup>

**Undercutting** [Fig. 31(c)] is the result of isotropic etching that will lead to lateral as well as vertical etching. When the isotropic component is strong (such as etching silicon with low bias  $\text{SF}_6$  or  $\text{NF}_3$  plasmas), a profile similar to the one obtained by wet etching is observed. This is caused by a chemical attack by neutral species [F for all forms of Si and Cl for  $n^+$ -Si (see Fig. 15), Cl and  $\text{Cl}_2$  for Al]. It is possible, however, to increase the vertical component (by increasing the bias power, for instance), to reduce the relative undercut. To avoid undercutting completely in these situations, a sidewall protection scheme is necessary (See discussion on aluminum etching, Sec. VC 6 below) Often the application of bias leads to formation of by-products that aid in this sidewall protection, such as resist erosion during Al etching.

**Tapered** profiles [Fig. 31(d)] often result from deposition on the sidewall during etching, effectively increasing the mask width as etching progresses. The deposited material

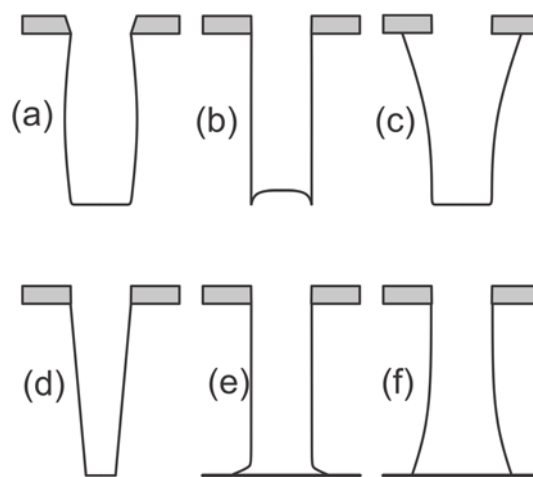


Fig. 31. Various profiles obtained during plasma etching: (a) bowing due to faceting of the mask; (b) microtrenching due to enhanced ion flux along the sidewall; (c) Undercutting due to an isotropic component in the etch process; (d) tapered profile due to deposition on the sidewall; (e) notching at the interface due to inadequate sidewall passivation or charging effects; (f) Re-entrant profile (overcutting) due to inadequate sidewall passivation and/or ion scattering.

can be either polymer formed during the etch process combined with etch by-product, or material being sputtered during etching. An example of the former is the excessive amount of sidewall passivation films that deposited during aluminum etching,<sup>227</sup> while the latter could be sidewall deposits of nonvolatile by-products from sputtered copper or gold.<sup>228</sup>

**Notching** at bottoms of etched features [Fig. 31(e)], at the interface with the layer below, can occur for a number of reasons. One can be positive charging of the underlying layer that can deflect positive ions toward the sidewall.<sup>229</sup> This is usually observed at low bias power in, for instance, gate overetch, where the low power is needed to preserve the thin gate oxide. Another mechanism occurs in etch processes that rely on sidewall passivation to achieve anisotropy. The sidewall protective layer near the interface may be too thin to provide protection, leading to isotropic etching at the interface. This can occur, for instance, in Al etching with a hard mask, using a  $\text{Cl}_2$  and  $\text{HBr}$  mixture to generate by-products that passivate the sidewalls.<sup>230</sup> The passivation layer at the bottom of the feature is too thin to protect the aluminum from the highly isotropic etch by  $\text{Cl}_2$ .<sup>230</sup> Notches at the bottoms of etched features could sometimes be desirable, such as in the formation of a notched gate (T-gate), to reduce the overlap capacitance between the gate and source and drain regions.<sup>231</sup>

**Reentrant** profiles, [Fig. 31(f)] could be the result of either inadequate passivation as the etch progresses deeper,<sup>232</sup> the result of ion-scattering by the etch-stop layer,<sup>233,234</sup> or a divergent ion flux.<sup>235</sup>

## B. Etch chemistries

The etch chemistry chosen for a particular application is based on the material being etched, the etchers being used and other considerations such as uniformity, selectivity, etch rate, etc. discussed in the previous sections.

### 1. Dielectrics

Fluorocarbon and hydrofluorocarbon gases, usually with some additives, are typically used for dielectric etching, such as  $\text{SiO}_2$ ,  $\text{Si}_3\text{N}_4$ ,  $\text{SiN}$ , and various low- $\kappa$  dielectrics.  $\text{CF}_4$  [Freon® 14 (Ref. 236)],  $\text{C}_2\text{F}_6$  (Freon 116), and  $\text{C}_3\text{F}_8$  (Freon 218) were used in the early days to etch  $\text{SiO}_2$ ,<sup>28,29</sup> usually with addition of  $\text{O}_2$  when selectivities to resist and/or silicon were not critical, and polymer control was important. Hydrogen addition to the above fluorocarbons was used to increase selectivity to silicon,<sup>28,29,237</sup> with the drawbacks of polymer formation, decreased etch rate,<sup>237,238</sup> and deep penetration of hydrogen into the silicon substrate<sup>239–247</sup> that can lead to device degradation if not annealed properly. In applications where this is not an issue (such as patterning of waveguides), hydrogen may be used as an additive to control selectivity to silicon and/or photoresists.

$\text{CHF}_3$  (Freon 23),<sup>28,29,37</sup> with some additives that vary with tool and application, has been used for many generations of device for  $\text{SiO}_2$  and  $\text{SiN}$  etching. The additives are needed to control polymer build-up on the wafer as well as

the chamber wall.  $\text{O}_2$  and  $\text{CO}_2$  were common additives in batch reactors; however, as the industry migrated to single wafer etchers, mixtures of  $\text{CHF}_3$  with  $\text{CF}_4$  became more common, usually with Ar as a diluent. The selectivity with respect to silicon could be controlled by the amount  $\text{CF}_4$  added to the mixture; increased  $\text{CF}_4$  concentration yields lower selectivity but less polymer formation.<sup>217</sup> Over the years, etching chemistries for dielectrics evolved too, with the introduction of gases with lower fluorine-to-carbon ratios (F:C) to increase selectivity both to silicon and photoresist masks.

Gases, such as  $\text{c-C}_4\text{F}_8$  (Refs. 28 and 29) (octafluorocyclobutane—F:C = 2),  $\text{c-C}_5\text{F}_8$  (Ref. 248) (octafluorocyclopentene—F:C = 1.6), and  $\text{C}_4\text{F}_6$  (Ref. 249) (hexafluoro-1,3-butadiene—F:C = 1.5), became the chemistries of choice in the newer generation of etchers. Although the migration to these gases was driven primarily by performance issues, there were environmental considerations as well. The motivation for the introduction of  $\text{C}_5\text{F}_8$ , for instance, was its short atmospheric lifetime [0.3 years<sup>248</sup> versus 3200 years for  $\text{C}_4\text{F}_8$  and 270 years for  $\text{CHF}_3$  (Ref. 250)] and reduced global warming potential. Comparisons have been made of etching of high aspect-ratio contacts<sup>251</sup> using  $\text{c-C}_4\text{F}_8$  to  $\text{c-C}_5\text{F}_8$  and  $\text{C}_4\text{F}_6$  in a modified Gaseous Electronic Conference Reference Cell.<sup>252</sup> However, the performance of these gases in a commercial reactor may be different and will depend on the particular etcher used.

Common additives include  $\text{O}_2$ , Ar,  $\text{CO}_2$ , and CO. The latter is used to control selectivity, since it tends to minimize the amount of fluorine-rich species.<sup>253</sup> Special care is needed with CO since it reacts spontaneously with nickel. Therefore all gas delivery hardware must be void of any exposed nickel surfaces (such as nickel gaskets). Type 316 stainless steel is an acceptable choice as gasket material (and tubing) for CO.

Although most chemistries that will etch  $\text{SiO}_2$  will etch silicon nitride films (stoichiometric or nonstoichiometric LPCVD or plasma-enhanced CVD, collectively referred to as  $\text{SiN}$ ), there are applications when one has to be etched selectively with respect to the other. Etching  $\text{SiO}_2$  selectively over  $\text{SiN}$  can be accomplished by a polymer-producing plasma that will sustain etching as long as oxygen by-products are released to the plasma from the etched film, but will stop on the nitride film, producing polymer deposits.<sup>253</sup> This process is extremely useful in etching self-aligned contacts (SAC) (to be discussed later), but difficult to implement in etching a bulk  $\text{SiO}_2$  film on top of  $\text{SiN}$  (such as silicon trench isolation). The reverse, etching  $\text{SiN}$  selectively to  $\text{SiO}_2$ , is needed in cases where a thin  $\text{SiO}_2$  film serves as an etch stop layer, to avoid exposure of the Si substrate to the plasma, such as in a local-oxidation-of-silicon (LOCOS) structure, where subsequent oxidation can create oxidation-induced stacking faults.<sup>254</sup> This can be accomplished in a number of ways.  $\text{SiN}$  can be etched with selectivities of 3:1 or higher by  $\text{SF}_6$  or  $\text{SF}_6/\text{O}_2/\text{N}_2$  mixtures under low-bias conditions.<sup>255</sup> Best results are obtained in the so-called “plasma” configuration, where the wafer is placed on the grounded electrode. Higher selectivities, however, can be obtained with  $\text{SF}_6/\text{CH}_4$ ,  $\text{NF}_3/\text{CH}_4$  or  $\text{CF}_4/\text{CH}_4$  mixtures<sup>256</sup> or



hydrofluorocarbons with F:C ratio less than 3,<sup>257</sup> such as  $\text{CH}_3\text{F}$  and  $\text{CH}_2\text{F}_2$ . The mechanism proposed<sup>257</sup> is the suppression of  $\text{CF}_3^+$  that are critical for etching  $\text{SiO}_2$ , but the process may be much more complex, as discussed above. With the proper additives, and by using the right process parameters (which are tool-dependent), extremely high selectivities to  $\text{SiO}_2$  or Si can be achieved. Once the layer below the SiN is exposed, a high rate of polymer deposition often ensues.

Low- $\kappa$  dielectrics in use consist of organosilicate glass, which was nonporous in older applications, but highly porous in current and future technologies (the requirement for the 22 nm node and beyond is  $\kappa \sim 2.2$ ). Fluorocarbon chemistry is used to etch the low- $\kappa$  dielectric, stopping on the capping layer below.  $\text{C}_4\text{F}_8/\text{CO}$  based chemistry was common at early stages of implementation of low- $\kappa$  materials,<sup>258</sup> however, with the migration to porous materials, the F:C ratio is adjusted to minimize residues at the end of the etch. The key to successful integration is the postetch resist strip, which can affect the final  $\kappa$ -value of the dielectric. This will be discussed below in Sec. VC7, where damascene structures are covered in detail.

## 2. Silicon

Silicon (crystalline, polycrystalline, and amorphous) is etched in chlorine, bromine, and fluorine based plasmas; the choice depends on the application. Generally, plasmas that generate large amounts of F atoms will etch Si faster than plasmas that contain large amounts of Cl or Br, but profile control and loading are harder to achieve, due to the fast isotropic etching by F atoms (see above and Fig. 15).  $\text{Cl}_2$ , HBr, or their mixture are better choices when vertical or near vertical walls are desired. When large heights or depths must be created in Si, for applications such as micromachining for MEMS or through-Si-vias (TSV), high etching rates and large selectivity to the mask are required. Here,  $\text{SF}_6$  plasmas, usually with added  $\text{O}_2$ , are the chemistry of choice. Since etching is substantially isotropic, the process alternates between an etching plasma containing  $\text{SF}_6$ , and a polymer depositing plasma containing most commonly  $\text{C}_4\text{F}_8$  to protect the sidewalls from lateral etch. More detailed discussion will follow in the sections discussing the various structures.

## 3. Silicides

Various silicides have been used in semiconductor applications, mostly as the top layer in a gate stack.<sup>259</sup> It can either be etched together with the silicon layer below to form the gate-stack, or formed after polysilicon etch and spacer formation (see below) in a silicidation process.<sup>259</sup> The most common silicide in the former is tungsten-silicides, but tantalum and titanium silicides have been used as well. A silicon-rich silicide is usually sputtered on top of a poly-Si or amorphous Si layer, and the best etching results are obtained before the film is sintered. In conventional RIE reactors various chlorofluorocarbons, such as  $\text{CFCl}_3$  (Refs. 260 and 261) and  $\text{CF}_2\text{Cl}_2$ ,<sup>260</sup> were popular etching gases, but due to environmental concerns, as well as issues with

polymer residues, they were replaced in later generation etchers by  $\text{Cl}_2$  (Ref. 262) or  $\text{Cl}_2$  and HBr mixtures, sometimes with the addition of oxygen, especially when the etched material is tungsten silicide. The ability to etch tungsten silicide with  $\text{Cl}_2$  is not obvious, since tungsten does not form volatile chlorides at room temperature. However, tungsten silicide is etched at room temperature, at etch rates comparable to or higher than the etch rate of the polysilicon layer below. It is possible that residual oxygen in the chamber or buried in the film helps in the creation of somewhat volatile tungsten oxychloride ( $\text{WOCl}_4$ ).<sup>263</sup>

## 4. Aluminum

Aluminum and aluminum alloys (with silicon or copper below 0.5%) are generally etched in  $\text{Cl}_2$  based chemistries. Detailed discussion will follow in the discussion of metallization structures below.

## 5. Titanium and titanium nitride

Both Ti and TiN are used in aluminum metallization stacks.  $\text{Cl}_2$  or  $\text{BCl}_3/\text{Cl}_2$  chemistries are the most commonly used. Detailed discussion will follow in the discussion of metallization structures below.

## 6. Chromium

The main use of Cr is in creating patterns on lithographic masks.  $\text{Cl}_2$  and  $\text{O}_2$  mixtures<sup>264</sup> are used at moderate pressures (tens of mTorr). The process relies on formation of chromium oxychloride ( $\text{CrO}_2\text{Cl}_2$ ) as a volatile by-product. When a hard mask or a silicon-containing resist is used (both erode slowly), there is a slight undercut.<sup>265</sup> The addition of nitrogen to the plasma helps in reducing the undercutting.<sup>265</sup>

## 7. Nickel and nickel alloys

Nickel does not form volatile alloys easily. However, it is possible to etch nickel with a  $\text{CO}/\text{NH}_3$  plasma. See detailed discussion below on magnetoresistive random-access-memory (MRAM).

## 8. Other materials

Cu, Au, Pt, Ir, PZT ( $\text{Pb}[\text{Zr}_x\text{Ti}_{1-x}]\text{O}_3$  with  $0 < x < 1$ ), BST ( $\text{Ba}_{1-x}\text{Sr}_x\text{TiO}_3$  with  $0 < x < 1$ ), and others that do not form volatile compounds at room temperature can be etched in specially designed etchers with chucks that can be heated to a few hundred degree Celsius,<sup>63</sup> using a hard mask or by reactive sputtering.<sup>266</sup> The etch chemistry will be material dependent.

There are number of reports of gold etching in  $\text{HBr}/\text{Ar}$ ,<sup>228</sup>  $\text{Cl}_2/\text{Ar}$ ,<sup>228</sup>  $\text{Cl}_2$ ,<sup>267</sup>  $\text{CF}_4/\text{Cl}_2$ ,<sup>267</sup> and  $\text{CF}_4/\text{CCl}_4$  (Ref. 267) containing plasmas, but the samples were not heated, and sputtering rather than the creation of volatile compounds took place. When substrates were heated to 125 °C and above,<sup>268–270</sup> Au etching rates in  $\text{Cl}_2$  as high as 980 nm/min with 10:1 selectivity to the  $\text{SiO}_2$  hardmask was realized.<sup>270</sup> There was no evidence of deposition on the sidewalls and 0.5  $\mu\text{m}$  wide features, 1  $\mu\text{m}$  high, appear to be vertical.

### C. Structures

Various structures that are created with the aid of plasma etching are listed below. It is not possible to cover all applications, so the attempt here is to address structures in use in modern ICs. Therefore, older application for structures and techniques such as LOCOS, poly-Si buffered LOCOS, plasma planarization, “champagne glass” contact, etc., have been left out.

#### 1. Shallow trench isolation

To achieve wafer planarity and enable higher device density, shallow trench isolation (STI) has replaced LOCOS as the isolation scheme for modern devices. It consists of etching trenches into silicon, filling them with  $\text{SiO}_2$ , followed by planarization, using chemical–mechanical-polishing (CMP) to achieve a nearly planar structure on which the device is to be built (Fig. 32).

The process involves deposition of a silicon-nitride film on a thin layer of oxide, followed by patterning with photoresist and then etching the nitride and oxide layer with fluorocarbon etch chemistry (e.g.,  $\text{CHF}_3/\text{CF}_4/\text{Ar}$ —Sec. VB, above). The photoresist can be either left in place, or removed prior to the silicon etch. In the latter case, the silicon-nitride serves as a hard mask during etching, so the etch chemistry must be selective to nitride. The requirements are to have a slightly tapered trench wall (to facilitate a good trench-fill), flat bottom and rounded corner at the bottom of the trench. Rounded corners at the top of the trench are necessary as well, but this can be accomplished in postetch processing.<sup>271</sup>

$\text{Cl}_2$  plasmas can etch Si with high selectivity to silicon-nitride, but the profile is inadequate and leads to microtrenching.<sup>169,223–225</sup> HBr or HCl (Ref. 226) containing plasmas lead to highly tapered profiles, but a mixture of  $\text{Cl}_2$  and HBr gives the desired profile, usually with the addition of oxygen. The latter is added mainly to increase selectivity to the mask, but it leads to the deposition of etch by-products on the trench wall.<sup>272</sup> The process is highly sensitive to oxygen concentration and the addition of too much oxygen can lead to heavy deposits on the entire wafer. Therefore, to achieve better control, the oxygen is often diluted in helium (usually 20%  $\text{O}_2$  in He).

When silicon-on-insulator (SOI) wafers are used, the buried-oxide (BOX) layer is a natural etch-stop for the process. With Si wafers, or when the SOI trench does not reach the BOX layer, uniformity is extremely crucial for consistent trench depths and device performance across the wafer.

The SiN mask remains on the wafer during the trench fill process and the subsequent CMP step. The CMP step is selective to SiN and the planarization is stopped once the SiN layer is exposed. The SiN layer is then removed, and after subsequent wet cleans (which include dipping in HF solution) the surface of the wafer is nearly planar.

#### 2. Gate

Polysilicon and amorphous silicon with or without a top conducting layer (silicide or TiN) have been used as the gate

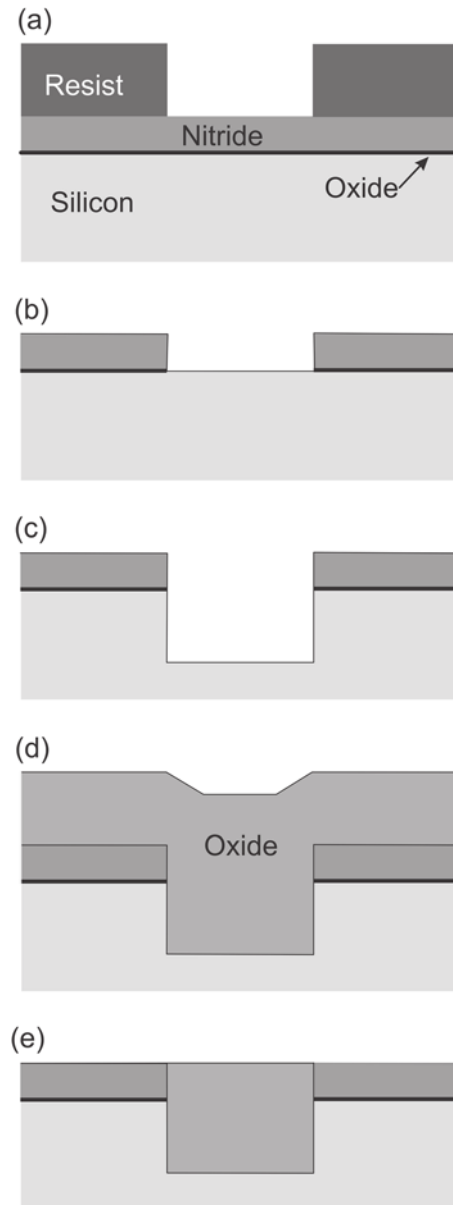


FIG. 32. STI process flow: (a) pattern definition; (b) nitride and oxide etch, and resist strip; (c) trench etch; (d) oxide fill; (e) CMP oxide, stopping on nitride.

materials for many device generations. The gates are formed by depositing a poly-Si (or amorphous Si) layer on a thin layer of oxide (either oxidized silicon, or high- $\kappa$  dielectric, usually  $\text{HfO}_2$ -based). The poly-Si is doped with proper impurities, usually by ion-implantation, and in symmetric complementary metal oxide semiconductor (CMOS) devices, both  $p$ - and  $n$ -type gate materials are present on the same wafer (in some devices only  $n$ -type poly-Si is used and that can be achieved either *in-situ* or by postdeposition doping). In some instances, other conductive layers such as a silicide (most commonly  $\text{WSi}_x$ , but historically  $\text{TaSi}_x$  and  $\text{TiSi}_x$ ) have been used.<sup>259</sup> In other schemes, the silicidation takes place after the gate formation, where the silicide is formed on the gate source and drain simultaneously.

The mask can be photoresist or a hard mask (e.g.,  $\text{SiO}_2$  or SiN). Though adding complexity, the hard mask offers

advantages of higher selectivity to oxide, and better CD control, especially when differences between isolated and nested lines have to be minimized. If photoresist is used as a mask, the eroded resist becomes part of the etch chemistry; it can lead to deposits on the sidewalls and lower selectivity toward  $\text{SiO}_2$ , hence leading to erosion of the underlying gate oxide layer.<sup>273</sup> When a hard mask (e.g.,  $\text{SiO}_2$  or  $\text{SiN}$ ) is to be used, it is deposited on top of the gate stack, followed by an antireflective coating (ARC), resist application and lithography. The ARC can be either organic or inorganic. Organic ARCs can be etched either in  $\text{O}_2$  or  $\text{CO}_2$  plasmas while the inorganic ARC can be etched with the same chemistry used to etch the hard mask below (using  $\text{CHF}_3/\text{CF}_4/\text{Ar}$  chemistry, for instance). The resist is then stripped followed by the proper wet cleans (Fig. 33).

In some cases, the resist is trimmed prior to hard mask etching to obtain dimensions not attainable by the lithographic process. This is accomplished in oxygen plasmas under conditions yielding an isotropic etch process. Etch

uniformity is extremely critical, and this process will inevitably increase the relative variability in CD control. For example, if the desired gate width is  $0.1\text{ }\mu\text{m}$  and the gate is printed at  $0.15\text{ }\mu\text{m} \pm 10\%$ , the best that can be achieved after the trim will be  $0.1\text{ }\mu\text{m} \pm 15\%$ , assuming no additional variability added by the trimming process.

The gate etch process usually consists of multiple steps. First, there is a breakthrough step to remove the native oxide and initiate etching. It usually consists of  $\text{Cl}_2$  or  $\text{Cl}_2/\text{Ar}$ , at relatively high bias power. This is followed by an etch process optimized for good CD control but not necessarily selective to oxide. The etch chemistry usually consists of a  $\text{Cl}_2/\text{HBr}$  mixture, sometimes with the addition of small amounts of  $\text{O}_2$  diluted in He. The  $\text{Cl}_2/\text{HBr}$  ratio will depend on the application. In pure  $\text{Cl}_2$ , highly  $n$ -doped polysilicon tends to etch isotropically (and faster than  $p$  or undoped polysilicon), and therefore, higher concentrations of HBr will be required, since the isotropic etching rate of  $n^+$ -Si by Br atoms is much slower than by Cl atoms (see Fig. 15). Once endpoint is detected, usually by optical emission (see Sec. III F), an overetch step follows. This step is intended to clear residual poly-Si remaining on the wafer due to nonuniformity, and in some cases, due to topography. The overetch step usually involves adding (more)  $\text{O}_2$  to a  $\text{Cl}_2/\text{HBr}$  (or just HBr) plasma and reducing the bias voltage. In critical cases, where extremely thin gate oxide is used, the overetch step is initiated before the polysilicon is cleared. An endpoint prediction scheme, relying on interferometry with an external light source, can be used to terminate the main etch step as little as 10 nm before endpoint.<sup>96–98</sup> The remaining gate oxide after etch cannot be measured reliably. From wet etch-rate measurements,<sup>96,274</sup> it appears to be a porous material.

When silicide or TiN is used as a top layer, the etch process may include another step optimized to etch that particular layer. This step is usually  $\text{Cl}_2$  or  $\text{Cl}_2/\text{HBr}$  based, and in the case of silicide, it may be advantageous to add small amounts of oxygen to increase the silicide:poly-Si etch-rate ratio. When TiN is used as the top layer, large amounts of oxygen added to the plasma will hinder the etch process.  $\text{Cl}_2$ , possibly with the addition of inert gases, is the most suitable etch gas.

The above approach has been used for gate formation and is known as the “*gate first*” approach where the gate is formed before the source and drain are constructed, by doping, epitaxially raised and/or silicided. In some cases, after spacer formation (see below), the hard mask is removed, and source, drain, and gate are silicided simultaneously.

A further evolution of the gate first approach is the introduction of high- $\kappa$  dielectrics (currently  $\text{HfO}_2$  based, but earlier investigations included  $\text{ZrO}_2$  based dielectrics as well<sup>275</sup>) and metal gates for added performance. The details are proprietary and will vary between manufacturers, but the gate metal under poly-Si is different for the  $p$ - and  $n$ -channel gates.<sup>276</sup> If TiN based metal is used for the gate, a  $\text{Cl}_2/\text{HBr}$  based<sup>277</sup> chemistry is used for etching the gate and  $\text{BCl}_3$  based chemistry (possibly with some additives) is used to remove the high- $\kappa$  dielectric after the gate is etched,<sup>277–280</sup> sometimes at elevated temperature.

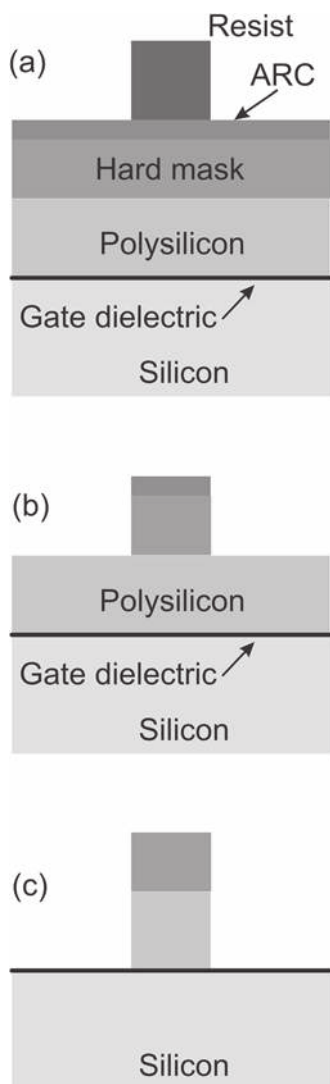


FIG. 33. Polysilicon gate process flow, using a hard mask: (a) pattern definition; (b) hard mask etch and resist strip; (c) polysilicon etching. When the ARC is organic, it is stripped with the photoresist; if inorganic, it will stay in place during the gate etching.



Another more recent approach, known as “*gate last*” (Fig. 34), relies on forming a poly-Si dummy gate (using a hard mask) that stays in place while the source and drain are being formed. There are two flavors to this approach: “*high- $\kappa$  first*”<sup>276,281</sup> and “*high- $\kappa$  last*.”<sup>281</sup> In the former, the polysilicon gate is formed over a high- $\kappa$  dielectric, in an identical fashion described in the gate first approach. After the formation of source and drain, a SiO<sub>2</sub> layer is deposited over the entire wafer, which is then planarized using CMP, until the top of the polysilicon gate is exposed. The poly-Si is then removed selectively, and the cavity is filled with the appropriate metal layers. A metal CMP step then follows to remove the metal everywhere but the gate cavity. The high- $\kappa$  last approach is similar, except that the sacrificial poly-Si gate is constructed on a sacrificial SiO<sub>2</sub> layer, to be removed

after removal of the poly-Si. A high- $\kappa$  dielectric layer is then deposited, followed by metal deposition and CMP to form the gate.<sup>281</sup>

In either “*gate last*” approaches, it is possible to etch back the metal gate to create a recess to be filled with a dielectric (e.g., SiN). This will be useful in the formation of self-aligned contact, to be discussed below.

### 3. Gate spacer

This sidewall, intentionally deposited on the sides of the gate (Fig. 35), serves multiple purposes. For simultaneous silicidation of gate, source, and drain, it prevents the shorting of these areas. It is also used as an implant mask in the creation of lightly doped-drain. Either SiO<sub>2</sub> or SiN<sub>x</sub> can be used as the spacer material. The latter is useful in the fabrication of self-aligned contacts, to be discussed below.

After fabricating the gate, a layer of oxide (or nitride) is deposited over the entire wafer, followed by a blanket etch-back. The process is terminated based on optical emission endpoint with some overetch. A typical etch chemistry for this step is CHF<sub>3</sub>/CF<sub>4</sub>/Ar, which will etch SiO<sub>2</sub> as well as SiN, and depending on the CF<sub>4</sub> concentration, will be selective to silicon. In some integration schemes, when nitride is

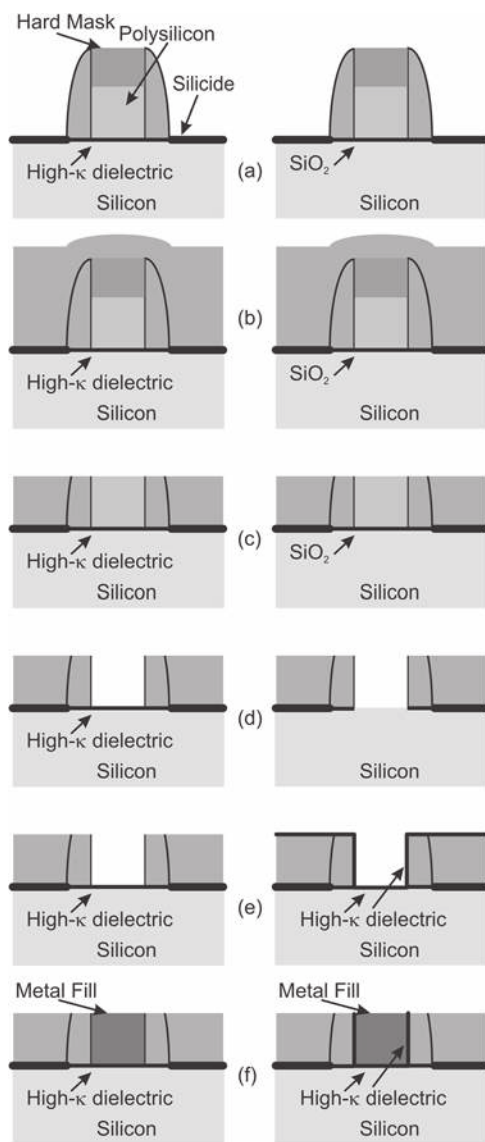


FIG. 34. Gate last process flow: Left: high- $\kappa$  first; Right: high- $\kappa$  last. (a) Polysilicon gate after spacer formation, implant and silicidation; (b) dielectric deposition; (c) CMP exposing the disposable gate; (d) polysilicon removal, removal of SiO<sub>2</sub> to expose substrate in high- $\kappa$  last scenario; (e) deposit high- $\kappa$  dielectric in high- $\kappa$  last scenario; (f) metal gate fill and CMP to create the gate.

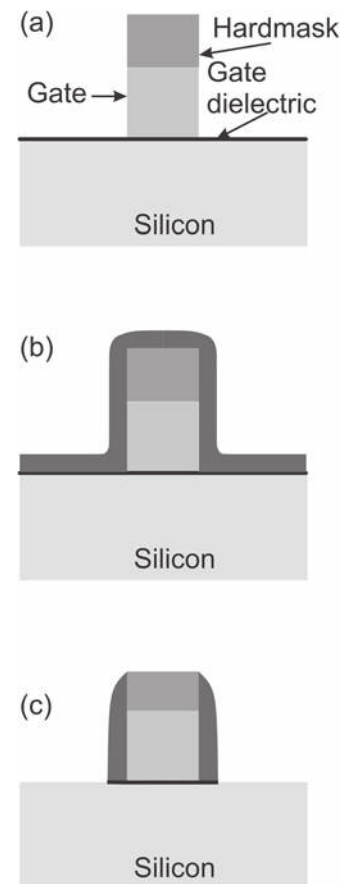


FIG. 35. Spacer process flow: (a) Gate with hard mask (b) after spacer-dielectric deposition (c) after etchback and gate-dielectric removal. Hard mask may or may not be present. The hard mask is typically SiO<sub>2</sub> or SiN; the spacer dielectric may or may not be the same dielectric.

used and it may be desired not to expose the Si substrate to the plasma, a thin layer of oxide is formed before the nitride deposition, and the etchback may consist of one or two steps, depending on the thickness of the nitride. The last step, selective to  $\text{SiO}_2$ , is carried out in a  $\text{CH}_3\text{F}$  (or  $\text{CH}_2\text{F}_2$ ) containing plasma that can be adjusted to obtain high nitride:oxide selectivity. The oxide layer can then be removed, exposing the silicon substrate below.

#### 4. Contacts

In this step, contacts are opened both to the gate and silicon substrate. If the first dielectric layer is planar, the depths of these contacts can be significantly different, depending on whether the contact is to be made to the gate or source and drain. Therefore, the selectivity to the gate material has to be high. The chemistries used for this step are usually  $\text{C}_4\text{F}_8$ ,  $\text{C}_5\text{F}_8$ , or  $\text{C}_4\text{F}_6$  based, and typically, a medium density plasma such as in a MERIE or multiple-frequency capacitively coupled etcher is used. A slightly tapered profile ( $88^\circ$ – $89^\circ$ ) is often desired to facilitate a good contact metal-fill. ARDE control is extremely important in this step. Although this step calls for equal size openings, there could be slight variability across the wafer. In addition, since the final aspect ratio of contacts to the source and drain regions can be considerably higher than the one to the gate, any etch rate reduction due to ARDE will inevitably lead to a long overetch of contacts to the gate (this is one motivation for using elevated source and drain regions). Selectivity to the underlying layer (Si,  $\text{SiN}$ , or silicide) is controlled by the thickness of the fluorocarbon film.<sup>282</sup> When the contact is terminated on silicide, excessive exposure of the silicided source and drain to ion bombardment can lead to junction degradation. This is generally addressed by a highly selective etch process that relies on a thick fluorocarbon layer for protection. In some integration schemes, an etch stop layer such as  $\text{SiN}_x$  covers the silicided gate, source, and drain, and a “soft” etch is used to clear all contacts simultaneously with minimal overetch. This approach is also used to form a borderless-contact,<sup>283</sup> where the contact to source or drain may overlap the isolation region and excessive oxide overetch is undesirable. When  $\text{SiN}_x$  is used for the etch-stop layer, a number of fluorocarbon gases can be used for etching; when high selectivity to  $\text{SiO}_2$  is desired, either  $\text{CH}_3\text{F}$  or  $\text{CH}_2\text{F}_2$  can be used for the nitride etch.

#### 5. Self-aligned contacts

In many instances, such as memory devices, it is desirable to have the contact to source or drain extremely close to the gate. Unfortunately, due to misalignment, the printed contact may overlap the gate, and eventually, once the contact is filled with metal, the gate and source (or drain) will be shorted. This can be overcome by encapsulating the gate with a dielectric resistant to the  $\text{SiO}_2$  etch chemistry used for opening the contact. Using  $\text{SiN}$  as the hard mask and spacer will achieve this goal.<sup>283</sup> The etch chemistry used for this

step is typically  $\text{C}_4\text{F}_8$  based which can be tuned to achieve high selectivity with respect to the nitride.<sup>282,284</sup> Once the  $\text{SiO}_2$  is cleared, a short step to remove the  $\text{SiN}$  and expose the source or drain is then performed (Fig. 36).

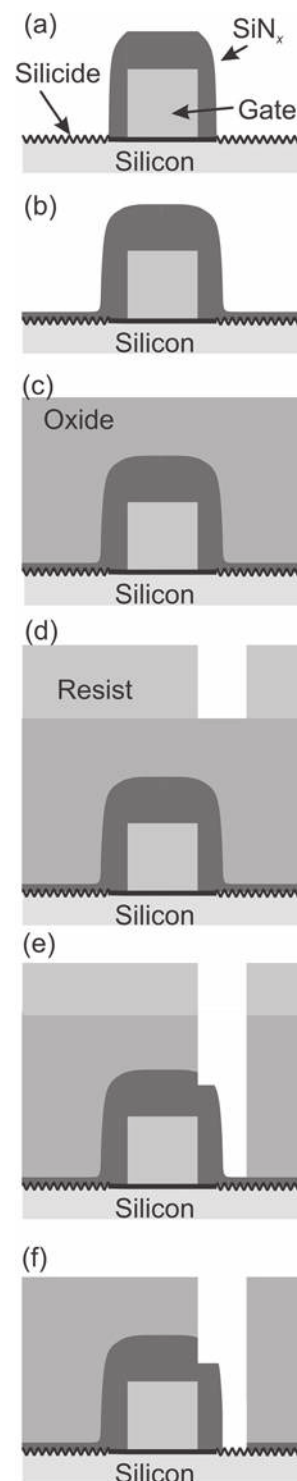


FIG. 36. One of many ways of self-aligned contact formation. (a) Gate is encapsulated with a blocking material that could be, for instance, LPCVD  $\text{Si}_3\text{N}_4$ , plasma CVD nitride or another blocking material. (b) A thin layer of blocking material is deposited. (c) First dielectric (usually BPSG) is deposited and planarized. (d) Lithography step to pattern contacts that could be misaligned. ARC, if used, is not shown. (e) Etching of BPSG selective to the blocking layer. (f) Etching of the blocking layer to expose the silicided source or drain and stripping of the resist.

## 6. Aluminum

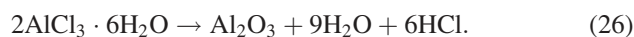
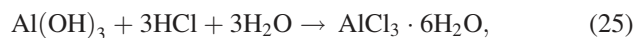
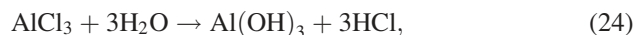
Aluminum based alloys were the dominant conductors for interconnect in VLSI circuits before the introduction of copper, although other metals, such as tungsten,<sup>263,285</sup> have been used occasionally. The aluminum alloys usually contain small amount of silicon and/or copper—the former to improve contact resistance when contact is made to the silicon substrate and the latter to control electromigration.<sup>286</sup> Since copper does not form volatile compounds with the chemistries used for aluminum etching (at the standard operating temperatures), its concentration is limited to less than 5%. When the Al layer is “sandwiched” between TiN layers, the same chemistry is used to etch the TiN layers (and the Ti that is used as an adhesion layer below the lower TiN layer) with possible variation of process conditions tailored for each layer.

Al will etch spontaneously in Cl<sub>2</sub> gas, but the presence of surface oxide inhibits etching. BCl<sub>3</sub>/Cl<sub>2</sub> mixtures<sup>287,288</sup> are commonly used for etching of Al, usually in a high-density plasma reactor, such as an ICP or ECR system. CCl<sub>4</sub>,<sup>288</sup> SiCl<sub>4</sub>,<sup>288</sup> and BBr<sub>3</sub> (Ref. 289) feed gases have also been used less frequently. The role of BCl<sub>3</sub> is to remove the native oxide on the aluminum,<sup>290</sup> scavenge any moisture in the chamber that may inhibit the etch process, and possibly to inhibit sidewall etching.<sup>291</sup> The interaction of the plasma with photoresist leads to formation of a layer on the sidewall that will prevent lateral etch of the aluminum,<sup>292</sup> but may lead to subsequent corrosion (discussed below). Sometimes an additive to the feed gas helps in the formation of sidewall passivation and can also be used to taper the metal lines. Typical additives are N<sub>2</sub> and CHF<sub>3</sub>,<sup>227</sup> but other polymer-forming additives have been used as well [e.g., CHCl<sub>3</sub> (Ref. 293)]. Although the additive may have a positive effect on the etched profile, it can cause particulate formation on the wafer due to the flaking off of deposits from the chamber walls. Therefore, the amount and type of the additives are important in establishing the optimum tradeoff between a desired profile and minimum wall deposits.

A hard mask can also be used for the pattern transfer. It has the advantage of minimized variation between isolated and nested aluminum lines, but since a major component of the etching process, the eroding photoresist, is absent, the etching process has to be modified. Etching in a low pressure (~2 mTorr) Cl<sub>2</sub>/HCl/N<sub>2</sub> plasma has been used successfully to pattern an aluminum stack consisting of TiN/Al/TiN/Ti.<sup>230</sup>

Etching uniformity is one of the challenges in aluminum etching.<sup>288</sup> Generally, the etch rate at the edge of the wafer is higher than the center and the metal is cleared in “bullseye” pattern. However, by process optimization and the use of focus-rings, the effect can be minimized.

Postetch corrosion is a major concern and it can be either purely chemical or galvanic. The chemical corrosion is associated with residual chlorides present on the wafer, especially on the sidewalls. Although during etching the wafer is heated to 50–70 °C to help volatilize the etch by-products, some AlCl<sub>3</sub> is embedded in the sidewall deposits, leading to chemical reactions with moisture in the air<sup>294</sup>



Al is also consumed by aqueous HCl



The process continues to corrode the aluminum, creating “worm”-like residues that are easily observed in an optical microscope (Fig. 37). The standard procedure to avoid chemical corrosion is to minimize sidewall deposits, heat the wafer during etching to the maximum temperature that will not reticulate the photoresist, and use a passivation step, combined with a partial or complete stripping of the photoresist. The passivation/strip is carried out by transferring the substrates in a load-lock, under vacuum, to a separate chamber designed specifically for that purpose (in earlier batch metal etchers, resist strip was carried out *in-situ* using an oxygen plasma with small amount of fluorine containing gas,<sup>227</sup> with the intention to convert the chlorides to noncorrosive fluorides). The passivation step is intended to convert the residual chlorides to volatile HCl and is accomplished by hydrogen-containing plasmas, typically water vapor.<sup>295</sup> Additional steps to reduce chemical corrosion are to heat the wafer after the passivation step on a hot stage in the etch tool, keeping the wafer under vacuum until the entire lot is etched, water rinse immediately after venting to dissolve any residues that are left, and chemical sidewall removal, followed by another resist ashing step to insure complete resist removal. Wafers should be kept in a dry-box before a capping oxide layer is deposited. The time interval between completion of the etch and the deposition step should be short, preferably less than 24 h.

Galvanic corrosion takes place when a galvanic cell is formed between two dissimilar metals in the presence of an electrolyte. The two metals in this case are the aluminum metal and the TiN layer(s) if used, and the electrolyte is the

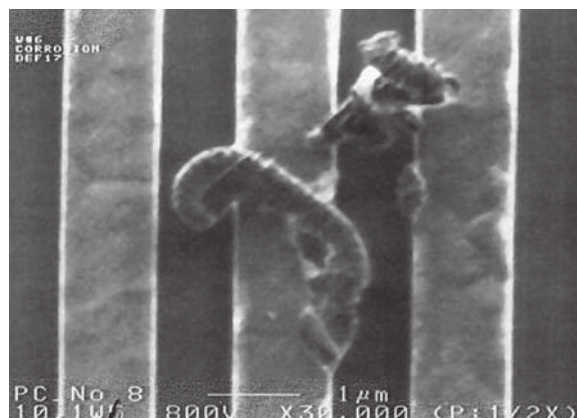


FIG. 37. Aluminum corrosion. The reaction by-products of the reaction between the chlorine-based residues, moisture, and aluminum are evident on top and the side of the etched metal lines. See text for details.



residual chlorides dissolved in water. This galvanic corrosion looks different than the chemical corrosion described above and is characterized by voids in the aluminum, while the TiN layer(s) is (are) intact. Usually, the TiN is oxidized, preventing the formation of the galvanic cell; however, if there are discontinuities in the film the cell can form, and often, galvanic corrosion is observed in a small number of sites. The galvanic corrosion is prevented by minimizing sidewall deposits, and a postetch rinse in an adequate amount of water: quick-dump-rinse or overflow-rinse are preferable to spin-rinse.

The major component in prevention of the two type of corrosion is the minimization of sidewall deposits. However, these deposits are necessary for anisotropic etch. The optimized etch process has to take into account these diametrically opposite requirements: just enough sidewall deposits to prevent undercut, but not enough to trap large amounts of residual chlorides.

## 7. Damascene structure

Modern metallization schemes utilize copper wiring inlaid in a dielectric,<sup>296,297</sup> producing structures similar to damascene ornaments, where precious metal is inlaid in another metal.<sup>298</sup>

Since metallization schemes involve a large number of metal layers, the entire structure is repeatedly planarized at every level. The first dielectric level, encapsulating the active area, is doped SiO<sub>2</sub> glass with metal (e.g., tungsten) filled contacts to the source, drain, and gates. All subsequent dielectric layers consist of low dielectric-constant material, such as organosilicate glass, which was solid in early implementations, and porous in subsequent technologies. The etching is accomplished with fluorocarbon-based plasmas and the F:C ratio is adjusted to minimize residues. Trenches (for intralevel interconnect) and vias (for interlevel interconnect) are formed within these layers, to be filled in subsequent steps with copper (in early versions with aluminum) and planarized by CMP. The resulting structure is a planar surface on which the next level is to be built in a similar fashion.

In a single-damascene scheme, contacts are made first to the level below through vias formed within the dielectric, to be filled with metal and polished to achieve planarity. The intralevel connection is achieved by another deposition of dielectric in which trenches are formed and filled with metal in a similar fashion described above. The more common process, however, is the dual-damascene scheme, where vias and trenches are etched before the metal fill step.

There are a number of approaches to create a dual-damascene structure with and without an intermediate etch layer that provides an etch-stop for the trench etching. The “via first” approach shown in Fig. 38(a) has evolved with time and has been the preferred implementation of dual-damascene structures. The version shown in this figure shows more recent implementation of the structure where no trench etch-stop layer is present within the low- $\kappa$  dielectric. In this approach, the via is etched to completion, resist is

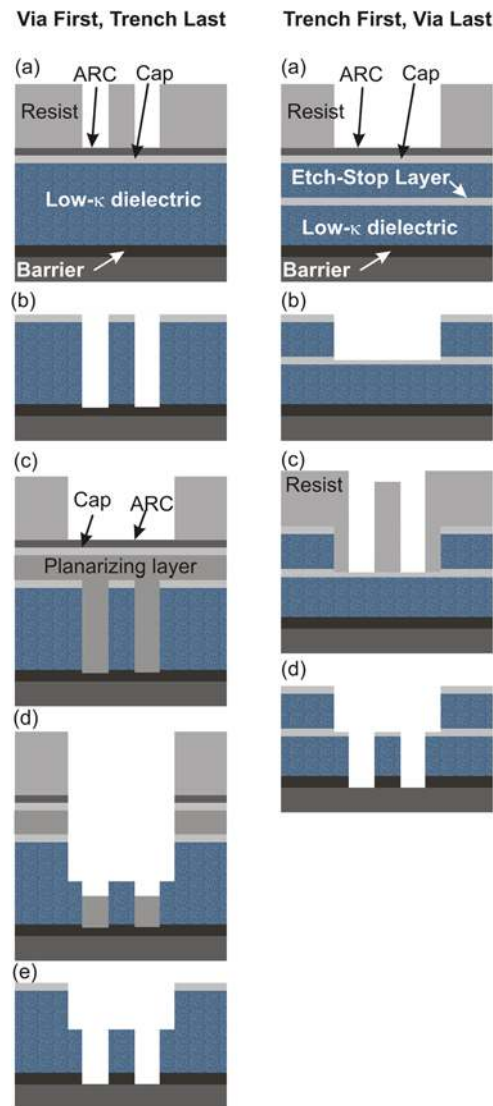


FIG. 38. (Color online) Dual damascene process flow. **Left: Via first, trench last.** (a) Via patterning on top of ARC and a cap layer; (b) Via pattern transfer and resist strip; (c) Trench patterning utilizing a planarizing layer to smooth the topography; (d) Trench pattern transfer with partial removal of the planarizing layer in the vias; (e) Complete removal of the planarizing layer, resist stripping, and barrier etch. **Right: Trench first, via last.** (a) Trench patterning on top of cap layer and ARC; (b) Trench pattern transfer, stopping on an etch-stop layer; (c) Via patterning; (d) Via pattern transfer, resist strip and barrier etch.

stripped (discussed below), followed by lithographic and etch steps to form the trench. A planarizing layer, capping layer (both absent in early implementations) and ARC are also shown. The role of the planarizing layer is to smooth the topography and, combined with the capping layer, it enables the use of a thin imaging layer. The pattern is first transferred to the capping layer (which could be either SiO<sub>2</sub> or SiN<sub>x</sub>, serving as a pattern-transfer layer) followed by a pattern transfer to the planarizing layer. The etch chemistry for the latter step is either O<sub>2</sub> or CO<sub>2</sub> based; the latter gives a more anisotropic profile than the former. Sometimes the ARC layer can serve in dual role as an antireflective layer as well as a pattern-transfer layer.

In the “trench first” approach [see Fig. 38(b), shown with a trench etch-stop layer], after the deposition of the low- $\kappa$  dielectric, trenches are patterned first by standard lithographic technique and etched to a finite depth into the dielectric. After resist removal, another lithographic step defines the via, and the etch process continues all the way to form the contact to the metal level below. A capping layer on top of the metal below is then etched in a low-bias process to reduce sidewall formation.

Since oxygen plasmas can degrade the low- $\kappa$  dielectric,<sup>299</sup> resist ashing is not performed in an oxygen plasma asher, but rather in a medium-density plasma (e.g., capacitively coupled plasma etcher), using plasmas with low-oxygen concentration or other chemistries, such as  $N_2/H_2$  based chemistry. Regardless of the ashing process used, some degradation of the dielectric is observed,<sup>299,300</sup> which is substantial for ultra low  $\kappa$  ( $\kappa < 2.3$ ) dielectrics. Therefore, newer dual-damascene schemes such as the trench first metal hard mask (TFMHM) approach attempt to minimize exposure of the low- $\kappa$  dielectric to resist-stripping plasmas.

TFMHM is the latest evolution in dual-damascene implementation, where the low- $\kappa$  dielectric is etched with a metal hard mask. In this approach, metal (usually TiN) is patterned first (Fig. 39) with a trench pattern and etched. After resist strip, the vias are patterned and partially etched into the dielectric, followed by resist strip, and simultaneous etching of trenches and vias. There are a number of advantages to this method, such as self-aligned vias,<sup>301,302</sup> and reduced degradation of the low- $\kappa$  dielectric associated with resist stripping.<sup>303</sup> However, other issues have to be dealt with, such as hard mask etching, and a clean etch of the dielectric without residues associated with sputtered hard mask material.<sup>301,302,304</sup>

## 8. FinFETs

To achieve higher performance at lower voltages, three dimensional transistors are finding their way into advanced devices. The fabrication involves creating “fins” in the substrate on which field effect transistors are built.<sup>305–307</sup> The gate wraps around the fins (Fig. 40) and depending on the number of the sides of the fin used to form the device, bigate or trigate FETs are created.<sup>308</sup> Figure 40 depicts a trigate device, while a bigate FET will have an insulator on top of the fin. There are two approaches for fabricating these devices, depending on the substrate—SOI or bulk silicon. These two approaches are shown in Figs. 40(a) and 40(b) for SOI and bulk silicon, respectively. The approach taken will depend on a number of factors, one of which is the cost of the substrate.<sup>309</sup> The gate width for a single-fin tri-gate device will be the sum of twice the height plus the width. Multiple fins can be used to achieve wider gates.

The height of the fins depends on the technology-node. For instance, at the 22 nm node, the fin is about 8 nm wide at its midheight and 34 nm high.<sup>310</sup> With SOI substrates, where the device-layer thickness equals the targeted fin-height, trench isolation is performed first, and then the fins are etched into the device layer, stopping on the buried-oxide

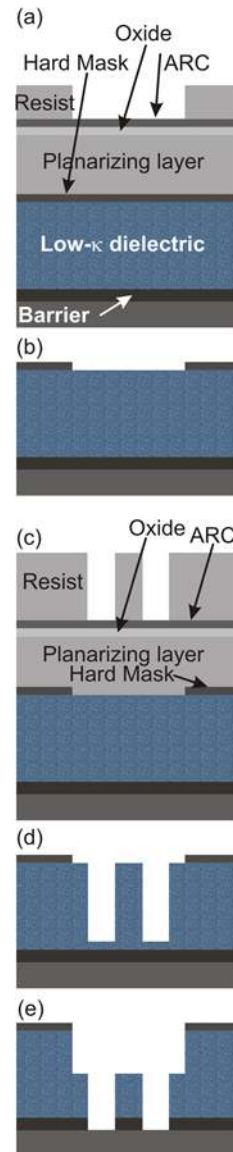


FIG. 39. (Color online) Dual damascene process flow—TFMHM. (a) Trench patterning on top of ARC, pattern-transfer layer (oxide), planarizing layer, and metal hard-mask; (b) Trench pattern in metal hard mask; (c) Via patterning; (d) Via pattern transfer into low- $\kappa$  dielectric; (e) Trench etching into the low- $\kappa$  dielectric, using the metal as a mask and barrier removal. Metal hard mask is removed in subsequent steps.

layer. If bulk silicon is used, the fins are etched at the same time as the isolation trenches, using a hard mask. Ideally, vertical fins are desired, and the etch is carried out in two step—the first to create the vertical profile needed for the fins, followed by an etch step that creates a tapered profile needed for the trench.<sup>311</sup> After oxide deposition and planarization, the oxide in the fin areas is etched back to the appropriate depth to expose the fins. Since the sidewalls of the fins are used for the active devices, surface roughness associated with the etch can lead to creation of interface-traps. This can be addressed by the etch process<sup>311</sup> and/or postetch surface treatment.

Once the fins are created, gate formation follows with either “gate first” or “gate last” approaches. The only difference between formation of planar and FinFET gates is the

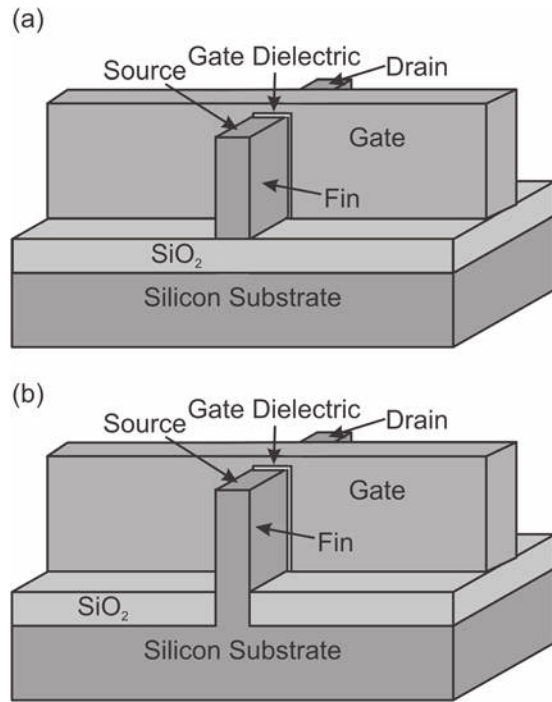


FIG. 40. FinFET with (a) SOI substrate and (b) bulk silicon substrate. The gate and the gate dielectric wrap the fins formed by etching silicon. The structure shown is a trigate, where three surfaces of the fin are used to form the gate.

long overetch-steps associated with the topography. In the gate-first approach, both metal-gate and hard mask have to be cleared,<sup>312</sup> while in the gate-last approach, the sacrificial polysilicon has to be etched in its entirety without penetrating the SiO<sub>2</sub> layer below. In both cases, the spacer formed before the source and drain construction must be cleared from the walls of the fins, while leaving the gate (or sacrificial gate) protected.

Evolution to more complex 3D devices is expected. The “Pi-Gate,” “Omega-FET,” and “Gate-All Around” as well as the use of new materials<sup>313,314</sup> will, no doubt, pose some integration and etching challenges in the future.

## D. Micromachining

Silicon-based MEMS can be fabricated by techniques similar to those used in silicon IC fabrication. Although ceramics, polymers, and metals are also MEMS materials, the focus of this review is on silicon-based systems only. As will be discussed below, etching techniques used for bulk micromachining have been adopted for etching TSV to facilitate electrical connections to the backside of the wafer.

Some MEMS involves fabrication of devices only on the surface of a silicon wafer, and the techniques used to fabricate these devices fall into the class of surface micromachining. Bulk micromachining involves utilizing a greater portion of the silicon wafer, typically more than 10  $\mu\text{m}$  of silicon.

### 1. Surface micromachining

The etch processes used for surface micromachining are similar, with some modifications to etch processes used in

IC fabrication. Cl<sub>2</sub> or HBr based processes are used to etch silicon, but in most cases, high selectivity to oxide is not required. CD control is important in some cases, and controlling CD when high aspect-ratio structures are desired could be quite challenging, similar to that encountered in the fabrication of trench capacitors in DRAMs.

In many cases, especially when high-aspect ratio structures are to be etched, a hard mask (SiO<sub>2</sub> or SiN<sub>x</sub>) is used. For these applications, SF<sub>6</sub>-based chemistry can be used. Profile control is a challenge, since SF<sub>6</sub> will tend to etch Si isotropically, but with the proper additive for sidewall passivation (e.g., C<sub>4</sub>F<sub>8</sub>, Cl<sub>2</sub>, or HBr), anisotropic profiles can be achieved (Fig. 41). If the process is terminated on an etch-stop layer, such as the BOX layer used in SOI wafers, the overetch step usually differs from the main etch step to avoid undercut during the overetch. This is accomplished either by modifying the gas flows and/or bias conditions, or switching to another etch chemistry, such as Cl<sub>2</sub>/HBr.

## 2. Bulk micromachining

Silicon bulk micromachining requires etching to depths greater than 10  $\mu\text{m}$ . It is commonly referred to as “deep reactive-ion-etching” (deep RIE or DRIE) and etch tools are modified high plasma-density etchers, with additional features to facilitate high etch rates with some degree of profile control.

To achieve high etch rates, SF<sub>6</sub> is the source gas, sometimes with the addition of O<sub>2</sub> primarily to reduce the chances of sulfur build-up in the exhaust line. To obtain anisotropy, the sidewalls of the features being etched must be passivated. One approach is to cool the substrate<sup>315–317</sup> to typically below 220 K (Ref. 317) and slow the rate of isotropic etching by F-atoms (see Fig. 15). (Ion-assisted etching processes typically have little or no temperature dependence.) The cold temperatures also lead to a buildup of SiO<sub>x</sub>F<sub>y</sub> by-products on the sidewalls, also suppressing isotropic etching.<sup>315,317</sup> It produces smoother sidewalls than the switched process described next, but sufficient time is needed for wafer cooling and warming before and after the etch, respectively. Once the wafer is warmed, the protection layer is volatilized, and if additional etch time is needed after

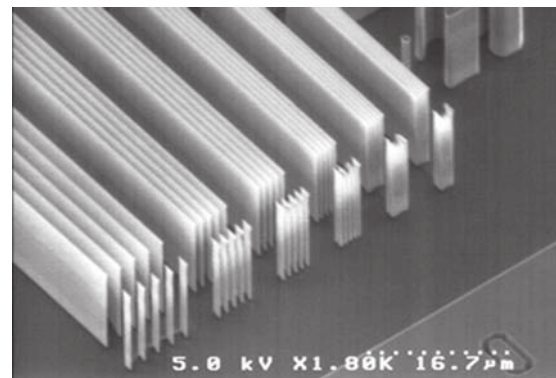


FIG. 41. Surface micromachining. The height of these features is 12  $\mu\text{m}$ , and the minimum dimension is 0.25  $\mu\text{m}$ .



postetch inspection, undercutting will occur due to the absence of a protection layer on the sidewall.<sup>317</sup>

A second method, known as the Bosch Process,<sup>318,319</sup> is a switched-gas process that utilizes alternate steps of etching with  $\text{SF}_6$  as the feed gas, and polymer deposition, usually with  $\text{C}_4\text{F}_8$  as the feed gas. The switched process is the one more commonly used, and it requires fast acting mass-flow-controllers to switch between etch and deposition steps, which occur every few seconds. An ICP etching tool is commonly used for the process and bias power is turned on only during the etch step and is kept low—only a few watts. Source power during the etch step depends on the total gas flow (to be discussed below). During the deposition step, polymer is being formed on the horizontal surface as well as on the sidewall. The etch step then removes the polymer from the horizontal surface, and proceeds with etching of silicon, while the remaining polymer on the sidewall, even though it is being eroded, provides protection against lateral etching. The resulting sidewalls show striations (Fig. 42), and may be an issue when smooth sidewalls are needed (e.g., mirror surface).

It is desirable to use etch mask and etch stop materials (if needed) that are resistant to the fluorine plasma.  $\text{SiO}_2$ ,  $\text{Al}_2\text{O}_3$ , and photoresist etch masks etch very slowly with selectivities with respect to silicon of 250:1, >10,000:1, and 50:1, respectively.<sup>320</sup>  $\text{SiO}_2$  and  $\text{Al}_2\text{O}_3$  can also be used as an etch stop material. Care must be used when choosing the etch stop and etch mask material such that the material chosen does not sputter during the etch to deposit nonvolatile products. This will cause “grass” to form in the etched areas due to micromasking.<sup>321</sup>

In many instances, the etch depths are hundreds of  $\mu\text{m}$ , sometimes the full thickness of a silicon wafer ( $725 \pm 25 \mu\text{m}$  for 200 mm diameter wafer). Therefore, a high etching rate is important. Etching rates can be increased by increasing gas flow, coupled with an increase in source power (Fig. 43). However, selectivity is reduced (the Si etching rate increases at a slower rate than does erosion of the mask), and it is claimed that this is due to increased ion flux.<sup>229</sup> Plasma

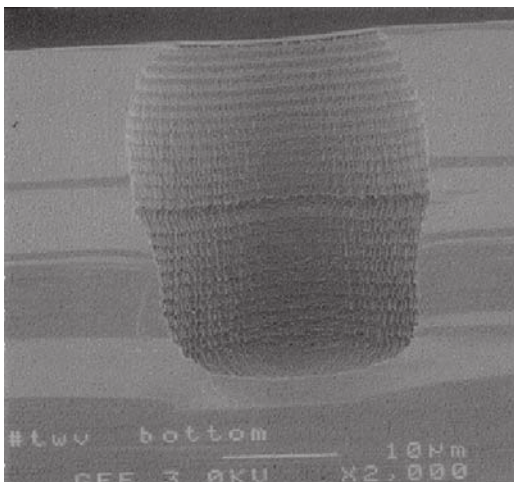


Fig. 42. Scallop associated with a switched (Bosch) process. The scallops are the result of alternate etch and deposition steps.

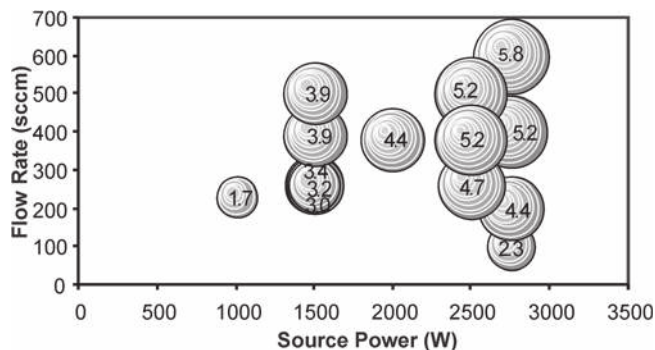


Fig. 43. Si etching rate in an  $\text{SF}_6$  plasma as a function of source power and flow-rate. Etching rates are given in  $\mu\text{m}/\text{min}$ . The “bubble” sizes are proportional to the etching rate.

source power affects ion energy distributions as well as ion flux. Ion-flux/energy control, offered on some etchers, is the key to achieving high etching rates without the adverse effects such as degraded selectivity mentioned above. One approach is to use pulse shape biasing.<sup>322,323</sup>

Etching of Si for MEMS devices has many of the same issues as for Si integrated circuit manufacturing. Etch rates are governed by the flux of reactants reaching the substrate surface. Therefore, etch rates drop as the total silicon area exposed to the plasma is increased (i.e., loading effect—Fig. 44). Therefore, Si etch rates for via patterning will be higher than for trench patterning. Although absolute etch rate is an important consideration, uniformity of the etching rate is important as well. Etching nonuniformity is less important when an etch stop layer is used, but selectivity and thickness of the etch stop layer must be adequate to offset the etching nonuniformity.

Another important structure in advanced MEMS as well as integrated circuits is a TSV, also known as through-wafer-via.<sup>324</sup> In MEMS fabrication, it enables electrical routing on the back of the wafer, freeing important “real estate” on the front of the wafer. The structure can also be used for bonding various MEMS modules to create a highly complex system, which combines MEMS and low and high-voltage control circuitry in one assembly.<sup>325</sup> In IC fabrication TSVs are used for 3D interconnects. There are number of ways to create electrical interconnect using TSV structures. They all

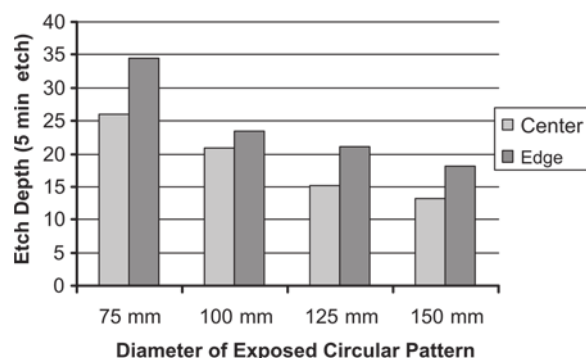


Fig. 44. Etch depth and uniformity (5 min in  $\text{SF}_6$  based etch) as total area of wafer exposed to plasma is increased. Process is not optimized for uniformity [after Bogart *et al.* (Ref. 321)].

involve creation of vias, depositing an insulating layer on the sidewalls, filling the via with conducting material, wafer thinning and stacking multiple wafers to create the 3D device.

### E. MRAM and FeRAM

Magnetoresistive and ferroelectric random-access-memory devices known as MRAM and FeRAM (or FRAM), respectively, are classes of nonvolatile RAM devices made of materials that do not form volatile compounds when etched in plasmas near room temperature.

**MRAM** memory cells utilize magnetic tunnel junctions to form a nonvolatile storage cell, integrated into the back-end processing of a CMOS device. Multiple stacked thin films form the cell. At a minimum, there are two magnetic layers separated by a thin dielectric layer. The magnetic moment orientation of one of the magnetic layers is fixed while the orientation of the moment of the second magnetic layer is free and it could be set by the control circuitry to be either parallel or antiparallel to the orientation of the fixed moment. The tunneling magnetoresistance will change based on the orientation of the moment of the free layer and that can be sensed by the CMOS circuitry. In reality, there are additional layers used to pin the moment of the fixed layer and prevent it from changing orientation during a “write” operation. The end result is a stack of thin (order of 1 nm or below) layers with  $\text{Al}_2\text{O}_3$  (Ref. 326) [or  $\text{MgO}$  (Ref. 327)] as the tunneling dielectric and magnetic materials such as Ni, Fe, Co, and their alloys, Ru, as well as IrMn or PtMn that serve as an antiferromagnetic pinning material (Fig. 45).

Unlike the etching of ferroelectric devices (see below), the etching of these stacks cannot be carried out at elevated temperatures due to the instability of the alloys used. Chlorine, bromine, and fluorine based chemistries can be used<sup>266,328,329</sup> to create compounds that are sputtered away, but postetch corrosion associated with residues on the wafer must be addressed.<sup>266</sup> In some instances ( $\text{NiFeCO}$ ), enhanced etch-rate in  $\text{Cl}_2/\text{Ar}$  plasmas with UV illumination has been observed,<sup>330</sup> but the mechanism is not well understood. Alternately, a

$\text{CO}/\text{NH}_3$  mixture has been demonstrated as another option, since it can form carbonyls that are volatile,<sup>331–334</sup> with some enhancement with the addition of Xe.<sup>335</sup> This process is not entirely chemical, however, and sputtering does take place, as evident from the thick sidewalls of redeposited sputtered material.<sup>336</sup> Another option to avoid patterning tough-to-etch materials is to use damascene structures. In this scenario, cavities are etched into the dielectric, and a stack of all of the above materials is deposited followed by planarization by CMP.<sup>266</sup> Although this solution seems simple, it basically transfers the difficulty from etch to the process of chemical–mechanical-polishing. There may be some other integration issues associated with this approach.

**FeRAM**, known also as FRAM or F-RAM, is a random access memory, where the memory cell consists of one capacitor and one access transistor, similar in structure to a DRAM. The dielectric in the capacitor is a ferroelectric material such as PZT, while materials such as Ir and  $\text{IrO}_2$  are used for the electrodes. Etching of the stack at temperatures above  $350^\circ\text{C}$  in a capacitively coupled plasma reactor with magnetic confinement yielded vertical profiles.<sup>63</sup> Chlorine and fluorine based gases together with oxygen and argon were part of the etch chemistry.

### VI. FUTURE

It has been said that “Studying the past is no sure guide to predicting the future.”<sup>337</sup> It has also been said, allegedly by Niels Bohr (and more recently, in a slightly different manner by others, including Yogi Berra), that “Prediction is very difficult, especially about the future.”<sup>338</sup> Nevertheless, for an industry with annual sale of roughly  $\$300 \times 10^9$ ,<sup>339</sup> some judicial assessment of future technologies is needed. The semiconductor industry, like others, develops and lives by roadmaps. The corresponding roadmap is the International Technical Roadmap for Semiconductors (ITRS, published in earlier editions by the Semiconductor Industry Association as the National Technical Roadmap for Semiconductors),<sup>340</sup> revised annually, with complete reports published biennially. Over time, changes in the ITRS may be significant; however, it is a blueprint for evolution of devices, technology, and processes, and it gives guidance to research and development efforts. The discussion below is based loosely on future device and technology requirements, covered in the relevant chapters of the 2011 edition of the ITRS.<sup>341–346</sup>

#### A. Patterning

Aside from advances in lithographic techniques, such as using next-generation-lithography tools, there are numerous techniques to achieve sub-lithographic features. Some involve pure lithographic methods, such as double-exposure,<sup>346</sup> some rely on combinations of lithography and etching, and other approaches use solely etching techniques to define features smaller than the capability of the lithographic tool. A number of methods have been proposed; some are beginning to find their way into manufacturing, while some are at the early stage of development and assessment of their capabilities and limitations. Some techniques are more

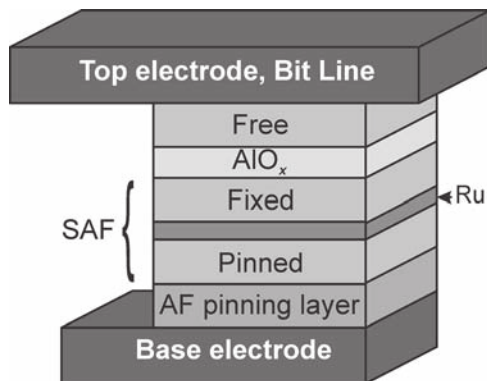


FIG. 45. MRAM capacitor structure. The free, fixed, and pinned layers are usually alloys of Co, Ni, and Fe. The fixed, pinned and ruthenium layers form a synthetic antiferromagnet (SAF) layer. The antiferromagnetic (AF) pinning layer (IrMn or PtMn) is used to prevent the SAF from responding to write operations [after Engel *et al.* (Ref. 326)].

appropriate for less dense logic devices, while others are intended for dense structures.

The method of **trimming** is discussed in the section on gate patterning, and it has been in use in production for a number of years. It is adequate for isolated lines, but not for creating dense patterns. Aside from CD control issues, there are also limitations associated with thinning of the resist as the result of the trimming operation.

The method of **double patterning** (DP)<sup>346–348</sup> utilizes two lithography and etch steps to pattern a single layer, which is then used to transfer the pattern to the target layer (e.g., gate, trench, etc.). It is often referred to as the litho-etch-litho-etch (LELE) method.<sup>346</sup> The technique is illustrated in Fig. 46; after the first lithographic step [Fig. 46(a)], a hard mask is etched, followed by resist strip [Fig. 46(b)] and another lithographic step [Fig. 46(c)], where additional features are printed and etched to create a dense pattern after the resist is stripped [Fig. 46(d)]. The resulting hard mask is then used to etch the target layer [Fig. 46(e)].

**Spacer double patterning** approaches come in two varieties, positive and negative tones. In the positive tone approach

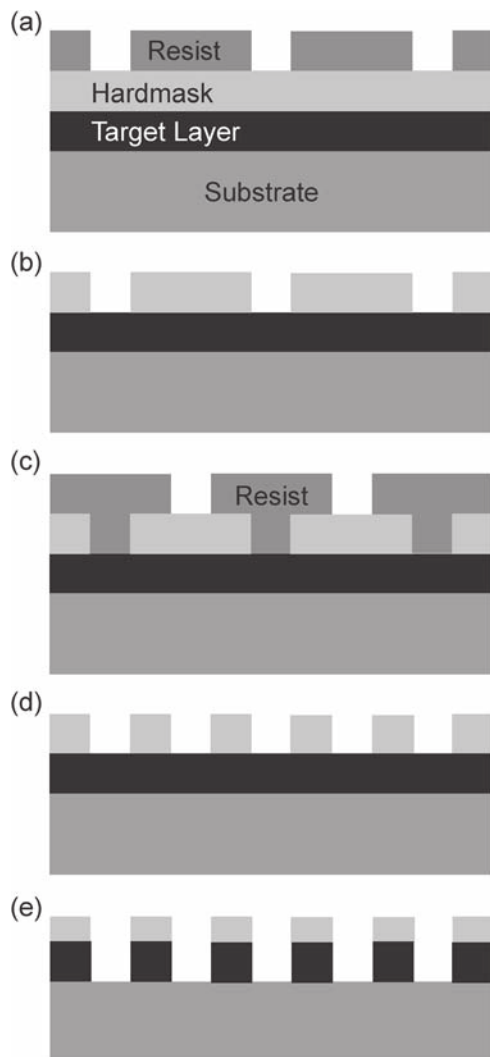


FIG. 46. Double patterning (DP): (a) First lithographic step. (b) Hard mask is etched, followed by resist strip. (c) Second lithographic step. (d) Hard mask etched and resist stripped. (e) Pattern transfer to the target layer.

(known also as **self-aligned double patterning**<sup>349–351</sup> or **side-wall image transfer**<sup>352</sup>), the sidewall-spacer is used as the hard mask for pattern-transfer to create features well under the lithographic capability of the lithographic tool. The concept is not new; it was first used by utilizing sidewall deposits formed during trilevel etching,<sup>353</sup> where the etched hard-baked resist was ashed away, leaving the sidewalls as the mask for the pattern transfer.<sup>354</sup> Similarly, small platinum features, 50 nm wide, were fabricated by sputtering away platinum films deposited on amorphous-silicon sacrificial structures that were subsequently removed by chemical dry etching.<sup>355</sup>

In the positive tone approach, the size of the features is controlled by the CVD and etch processes, while the space between the features is determined by lithography. The method, shown in Fig. 47, can be used when all the features are of equal size, such as the fins in FinFETs. The first step in using this technique is to create structures (mandrels), on top of the target layer [Fig. 47(a)] that will be used to construct the sublithographic features. After CVD and etch, sidewall-spacers are created [Fig. 47(b)], followed by the removal of the mandrels [Fig. 47(c)], pattern transfer and spacer removal to create the desired structure in the target layer [Fig. 47(d)]. The mandrel material will depend on the application. To fabricate the fins for FinFETs, for instance, the mandrel could be amorphous carbon, patterned with photoresist (possibly after trimming, discussed above, and using SiO<sub>2</sub> or SiN as the pattern-transfer layer), while the spacer material is SiO<sub>2</sub> or SiN. The spacer remaining after the ashing can be used as the hardmask for the pattern transfer directly into the silicon to create the fins. Another application of the technique is metal gates on high- $\kappa$  dielectrics.

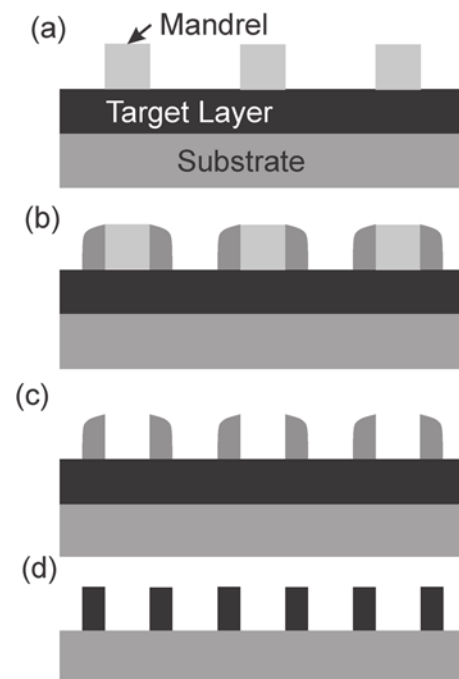


FIG. 47. Spacer double patterning—positive tone: (a) Create mandrels on top of the target layer. (b) Form sidewall spacers by CVD and etch-back. (c) Removal of the mandrels. (d) Pattern transfer and spacer removal to create the desired structure in the target layer.



In the negative tone approach, dense features can be created, and their widths need not be the same. In this case the spacers are disposable.<sup>351,356</sup> Following the formation of the mask [e.g., SiO<sub>2</sub>, SiN, or polysilicon, Fig. 48(a)] on top of the target layer (which could be either a device layer or a hardmask used for the pattern-transfer to the device layer), a spacer is formed by deposition and etchback [Fig. 48(b)]. A layer of oxide is then deposited to fill the gap between the feature [Fig. 48(c)], followed by etchback or CMP to expose the spacers [Fig. 48(d)]. The spacers are then removed to create a dense pattern shown in Fig. 48(e), which is then used to transfer the pattern to the target layer. The choice of materials will obviously depend on the application. Jung *et al.* used the technique to create a dense pattern in a target layer consisting of 50 nm SiON on top of 200 nm amorphous-carbon.<sup>356</sup> In this case, the mask was 200 nm polysilicon, the sacrificial spacer-sidewall was 20 nm fluorocarbon and the gap-fill material was spin-on glass.

**Self-aligned quadruple patterning (SAQP)**<sup>349,357</sup> is an extension of the self-aligned double patterning described above. In this case, the first mandrel is used to create a denser pattern in a 2nd mandrel layer, as shown in Fig. 49. After the formation of the first mandrel [Fig. 49(a)], spacers are formed [Fig. 49(b)], and the mandrels are removed

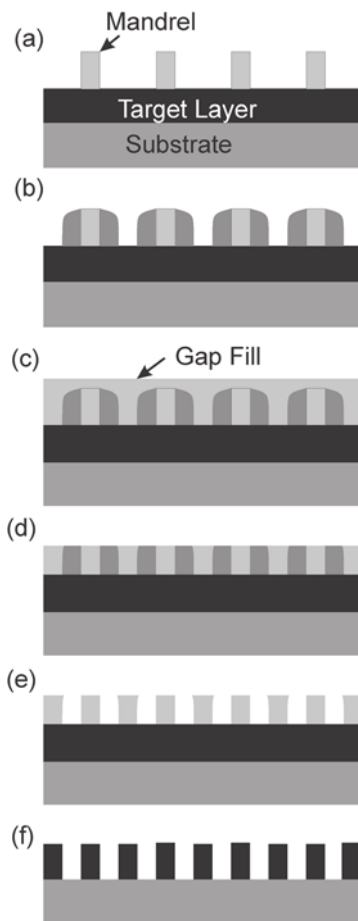


FIG. 48. Spacer double patterning—negative tone: (a) Create mandrels on top of the target layer. (b) Create sidewall spacers by CVD and etch-back. (c) Gap fill. (d) CMP or etch back to expose the spacers and the mandrels. (e) Remove the spacers. (f) Pattern transfer to the target layer.

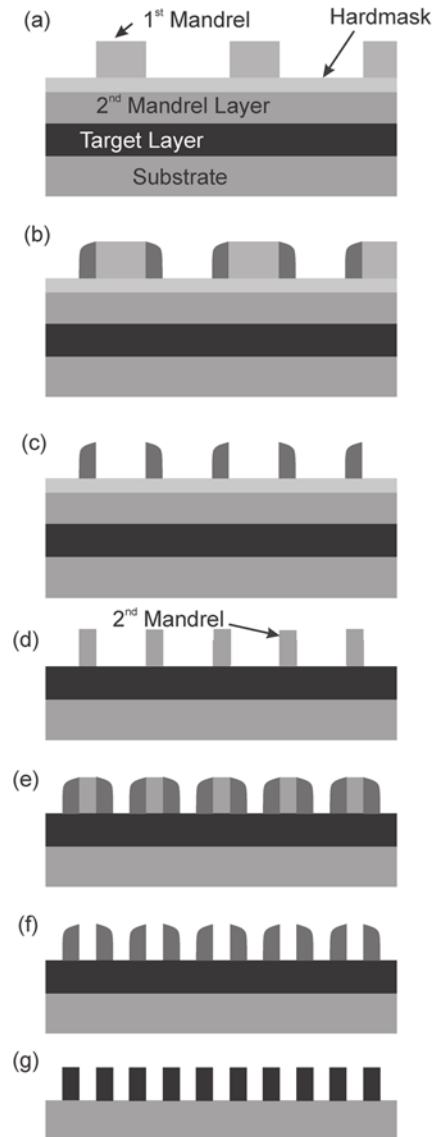


FIG. 49. SAQP: (a) Create first mandrels on top of a hard mask layer. (b) Form sidewall spacers by CVD and etch-back. (c) Remove first mandrels. (d) Use the features created by the previous step for pattern transfer into the second mandrel layer. (e) Form sidewall spacers by CVD and etch-back. (f) Remove second mandrels. (g) Transfer pattern to the target layer.

[Fig. 49(c)]. The remaining features are then used to transfer the pattern to the hard mask and form a second mandrel [Fig. 49(d)]. After spacer formation [Fig. 49(e)], and mandrel removal [Fig. 49(f)], the pattern is transferred to the target layer [Fig. 49(g)].

In another variation, **self-aligned triple patterning** is claimed to offer some advantages over the other multipatterning schemes.<sup>349,357,358</sup> The technique involves the creation of two consecutive spacers, the first of which is sacrificial. The mandrels in this case are not sacrificial, and can be used, in addition to the spacers, as the hard mask for the pattern transfer. Details can be found in the references cited.

## B. Linewidth roughness and line-edge roughness

Linewidth roughness (LWR) and line-edge roughness (LER) are related quantities that affect CD control. LWR is

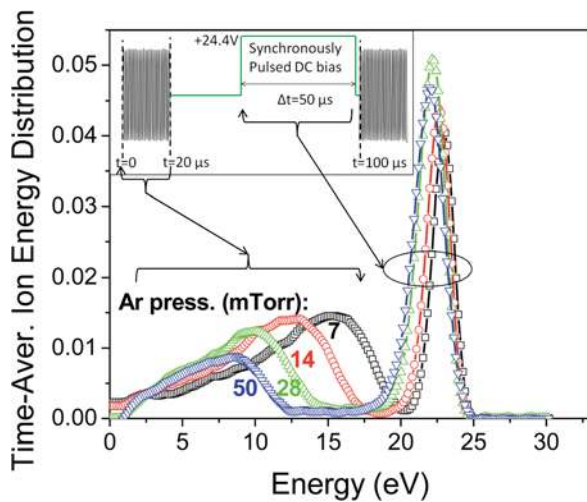


FIG. 50. (Color online) Ion energy distributions obtained in a pulsed ICP with synchronous pulsed DC bias of a boundary electrode (Ref. 434).

a measure of variation in width of the line expressed in  $3\sigma$ , while LER is the variation from a straight line along the edge of the line (also expressed in  $3\sigma$ ).<sup>359,360</sup> The guidelines for low-frequency LWR are generally less than 8% of the CD,<sup>346</sup> and it can occur immediately after the resist is patterned, with amplification during the pattern-transfer.<sup>361</sup> Low-frequency line-edge roughness is linked to fluctuation in CD,<sup>359,360</sup> while high frequency LER in polysilicon gate can lead to enhanced lateral diffusion, ultimately causing reduced channel-length.<sup>362</sup> The roughness is an issue that is becoming more critical as CD decreases, since LWR does not scale with linewidth shrink. In the etch process, it is associated with plasma interaction with the photoresist,<sup>361</sup> which roughens the surface, thus causing edge roughness, especially if the resist is chemically amplified.<sup>363,364</sup> Ion bombardment, plasma radicals, and polymers deposited during the etch are claimed to be contributors to the resist roughness.<sup>363</sup> Also, photons and heat have been shown to synergistically cause LER.<sup>361,364</sup> Although the etch process can be tuned to reduce the effect,<sup>365</sup> it is clear that more robust resists are necessary in the future to reduce LWR and LER in the patterned resist as well as in the postetch pattern. Nonchemically amplified resists are claimed to be the solution for the problem, but they may present a different set of challenges for the etching process. One option considered is the use of inorganic resists,<sup>366</sup> which, depending on the material, may be easy or difficult to remove after the etch. For instance, one candidate contains both Hf and Zr and exhibits  $>7:1$   $\text{SiO}_2$ :resist selectivity,<sup>367</sup> so removal of the material after the pattern transfer may be a challenge.

### C. New materials

Silicon continues to be the substrate material for the foreseeable future, but SiC is emerging as the material of choice in some applications.<sup>368</sup> In silicon devices, other materials are expected to be incorporated in the future. Alternate channel materials with high mobility are of great interest, and their integration to large-scale devices may be quite

challenging. The list of materials of interest is long and includes  $n$ -InGaAs and  $p$ -Ge in the near future, and other III-V materials,  $n$ -Ge, carbon nanotubes, and graphene in future technologies.<sup>344</sup> All of these materials are expected to be grown epitaxially (there may be other options for graphene<sup>369</sup>), but forming a good contact to some of these materials (e.g., graphene) is a major challenge.

The implementation of high- $\kappa$  materials as the gate dielectrics has addressed the high leakage current density associated with thin effective-oxide-thickness (EOT), but future devices may require even higher- $\kappa$  materials [e.g.,  $\text{TiO}_2$  (Ref. 344)] than the current Hf based dielectric to reduce EOT even further. Removal of these materials from the substrate with no appreciable damage will have to be addressed.

Although there is some discussion on using carbon nanotubes<sup>345</sup> as a potential interconnect material, in all likelihood copper will be the conductor of choice for some time, and the focus for improved performance will be the reduction of the dielectric-constant of the interlevel dielectric. The pore-volume in the dielectric is expected to increase, leading to  $\kappa$  values below 2.0. Etching the highly porous material, postetch-cleans as well as its integration into current metallization scheme are doable, but may not be simple extension of current processes. One material is pure-silica-zeolite<sup>370</sup> which, depending on its porosity, could reach  $\kappa$  values below 2.3, but with an increase in leakage current. Alternately, a nonporous low- $\kappa$  dielectric can be used. A polycarbosilane-based dielectric with a  $\kappa$  value as low as 2.32 and low leakage current is one choice.<sup>371</sup> The advantage of this material is that once it cured, it resists copper diffusion into the dielectric (attributed to the lack of oxygen in the dielectric), thus enabling copper metallization without the need for a barrier material in the vias and trenches. As a result, lower resistivity interconnects can be realized with this material compared to a dielectric where a barrier material is needed.<sup>342</sup> A carbon-rich fluorocarbon material with  $k < 2$  also has been reported.<sup>372</sup> The material is deposited by a plasma discharge of  $\text{C}_5\text{F}_8$  and Ar. It exhibits good adhesion to the SiCN barrier layer, and good thermal and mechanical properties. The ultimate goal for reduction of  $\kappa$  value is a number close to 1.0. This will be discussed in the following section.

High- $\kappa$  dielectrics have been introduced to DRAMs as well to maintain the capacitance as the device dimensions shrink. Current capacitor structures utilize TiN as the electrode material with high- $\kappa$  insulator as the dielectric (TiN/insulator/TiN or TIT structure).<sup>373</sup>  $\text{Hf}_x\text{Al}_y\text{O}_z$  dielectrics were used initially,<sup>373,374</sup> but they have been replaced by  $\text{ZrO}_2/\text{Al}_2\text{O}_3/\text{ZrO}_2$  (ZAZ)<sup>373,375</sup> at the 40–30 nm half-pitch technology nodes, to achieve EOT of 6.3 Å.<sup>375</sup> Future replacement with perovskite structure materials will have a higher  $\kappa$  value.<sup>376</sup> Etching of these materials is not required, since they are incorporated in a capacitor structure that currently requires formation of cylindrical cavities in oxide, with no need to etch these dielectrics (see discussion on structures below).

Other memory devices in the near future, phase-change memories (PCM, known also as phase-change random

access memory, or PRAM devices), utilize changes in resistivity of chalcogenides in their amorphous and crystalline states to create nonvolatile memories.<sup>340,344</sup> These devices are seen as a future replacement of Flash memory, and in some applications, as replacements for DRAM and static random access memory. PCM devices are already commercially available for mobile applications, with endurance of  $10^6$  write-cycles in current product offering,<sup>377</sup> and a potential of increased reliability in future devices ( $6.5 \times 10^{15}$  cycles in one recent publication).<sup>378</sup>

It seems that most of the new materials to be introduced in future devices will not require new etching processes and they will be incorporated into structures formed in traditional materials.

#### D. New structures

The ITRS lists a large number of emerging devices that are in different stages of research or development. Obviously, only a small number will be commercialized. At this stage, it is not clear what role plasma etching will play in the fabrication of these devices. In the following discussion, we will concentrate on structures where plasma etching may be important.

3D structures are expected in most if not all devices in the near and distant future. FinFETs are now used in manufacturing of advanced ICs and are expected to become more ubiquitous. The current trigate structure is expected evolve to “Pi-Gate,” “Omega-FET” and “Gate-All Around” structures (see discussion of FinFETs in Sec. V C). In forming these structures, control of the damage to the underlying substrate will be highly important. Various modifications of FinFETs have been implemented for DRAM applications. The combined structure of saddle FinFET (S-Fin)<sup>379</sup> and Recessed Channel Array Transistor<sup>380</sup> or R-FinFET seem to be the preferred structure for current and future generation of DRAMs.<sup>381</sup>

The DRAM capacitor has evolved over time too. Since minimum capacitance of roughly 25–30 fF per cell is required regardless of the technology node (as determined by the sensing circuit, data retention requirements, and single disrupting events, such as alpha particles and cosmic radiation<sup>382</sup>), the capacitor structure has evolved to maintain this minimum value with reduction in the area occupied on the device. The initial planar capacitor was replaced by a trench<sup>382</sup> and stacked capacitors.<sup>382,383</sup> The latter has evolved with time to a 3D, cylindrical-cavity structure<sup>383</sup> with the use of high- $\kappa$  dielectrics. The capacitor structure is expected to change to a pillar type as device dimensions and dielectric thickness shrink further.<sup>344</sup> Bonding of multiple DRAM chips vertically (with the use of through-wafer-vias) to form high-capacity devices is also expected.<sup>383–385</sup>

In interlevel metallization, the goal is to lower the dielectric constant with the ultimate goal of  $\kappa$  close to 1.0. One way to achieve this is by using nonconformal interdielectric deposition that will lead to void formation between the metal lines.<sup>386–389</sup> In this approach, the dielectric between the metal interconnect is etched away, followed by the

nonconformal deposition of the dielectric. An alternate approach is to use a sacrificial material to build the entire metallization structure, to be removed (at least partially) later-on,<sup>390</sup> creating a structure that is generally devoid of solid dielectric between the lines. Reactive gas can be used to remove some sacrificial materials.<sup>387,391,392</sup> Other sacrificial materials can be removed by thermal decomposition, with the resulting gases diffusing through the capping layer.<sup>393–395</sup> Regardless of the method used, numerous etching, integration, packaging, and reliability issues must be addressed before this scheme becomes viable.

Quantum computing is an area of active research that promises to deliver future computing power far exceeding what is available today.<sup>396,397</sup> Some of the approaches are based on a nuclear spin of  $^{31}\text{P}$  donor in silicon,<sup>398–400</sup> quantum dots,<sup>401–403</sup> and ion traps,<sup>404–410</sup> and many of the fabrication steps are similar to the ones used in IC and MEMS fabrication today.

Clearly, regardless the path chosen from the choices above, device dimensions will continue to shrink, and the requirements for high-fidelity pattern transfer as well as reduction in damage and particle formation will become ever more stringent. As new 3D structures are introduced, selective and residue-free etch processes will be even more challenging.

#### E. Improved processes and equipment

One obvious source of concern for future device technologies is the particles that may be generated in the chamber and end up on the wafer before or during etching. Since the size of particles must be much smaller than the smallest device dimension, the fraction of particles in a given size distribution that qualify as “killer defects” keeps increasing over time. Particles are generated by the process, as deposits flake from the chamber walls and fall on the wafer. They can also arise from erosion of materials in the chamber. Process generated particles can be addressed by frequent cleaning of the chamber wall (e.g., between wafers), or by trapping the particles in a polymer coating.<sup>54</sup> The approach taken will be process dependent. Particles generated by the degradation of material in the chamber can be mitigated by choice of better materials and/or replacement of components in the chamber at frequent intervals. Chamber materials, including coatings, will likely become even more important in the future for both particle generation and for consistency in etching behavior over time.

Better control of ion and neutral fluxes as well as ion energy will be required to address issues such as CD control, ARDE, line-edge roughness, and lattice damage due to ion bombardment. In addition, improvements in the precise control of amount of material removed and etch uniformity will be needed.

Since vertical dimensions (with the exception of the photoresist mask) do not decrease as much as the width of devices shrinks, aspect ratios of contacts and trenches continue to increase. Therefore, ARDE control is important both to compensate for variation in the lithography-defined features



as well as changing aspect-ratio with time. In principle, longer etch-time may be used to compensate for the etch-rate reduction; however, the thin photoresist may erode before the etch process is complete. It has been shown that control of the ion/neutral ratio is the key to reduction of aspect-ratio dependent etch rate of dielectrics.<sup>215,217</sup> This was accomplished by changing process parameters, such as pressure and fluorocarbon feed gas fraction.<sup>217</sup> However, these conditions tend to lead to high polymer deposition, which can suppress etching entirely, and do not offer sufficient selectivity to current thinner photoresist. Bias power pulsing seems to offer an additional means for controlling ARDE,<sup>53,54</sup> without changing pressure or gas flows, by operating in an ion-limited regime.<sup>162,411</sup> In this case, the neutral flux stays nearly constant, but ion-flux is controlled by the on/off cycle of the bias. Although etching rates may still be decreased by the increased aspect-ratio, the required longer etch times are not prohibitive. With bias pulsing, photoresist erosion is reduced more than the dielectric etching rates, increasing selectivity to photoresist as compared to continuous-wave plasmas.

As discussed above, line-edge roughness has been always a concern, but it has become more acute as device dimensions shrink. Roughness along the edges of photoresist has been shown to be induced by a combination of exposure to UV light, ion bombardment, and heat.<sup>80,412</sup> Preliminary results have shown<sup>53</sup> that time modulation of neutrals, where conditions are repeatedly switched from depositing polymer on the sides of the photoresist (and tops) to etching, can prevent rough edges on the photoresist. This is done while keeping the ion flux constant.

Using pulsed plasmas may be the potential solution to other concerns too, such as surface damage to the layer exposed to the plasma. In the past, the solution has been to remove the damaged layer either by chemical etching (e.g., downstream etching) or by oxidizing the surface and removing the oxide in HF solution. This loss of material is becoming less tolerable now and will be too high a price to pay in future device technologies.

Two general areas of research have re-emerged to address many of these issues: time-modulated plasmas and neutral beam etching. Pulsed plasmas have been an active area of research for many years.<sup>413–430</sup> In most of these early studies, the plasma-generating power was modulated; in a few instances, pulsed bias was also investigated. RF or microwave power is modulated at frequencies of typically  $\sim 10$  kHz, and  $\sim 50\%$  duty cycle. Within  $\sim 10$   $\mu$ s of the power being turned off,  $T_e$  drops from several eV to  $\sim 1$  eV and then more slowly to  $< 0.5$  eV. During this time, the positive ion density decays only some near the center of the plasma, but can stay constant or even increase near the edge of the plasma.<sup>429,431</sup> If the plasma is in a highly electronegative gas (e.g.,  $\text{Cl}_2$ ), then the electron density will decay rapidly in the afterglow (power off) period, due to dissociative attachment and formation of negative ions (e.g.,  $\text{Cl}^-$ ). Deep into the afterglow period in such plasmas, the negative ion density can greatly exceed the electron density, causing the sheaths to collapse and the negative ions can then reach surfaces, as

they are no longer repelled by the negative potential difference between surfaces and the plasma. If, under these ion-ion plasma conditions, a positive bias is applied to the substrate (usually the positive period of RF bias at frequencies well below the ion response frequency), then negative ions can be accelerated to the substrate surface.<sup>430</sup> With negative bias, positive ions bombard the surface, so with equal portion positive and negative bias at low RF bias frequencies, the differential charging problems obtained with electrons as the negative charge carrier can be greatly reduced.<sup>432</sup> Apparently, this approach has not been used in commercial etching processes to date, but could become important again in the future.

Pulsed plasmas also allow very narrow ion energy distributions to be obtained for most of the afterglow period.<sup>433,434</sup> By applying bias synchronously in the afterglow, a nearly monoenergetic IED can be obtained, as shown in Fig. 50. The wafer will of course be bombarded by ions during the power-on portion of the cycle, but with the bias off, and the pressure high enough that  $T_e < 2$ , the ion energy will not exceed  $\sim 10$  eV (the low energy portion of the IED in Fig. 50). This could allow very high selectivities to be obtained by tuning the IED to be above threshold for one material (e.g., Si) and below that for another (e.g.,  $\text{SiO}_2$ ), making it possible to obtain near-infinite selectivities. (Of course etching rates will be low, but for many applications this is not an important constraint.) As discussed above, when Si is etched in a  $\text{Cl}_2/\text{Ar}$  plasma under these conditions (Fig. 20), the etching rate increases with ion energy above a threshold energy in a manner that is consistent with beam studies, but with a substantial etching below the ion threshold energy. This component has been ascribed to etching assisted by the light generated by the plasma, mainly in the VUV.<sup>167</sup> It should be noted that pulsed plasmas produce little VUV light in the off portion, and therefore less average VUV light while maintaining high positive ion density. The ion flux during the off portion is reduced by  $\sim T_e^{-1/2}$ , so there should be a net gain in the ion-to-VUV photon flux ratio for pulsed plasmas, perhaps suppressing photo-assisted etching, photoresist degradation, and defect generation in sensitive regions of circuits. This could also be of added importance in future devices with small dimensions.

Synchronization of source and bias powers<sup>435</sup> as well as tailored the waveforms<sup>322</sup> have also been explored specifically for finer control of etching processes. The idea behind the tailored bias waveform is to invert the problem of letting the waveform determine the IED. Instead choose a desired IED and then determine the waveform that will produce that IED, synthesize it, and apply it to the substrate.<sup>436</sup>

Another way to suppress all forms of plasma damage associated with positive ions, electrons, or photons is to bring the substrate out of the plasma and use directed, energetic neutral beams instead of ions to induce etching. Since positive ions are neutralized before striking the surface, the energy dependence of the etching yields for neutrals is expected to be the same as those of ions. Neutral beam assisted etching was explored in the mid 1990s and then largely abandoned.<sup>437–439</sup> Recently, however, there has been

a re-emergence of interest in neutral beam etching. These studies extract neutral beams by allowing ions extracted from a plasma to make glancing angle collisions with the walls of high aspect ratio holes in a grid.<sup>440,441</sup> One such system for etching is shown in Fig. 51.<sup>442</sup>

Either positive or negative ions from an ICP are allowed to enter a high aspect ratio grid plate. For negative ions in a strongly attaching gas like chlorine, a pulsed plasma must be used and negative ions are extracted deep in the afterglow. The ions entering the grid are accelerated by an imposed potential, and are neutralized by specular collision with the grid wall, forming a highly directed, energetic neutral beam. The beam can retain a large portion of the velocity of the incoming ion.<sup>443</sup> This mostly neutral energetic beam, along with background gas, enters the processing chamber below. The etching mechanism is similar to the synergistic ion-assisted process, but with few charged species. These conditions have been used to etch various nanostructures including Si IC FinFETS<sup>440</sup> and Si quantum dots,<sup>440</sup> as well as GaAs/AlGaAs heterojunction nanopillars.<sup>444</sup> A transmission electron micrograph (TEM) of the Si quantum dot structure is reproduced in Fig. 52. The mask for this structure was ferritin, a 7 nm diameter spherical protein. The TEM reveals little if any disruption of the Si crystal lattice below the sidewall surfaces. The authors conclude that neutral beam etching creates such little damage because the VUV light levels are so much lower than in conventional plasma etching.

Atomic layer deposition (ALD) has become a mainstream technology for high- $\kappa$  dielectrics. In this process, two alternating half steps are carried out to first deposit a metal and then oxidize it. Each half step is self limited. The metal deposition follows Langmuir–Hinshelwood kinetics, leaving the surface covered with a saturated layer of metal that is up to one monolayer. This metal layer is then completely oxidized in the second half step. Rapid gas pulsing brings the process from one step to the next. The process is repeated many times to grow precisely the same amount of material all over the wafer.

Atomic layer etching (ALET), the analog to ALD, is attractive for similar reasons. For example, if an etching process could be made self-limiting in the same manner, it could

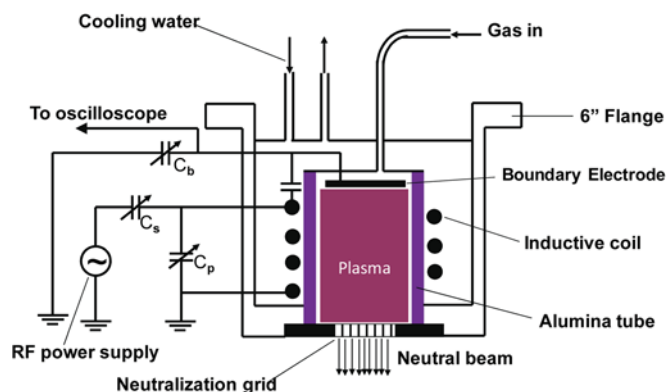


Fig. 51. (Color online) Neutral beam etching system developed by Panda, Economou, and Lee (Ref. 442).

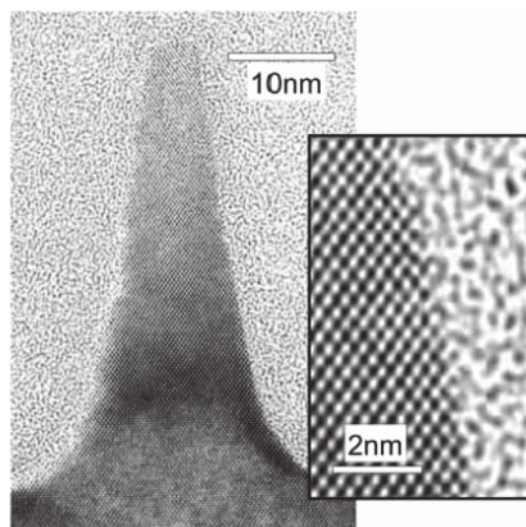


Fig. 52. Si nanopillar etched with a neutral beam by Samukawa and co-workers (Ref. 440).

eliminate ARDE. ALEt (sometimes referred to as “digital etching”) was first reported for GaAs etching with alternating  $\text{Cl}_2$  adsorption and electron beam etching.<sup>445</sup> Sasaue *et al.* used ion bombardment to effect ALEt of silicon, but the etch rate per cycle was less than a monolayer.<sup>446</sup> ALEt of silicon with one monolayer etched per cycle was achieved by Athavale and Economou.<sup>447</sup> Their approach, depicted in Fig. 53, consisted of four steps:<sup>448</sup> (1) Exposure of a clean substrate to a reactant gas, and adsorption of the gas onto the surface (*chemisorption step*). The reactant gas flow (chlorine in this case) is turned ON only during this chemisorption step. This process is self-limiting; chemisorption stops when all available surface sites are occupied. (Spontaneous etching must clearly not take place, otherwise etching with

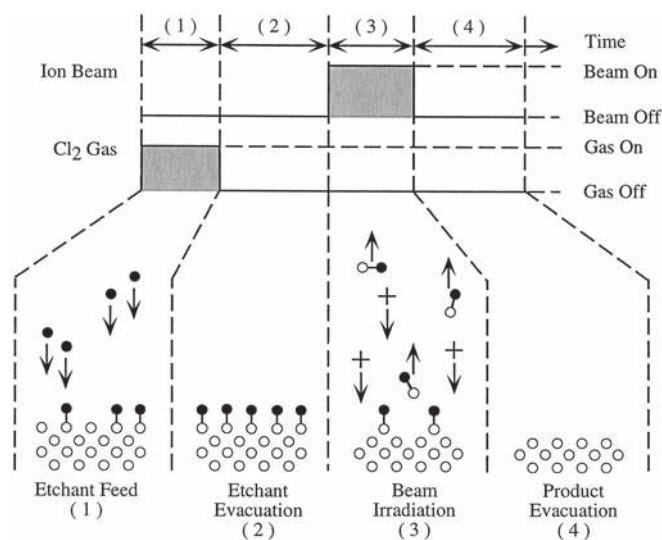


Fig. 53. ALEt cyclic process, consisting of four steps: (1) Chemisorption of a gas (chlorine in this case) on the surface (chemisorption step). (2) Chamber evacuation to remove all but the chemisorbed gas. (3) Ion irradiation to chemically sputter the top layer of substrate atoms (etching step). (4) Product evacuation to remove the etch products from the chamber (Refs. 447 and 448).

monolayer precision is not possible.) (2) Purging of excess  $\text{Cl}_2$  gas with inert (Ar) gas. (3) Exposure of the surface to ion bombardment in an Ar plasma, to induce chemical sputtering of the surface chlorinated layer (*etching step*). Ideally, this process is also self-limiting; ions react only with substrate atoms bonded to the chemisorbed gas. Once this top chlorinated layer is removed, further etching (physical sputtering now) of the substrate must not occur or be very slow. (4) Evacuation of the chamber to exhaust the etching products. If the periods of chemisorption (step 1) and etching (step 3) are long enough, the etching rate approaches one atomic layer per cycle, where the atomic layer thickness is that of the chlorinated layer, and not necessarily one monolayer of the substrate. If the substrate surface remains (atomically) smooth during repeated ALEt cycling, it is possible to achieve the ideal condition of removal of exactly *one monolayer* of the substrate per cycle.

This approach to ALEt process requires a very long  $\sim 150$  s per cycle.<sup>449</sup> While pulsed gas valves and fast switching mass flow controllers have improved in recent years, the cycle time is too low for this process to be widely applicable. Even with very fast, stable flow switching, the sticky halogen compounds [etching products<sup>121,122</sup> and even  $\text{Cl}_2$  (Ref. 143)] demand long purging times. Recently, a new method has been proposed in which rapid ALEt is achieved by pulsed bias.<sup>53,450,451</sup> The idea is to form a self-limited halogenated surface layer in the plasma with no bias on the substrate so that no etching occurs (*chemisorption step*). A bias pulse is then initiated and the halogenated layer is sputtered faster than it can reform (*etching step*). Etching will greatly slow after this layer is removed provided the ion energy is below the sputtering threshold. Bias is then turned off and a halogenated layer forms again (*chemisorption step*).

Finally, it is very difficult to predict what is beyond silicon CMOS devices and what role plasma etching will play in that technology. Such devices will have dimensions much smaller than conventional ICs. The smallest components will likely consist of single monolayers (e.g., graphene<sup>452</sup>), molecules<sup>453</sup> (e.g., carbon nanotubes<sup>454</sup>), or even single atoms.<sup>455</sup> As these emerging technologies find their way to commercial devices, the need for conventional circuitry and processing will likely remain for a long time. For example, an IC with carbon nanotube FETs still needs metallization, interlayer dielectric layers, vias, contacts, etc. If some future device required placing single molecules such as 1,4-benzenedithiol between two electrodes in trillions of locations, the need would still exist to fabricate those electrodes and create a separation between the electrodes (in this example, 0.85 nm) required for the covalent bond linkage.<sup>453</sup> It is highly unlikely that a fully bottom-up approach will ever be able to produce an advanced integrated circuit, hence some form of top-down fabrication is likely to continue and highly selective plasmas processes will be called upon to carry out patterning even on this scale. Low energy ion bombardment would be essential, but ultimately more processes may demand novel sidewall deposition of composite layers followed by isotropic etching to remove material sandwiched between two closely spaced layers.

## VII. SUMMARY

In the 1970s, plasma etching became an essential method for pattern transfer for silicon integrated circuits. As circuitry has become ever more complex with no sign of reaching the end of the roadmap for reduction in feature dimensions, the need for and importance of plasma etching continues to increase.

The need for plasma etching began roughly forty years ago when the undercutting of etch masks inherent in wet etching methods was no longer tolerable for transistor and interconnect formation. Silicon etching for transistor fabrication began in fluorine atom-generating plasmas such as  $\text{CF}_4/\text{O}_2$ , but it was quickly realized that the undercutting by F atoms was not desirable and much better profiles were possible in chlorine-containing plasmas. Parallel plate, capacitively coupled plasma reactors were used first for silicon etching but have largely been replaced by higher density inductively coupled or microwave-generated plasmas. Further improvements were realized with the addition of HBr to  $\text{Cl}_2$ . The etching of poly-Si and single crystal Si proceeds by a mechanism in which positive ions are accelerated across the sheath that develops adjacent to the wafer. The voltage drop across this sheath (and hence ion energy) is controlled by a separate bias power applied to the substrate stage. This energetic ion bombardment causes a disruption of a halogenated chemisorbed layer and induces chemical reactions that lead to the formation of volatile products.

Anisotropic etching of aluminum for interconnects was also developed with chlorine-based CCP plasmas and later also migrated to higher density ICPs. Here the mechanism is quite different. Cl and  $\text{Cl}_2$  react readily with Al in the absence of ion bombardment, which will lead to severe undercutting of masks. To prevent this, species such as  $\text{BCl}_3$  feed gas or  $\text{CCl}_x$  fragments of photoresist erosion are introduced and bare Al surfaces become coated with a passivating layer that prevents chemical etching of Al by Cl and  $\text{Cl}_2$ . Positive ion bombardment keeps horizontal surfaces relatively clean, allowing chemical etching to occur, with some added enhancement by ion bombardment. On vertical surfaces, the passivation layer prevents etching and anisotropic profiles are obtained.

Silicon dioxide etching for providing patterned insulating layers between interconnecting Al wires and Si transistors began around the same time. Fluorocarbon-containing plasmas emerged and remain the only way of achieving anisotropic etching that is selective toward Si.  $\text{SiO}_2$  etching evolved from CCP to ICP and back to CCP plasmas. The re-emergence of CCP for  $\text{SiO}_2$  etching has been accompanied by the use of radio frequency power at two (or even three) frequencies. The mechanism for etching of  $\text{SiO}_2$  has been well studied, due to its importance and highly complex nature. Etching occurs in the presence of a thin fluorocarbon film that also inhibits unwanted etching of Si. Ion bombardment of this fluorocarbon layer causes reactions to occur that lead to the generation of volatile  $\text{SiF}_4$ , CO,  $\text{CO}_2$ , and perhaps other etching products that must then diffuse out of the layer.



Recently, insulating materials with dielectric constants lower than SiO<sub>2</sub> have emerged. These films usually contain Si, C, and O and often have voids to further reduce the dielectric constant. Fluorocarbon plasmas etch these materials with a mechanism that is similar to SiO<sub>2</sub>. The same equipment that is used to etch SiO<sub>2</sub> is also used to etch these low- $\kappa$  materials.

Following the development of processes for Si, Al, and SiO<sub>2</sub> patterning, plasma etching was quickly called upon for etching a host of other conducting and insulating materials. For the first 25 years or so, plasma etching was used strictly for transferring patterns from photoresists to these materials, some of which (e.g., SiO<sub>2</sub> and amorphous Si) were used as hard masks for delineating underlying layers. In the last roughly 5–10 years, however, many applications have begun to emerge where plasma etching is taking on more of the task traditionally carried out by photolithography. These involve using a starting structure with a relatively wide line-width and then creating one, two, or even three narrower lines by trimming processes or by depositing thin layers on the sides of lines that are then removed. All indications are that the number of such processes will only increase in the future.

The future needs in plasma etching will be for evermore tighter control of process variability, higher selectivity and less damage. This may require one or more of the following: migration to pulsed plasmas, lower ion energies, tighter control of ion energy distributions, and reduced photon fluxes. Evolutionary transitions to atomic layer etching or neutral beam etching could become necessary if sensitive devices can no longer tolerate monolayer-scale damage produced by continuously immersing substrates in the plasma.

Future devices will certainly have smaller critical dimensions, will incorporate new materials and structures, and will be fabricated on larger wafers. Although self-assembly is considered as for some structures and materials, dry etching will still be used for most of the pattern transfer of the ever-shrinking lithographic features in the foreseeable future. In some cases, new materials will be incorporated in cavities formed in traditional semiconductor materials, and in other cases, these materials will require dry etching, and new etching processes will have to be developed. The choice of structures and materials will be influenced greatly by the capabilities of the dry-etching processes and equipment on hand. Control of selectivity (to the substrate as well as the mask), profile and CD control, lattice damage, plasma damage (which may be enhanced by photon flux), particle formation, process reproducibility, and equipment reliability will dominate future etching technologies and equipment.

Plasma etching technology has evolved from a manually loaded quartz tube with a coil wound around it to sophisticated automatic multimillion dollar machines, with advanced equipment and process control. This evolution continues.

## ACKNOWLEDGMENTS

The authors thank Lee Chen, John Coburn, Joel M. Cook, Richard A. Gottscho, Catherine B. Labelle, Michael Mocella,

Anthony E. Novembre, Richard E. Slusher, and Bruce Slutsky for providing information and for helpful discussions and suggestions. Special thanks to Catherine B. Labelle for a critical review of the manuscript. V.M.D. also thanks the Department of Energy, Office of Fusion Energy Science, contract DE-SC0001939, the National Science Foundation grant CBET 0903426, and the Department of Energy grant DE-SC0000881 for financial support.

<sup>1</sup>F. Faggin, M. E. Hoff, S. Mazor, and M. Shima, *IEEE Micro* **16**, 10 (1996).

<sup>2</sup>Source: Intel Chip History poster.

<sup>3</sup>O. Auciello and D. L. Flamm, *Plasma Diagnostics: Discharge Parameters and Chemistry* (Academic, New York, 1989).

<sup>4</sup>D. M. Manos and D. L. Flamm, *Plasma Etching: An Introduction* (Academic, New York, 1989).

<sup>5</sup>M. A. Lieberman and A. J. Lichtenberg, *Principles of Plasma Discharges and Materials Processing*, 2nd ed. (John Wiley & Sons, Inc., New York, 2005).

<sup>6</sup>Y. P. Raizer, *Gas Discharge Physics* (Springer-Verlag, Berlin, 1991).

<sup>7</sup>B. Chapman, *Glow Discharge Processes* (Wiley-Interscience, USA, Canada, 1980).

<sup>8</sup>W. R. Grove, *Philos. Trans. R. Soc. London* **142**, 87 (1852).

<sup>9</sup>F. Simeon, in *A Discussion on "The Making of Reflecting Surfaces"* (The Fleetway, Imperial College of Science and Technology, South Kensington, S.W.7, 1920), pp. 26.

<sup>10</sup>L. Tonks, *Am. J. Phys.* **35**, 85 (1967).

<sup>11</sup>I. Langmuir, *Proc. Natl. Acad. Sci. U.S.A.* **14**, 627 (1928).

<sup>12</sup>M. P. Lepselter, H. A. Waggener, R. W. MacDonald, and R. E. Davis, *Proc. IEEE* **53**, 405 (1965).

<sup>13</sup>M. P. Lepselter, *Bell Syst. Tech. J.* **45**, 233 (1966).

<sup>14</sup>C. M. Melliard-Smith, *J. Vac. Sci. Technol.* **13**, 1008 (1976).

<sup>15</sup>R. Glang and L. V. Gregor, in *Handbook of Thin Film Technology*, edited by L. Maissel and R. Glang (McGraw-Hill, New York, 1970).

<sup>16</sup>K. R. Williams, K. Gupta, and M. Wasilik, *J. Electromech. Syst.* **12**, 761 (2003).

<sup>17</sup>M. P. Lepselter, US patent 3,442,701 (6 May 1969).

<sup>18</sup>P. D. Davidse, in *13th National Vacuum Symposium of the AVS*, edited by W. J. Lange (San Francisco, 1966), pp. 51–52.

<sup>19</sup>P. D. Davidse, *J. Electrochem. Soc.* **116**, 100 (1969).

<sup>20</sup>H. S. Butler and G. S. Kino, *Phys. Fluids* **6**, 1346 (1963).

<sup>21</sup>S. M. Irving, in *ECS National Meeting* (Fall, 1967), Abstract 180.

<sup>22</sup>S. M. Irving, in *Kodak Photoresist Seminar Proceedings* (1968), Vol. II, pp. 26.

<sup>23</sup>S. M. Irving, *Solid State Technol.* **14**, 47 (1971).

<sup>24</sup>D. L. Tolliver, *Solid State Technol.* **23**, 99 (1980).

<sup>25</sup>J. J. Thomson, *Philos. Mag. Ser. 5* **32**, 321 (1891).

<sup>26</sup>S. M. Irving, K. E. Lemons, and G. E. Bobos, US patent 3,615,956 (26 Oct. 1971).

<sup>27</sup>T. C. Penn, *IEEE Trans. Electron. Dev.* **ED26**, 640 (1979).

<sup>28</sup>R. A. H. Heinecke, *Solid State Electron.* **18**, 1146 (1975).

<sup>29</sup>R. A. H. Heinecke, *Solid State Electron.* **19**, 1039 (1976).

<sup>30</sup>R. L. Bersin, *Solid State Technol.* **13**, 39 (1970).

<sup>31</sup>A. R. Reinberg, US patent 3,757,733 (11 Sept. 1973).

<sup>32</sup>N. Hosokawa, R. Matsuzaki, and T. Asamaki [*Proceedings of the 6th International Vacuum Congress*, 1974], *Jpn. J. Appl. Phys. Suppl.* **2**, 435 (1974).

<sup>33</sup>J. M. Harvilchuck, J. S. Logan, W. C. Metzger, and P. M. Schaible, US patent 3,994,793 (30 Nov. 1976).

<sup>34</sup>J. A. Bondur, *J. Vac. Sci. Technol.* **13**, 1023 (1976).

<sup>35</sup>J. W. Coburn and H. F. Winters, *J. Vac. Sci. Technol.* **16**, 391 (1979).

<sup>36</sup>S. Somekh and H. C. Casey, *Appl. Opt.* **16**, 126 (1977).

<sup>37</sup>H. W. Lehmann and R. Widmar, *J. Vac. Sci. Technol.* **15**, 319 (1978).

<sup>38</sup>F. D. Egitto, D. N. K. Wang, D. Maydan, and D. Benzing, *Solid State Technol.* **24**, 71 (1981).

<sup>39</sup>H. R. Koenig and L. I. Maissel, *IBM J. Res. Dev.* **14**, 168 (1970).

<sup>40</sup>C. M. Horwitz, *J. Vac. Sci. Technol. A* **1**, 60 (1983).

<sup>41</sup>D. Maydan, US patent 4,298,443 (3 Nov. 1981).

<sup>42</sup>J. Maher, *Semicond. Int.* **6**, 110 (1983).

<sup>43</sup>O. A. Popov, *High Density Plasma Sources, Design, Physics and Performance* (Noyes, Park Ridge, NJ, 1995).

- <sup>44</sup>Y. Horiike, H. Okano, T. Yamazaki, and H. Horie, *Jpn. J. Appl. Phys.* **20**, L817 (1981).
- <sup>45</sup>R. N. Castellano, *Semiconductor Device Processing: Technology Trends in the VLSI Era* (Gordon and Breach, New York, 1992).
- <sup>46</sup>V. J. Minkiewicz and B. N. Chapman, *Appl. Phys. Lett.* **34**, 192 (1979).
- <sup>47</sup>J. H. Thomas and B. Singh, *J. Vac. Sci. Technol. A* **10**, 3070 (1992).
- <sup>48</sup>G. J. Gorin, U.S. Patent 4,446,223 (7 August 1984).
- <sup>49</sup>R. Limpachert and K. R. MacKenzie, *J. Sci. Instrum.* **44**, 726 (1973).
- <sup>50</sup>V. J. Minkiewicz, M. Chen, J. W. Coburn, B. N. Chapman, and K. Lee, *Appl. Phys. Lett.* **35**, 393 (1979).
- <sup>51</sup>E. H. Lenz, US patent 6,602,381 (5 Aug. 2003).
- <sup>52</sup>V. Milosavljević, A. R. Ellingboe, C. Gaman, and J. V. Ringwood, *J. Appl. Phys.* **103**, 083302 (2008).
- <sup>53</sup>R. A. Gottscho and K. J. Kanarik, in *APS 64th Annual Gaseous Electronics Conference* (Salt Lake City, UT, 2011). Abstract available at: <http://meetings.aps.org/link/BAPS.2011.GEC.HW1.1>.
- <sup>54</sup>S. Sriraman, K. Kanarik, and R. A. Gottscho, in *AVS 59th National Symposium* (American Vacuum Society, Tampa, FL, 2012), pp. 73.
- <sup>55</sup>R. Dhindsa *et al.*, US patent 7,405,521 (29 July 2008).
- <sup>56</sup>W. T. Lai, C. J. Hwang, A. T. Wang, J. C. Yau, J. H. Liao, L. H. Chen, K. Adachi, and S. Okamoto, in *Proceedings of the 28th International Symposium on Dry Process* (Institute of Electrical Engineers, Nagoya, Japan, 2006).
- <sup>57</sup>E. Kawamura, M. A. Lieberman, A. J. Lichtenberg, and E. A. Hudson, *J. Vac. Sci. Technol. A* **25**, 1456 (2007).
- <sup>58</sup>E. Kawamura, A. J. Lichtenberg, and M. A. Lieberman, *Plasma Source Sci. Technol.* **17**, 045002 (2008).
- <sup>59</sup>L. Xu, L. Chen, M. Funk, A. Ranjan, M. Hummel, R. Bravenec, R. Sundararajan, D. J. Economou, and V. M. Donnelly, *Appl. Phys. Lett.* **93**, 261502 (2008).
- <sup>60</sup>L. Chen and M. Funk, in *63rd Annual Gaseous Electronics Conference and 7th International Conference on Reactive Plasmas* (American Physical Society, Paris, France, 2010), Abstract CTP.00154.
- <sup>61</sup>M. Honda, K. Yatsuda and L. Chen, in *AVS 55th International Symposium* (American Vacuum Society, Boston, MA, 2008), pp. 142.
- <sup>62</sup>J. C. Forster and J. H. Keller, in *High Density Plasma Sources*, edited by O. A. Popov (Noyes Publications, Park Ridge, NJ, 1995), pp. 76–99.
- <sup>63</sup>S. Marks, J. P. Almerico, M. K. Gay, and F. G. Celii, *Integr. Ferroelectr.* **59**, 333 (2003).
- <sup>64</sup>J. E. Stevens, in *High Density Plasma Sources*, edited by O. A. Popov (Noyes Publications, Park Ridge, NJ, 1995), pp. 312–379.
- <sup>65</sup>S. Kawamura, N. Itabashi, A. Makino, and M. Sakaguchi, *Hitachi Rev.* **51**, 95 (2002).
- <sup>66</sup>F. F. Chen, in *High Density Plasma Sources*, edited by O. A. Popov (Noyes Publications, Park Ridge, NJ, 1995), pp. 1–75.
- <sup>67</sup>F. F. Chen, *Plasma Phys. Controlled Fusion* **33**, 339 (1991).
- <sup>68</sup>R. Boswell, R. Porteous, A. Prytz, A. Bouchoule, and P. Ranson, *Phys. Lett. A* **91**, 163 (1982).
- <sup>69</sup>R. W. Boswell, *Phys. Lett. A* **33**, 457 (1970).
- <sup>70</sup>R. W. Boswell, A. J. Perry, and M. Emami, *J. Vac. Sci. Technol. A* **7**, 3345 (1989).
- <sup>71</sup>G. Campbell, R. W. Conn, and T. Shoji, US patent 4,990,229 (5 Feb. 1991).
- <sup>72</sup>H. Sugai, I. Ghanashev, and M. Nagatsu, *Plasma Sources Sci. Technol.* **7**, 192 (1998).
- <sup>73</sup>R. Bravenec, J. Zhao, L. Chen, and M. Funk, in *63rd Annual Gaseous Electronics Conference and 7th International Conference on Reactive Plasmas* (American Physical Society, Paris, France, 2010), Abstract CTP.00059.
- <sup>74</sup>J. Zhao, R. Bravenec, L. Chen, M. Funk, R. Sundararajan, Koji Koyama, T. Nozawa, and S. Samukawa, in *APS 63rd Annual Gaseous Electronics Conference and 7th International Conference on Reactive Plasmas* (American Physical Society, Paris, France, 2010), Abstract BT2.0000.
- <sup>75</sup>C. Cismaru, J. L. Shohet, and J. P. McVittie, *Appl. Phys. Lett.* **76**, 2191 (2000).
- <sup>76</sup>S. Samukawa, Y. Ishikawa, S. Kumagai, and M. Okigawa, *Jpn. J. Appl. Phys.* **40**, L1346 (2001).
- <sup>77</sup>S. Fujimura, K. Shinagawa, M. Nakamura, and H. Yano, *Jpn. J. Appl. Phys.* **29**, 2165 (1990).
- <sup>78</sup>N. Layadi, S. J. Molloy, A. Kornblit, J. T. C. Lee, T. M. Wolf, and D. E. Ibbotson, *Plasma Etching in Microelectronics* (American Vacuum Society, New York, 2001).
- <sup>79</sup>B. Thedjoisworo, D. Cheung, and V. Crist, *J. Vac. Sci. Technol. B* **31**, 021206 (2013).
- <sup>80</sup>D. Nest, D. B. Graves, S. Engelmann, R. L. Bruce, F. Weillnboeck, G. S. Oehrlein, C. Andes, and E. A. Hudson, *Appl. Phys. Lett.* **92**, 153113 (2008).
- <sup>81</sup>A. R. Reinberg, in *Plasma Etching—An Introduction*, edited by D. M. Manos and D. L. Flamm (Academic, New York, 1989), pp. 358.
- <sup>82</sup>P. A. Heimann and R. J. Schutz, *J. Electrochem. Soc.* **131**, 881 (1984).
- <sup>83</sup>M. Haverlag and G. S. Oehrlein, *J. Vac. Sci. Technol. B* **10**, 2412 (1992).
- <sup>84</sup>N. Blayo, R. A. Cirelli, F. P. Klemens, and J. T. C. Lee, *J. Opt. Soc. Am. A* **12**, 591 (1995).
- <sup>85</sup>D. W. Mills, R. L. Allen and W. M. Duncan, *Proc. SPIE* **2637**, 194 (1995).
- <sup>86</sup>E. O. Degenkolb, C. J. Mogab, M. R. Goldrick, and J. E. Griffiths, *Appl. Spectrosc.* **30**, 520 (1976).
- <sup>87</sup>W. R. Harshbarger, R. A. Porter, T. A. Miller, and P. Norton, *Appl. Opt.* **31**, 201 (1977).
- <sup>88</sup>R. G. Poulsen, *J. Vac. Sci. Technol.* **14**, 266 (1977).
- <sup>89</sup>J. E. Greene, *J. Vac. Sci. Technol.* **15**, 1718 (1978).
- <sup>90</sup>K. Hirobe and T. Tsuchimoto, *J. Electrochem. Soc.* **127**, 234 (1980).
- <sup>91</sup>P. A. Heimann, J. M. Moran, and R. J. Schutz, US patent 4,680,084 (14 July 1987).
- <sup>92</sup>T. J. Dalton, W. T. Conner, and H. H. Sawin, *J. Electrochem. Soc.* **141**, 1893 (1994).
- <sup>93</sup>H. H. Sawin, W. T. Conner, T. J. Dalton, and E. M. Sachs, US patent 5,450,205 (12 September 1995).
- <sup>94</sup>D. L. Flamm and G. K. Herb, in *Plasma Etching—An Introduction*, edited by D. M. Manos and D. L. Flamm (Academic, New York, 1989), pp. 1–89.
- <sup>95</sup>C. W. Jurgensen, R. R. Kola, A. E. Novembre, W. W. Tai, J. Frackowiak, L. E. Trimble, and G. K. Geller, *J. Vac. Sci. Technol. B* **9**, 3280 (1991).
- <sup>96</sup>A. Kornblit, in *Lam Research Corporation Technical Symposium* (San Francisco, CA, 1998) (unpublished).
- <sup>97</sup>A. Kornblit, J. T.-C. Lee, H. Lee, and H. L. Maynard, US patent 6,228,277 (8 May 2001).
- <sup>98</sup>N. Layadi, S. J. Molloy, T. C. Esry, T. Lill, J. Trevor, M. N. Grimbergen, and J. Chinn, *J. Vac. Sci. Technol. B* **17**, 2630 (1999).
- <sup>99</sup>D. L. Flamm, V. M. Donnelly, and J. A. Mucha, *J. Appl. Phys.* **52**, 3633 (1981).
- <sup>100</sup>E. A. Ogryzlo, D. E. Ibbotson, D. L. Flamm, and J. A. Mucha, *J. Appl. Phys.* **67**, 3115 (1990).
- <sup>101</sup>This quote is widely (and erroneously) attributed to Aristotle (4th century BCE), based on misinterpretation of statement in *Metaphysics*, Book 8, Sec. 1045a. See: Sheila Guberman and Gianfranco Minati, *Dialogue about Systems* (2007), Section C.4, pp. 181–182. It is true, however, that Aristotle says that there are instances that “...you may have the parts and yet not have the whole, so that parts and whole cannot be the same” (*Topics*, Book VI, Sec. 13, translated by W. A. Pickard-Cambridge).
- <sup>102</sup>H. F. Winters, J. W. Coburn, and T. J. Chuang, *J. Vac. Sci. Technol. B* **1**, 469 (1983).
- <sup>103</sup>H. F. Winters and J. W. Coburn, *Surf. Sci. Rep.* **14**, 162 (1992).
- <sup>104</sup>M. E. Barone and D. B. Graves, *J. Appl. Phys.* **78**, 6604 (1995).
- <sup>105</sup>P. R. McCurdy, K. H. A. Bogart, N. F. Dalleska, and E. R. Fisher, *Rev. Sci. Instrum.* **68**, 1684 (1997).
- <sup>106</sup>E. R. Fisher, *Plasma Process. Polym.* **1**, 13 (2004).
- <sup>107</sup>D. Liu, I. T. Martin, J. Zhou, and E. R. Fisher, *Pure Appl. Chem.* **78**, 1187 (2006).
- <sup>108</sup>N. E. Capps, N. M. Mackie, and E. R. Fisher, *J. Appl. Phys.* **84**, 4736 (1998).
- <sup>109</sup>J. Guha and V. M. Donnelly, *J. Vac. Sci. Technol. A* **27**, 515 (2009).
- <sup>110</sup>V. M. Donnelly, J. Guha, and L. Stafford, *J. Vac. Sci. Technol. A* **29**, 010801 (2011).
- <sup>111</sup>H. Singh, J. W. Coburn, and D. B. Graves, *J. Vac. Sci. Technol. A* **17**, 2447 (1999).
- <sup>112</sup>H. Singh, J. W. Coburn, and D. B. Graves, *J. Vac. Sci. Technol. A* **18**, 299 (2000).
- <sup>113</sup>J. Benedikt, A. Hecimovic, D. Ellerweg, and A. v. Keudell, *J. Phys. D: Appl. Phys.* **45**, 403001 (2012).
- <sup>114</sup>I. P. Herman, *Optical Diagnostics for Thin Film Processing* (Academic, San Diego, 1996).
- <sup>115</sup>K. H. A. Bogart and V. M. Donnelly, *J. Appl. Phys.* **86**, 1822 (1999).
- <sup>116</sup>V. M. Donnelly, *J. Vac. Sci. Technol. A* **14**, 1076 (1996).
- <sup>117</sup>R. A. Gottscho and V. M. Donnelly, *J. Appl. Phys.* **56**, 245 (1984).

- <sup>118</sup>M. V. Malyshev and V. M. Donnelly, *J. Appl. Phys.* **88**, 6207 (2000).
- <sup>119</sup>N. C. M. Fuller, M. V. Malyshev, V. M. Donnelly, and I. P. Herman, *Plasma Sources Sci. Technol.* **9**, 116 (2000).
- <sup>120</sup>G. Cunge, M. Kogelschatz, and N. Sadeghi, *Plasma Sources Sci. Technol.* **13**, 522 (2004).
- <sup>121</sup>R. Khare, A. Srivastava, and V. M. Donnelly, *J. Vac. Sci. Technol. A* **30**, 051306 (2012).
- <sup>122</sup>R. Khare, A. Srivastava, and V. M. Donnelly, *J. Vac. Sci. Technol. A* **30**, 051307 (2012).
- <sup>123</sup>M. V. Malyshev, N. C. M. Fuller, K. H. A. Bogart, V. M. Donnelly, and I. P. Herman, *Appl. Phys. Lett.* **74**, 1666 (1999).
- <sup>124</sup>M. V. Malyshev, N. C. M. Fuller, K. H. A. Bogart, V. M. Donnelly, and I. P. Herman, *J. Appl. Phys.* **88**, 2246 (2000).
- <sup>125</sup>J. W. Coburn and M. Chen, *J. Appl. Phys.* **51**, 3134 (1980).
- <sup>126</sup>R. d'Agostino, F. Cramarossa, S. D. Benedictis, and G. Ferraro, *J. Appl. Phys.* **52**, 1259 (1981).
- <sup>127</sup>R. d'Agostino, F. Cramarossa, S. D. Benedictis, F. Fracassi, L. Laska, and K. Masek, *Plasma Chem. Plasma Process.* **5**, 239 (1985).
- <sup>128</sup>V. M. Donnelly, D. L. Flamm, W. C. Dautremont-Smith, and D. J. Werder, *J. Appl. Phys.* **55**, 242 (1984).
- <sup>129</sup>M. Schabel, V. M. Donnelly, A. Kornblit, and W. Tai, *J. Vac. Sci. Technol. A* **20**, 555 (2002).
- <sup>130</sup>E. Karakas, V. M. Donnelly, and D. J. Economou, *Appl. Phys. Lett.* **102**, 034107 (2013).
- <sup>131</sup>J. P. Booth, O. Joubert, J. Pelletier, and N. Sadeghi, *J. Appl. Phys.* **69**, 618 (1991).
- <sup>132</sup>R. E. Walkup, K. L. Saenger, and G. S. Selwyn, *J. Chem. Phys.* **84**, 2668 (1986).
- <sup>133</sup>A. R. Godfrey, S. J. Ullal, L. B. Braly, E. A. Edelberg, V. Vahedi, and E. S. Aydi, *Rev. Sci. Instrum.* **72**, 3260 (2001).
- <sup>134</sup>S. J. Ullal, H. Singh, J. Daugherty, and V. Vahedi, *J. Vac. Sci. Technol. A* **20**, 1195 (2002).
- <sup>135</sup>C. C. Cheng, K. V. Guinn, V. M. Donnelly, and I. P. Herman, *J. Vac. Sci. Technol. A* **12**, 2630 (1994).
- <sup>136</sup>C. C. Cheng, K. V. Guinn, I. P. Herman, and V. M. Donnelly, *J. Vac. Sci. Technol. A* **13**, 1970 (1995).
- <sup>137</sup>I. P. Herman, V. M. Donnelly, K. V. Guinn, and C. C. Cheng, *Phys. Rev. Lett.* **72**, 2801 (1994).
- <sup>138</sup>J. Y. Choe, I. P. Herman, and V. M. Donnelly, *J. Vac. Sci. Technol. A* **15**, 3024 (1997).
- <sup>139</sup>J. Y. Choe, N. C. M. Fuller, V. M. Donnelly, and I. P. Herman, *J. Vac. Sci. Technol. A* **18**, 2669 (2000).
- <sup>140</sup>P. F. Kurunczi, J. Guha, and V. M. Donnelly, *J. Phys. Chem. B* **109**, 20989 (2005).
- <sup>141</sup>P. F. Kurunczi, J. Guha, and V. M. Donnelly, *Phys. Rev. Lett.* **96**, 018306 (2006).
- <sup>142</sup>J. Guha and V. M. Donnelly, *J. Appl. Phys.* **105**, 113307 (2009).
- <sup>143</sup>J. Guha, V. M. Donnelly, and Y.-K. Pu, *J. Appl. Phys.* **103**, 013306 (2008).
- <sup>144</sup>J. Guha, R. Khare, L. Stafford, V. M. Donnelly, S. Sirard, and E. A. Hudson, *J. Appl. Phys.* **105**, 113309 (2009).
- <sup>145</sup>J. Guha, P. Kurunczi, L. Stafford, and V. M. Donnelly, *J. Phys. Chem. C* **112**, 8963 (2008).
- <sup>146</sup>J. Guha, Y.-K. Pu, and V. M. Donnelly, *J. Vac. Sci. Technol. A* **25**, 347 (2007).
- <sup>147</sup>G. S. Oehrlein, K. K. Chan, and M. A. Jaso, *J. Appl. Phys.* **64**, 2399 (1988).
- <sup>148</sup>G. S. Oehrlein, A. A. Bright, and S. W. Robey, *J. Vac. Sci. Technol. A* **6**, 1989 (1988).
- <sup>149</sup>G. S. Oehrlein, J. F. Rembetski, and E. H. Payne, *J. Vac. Sci. Technol. B* **8**, 1199 (1990).
- <sup>150</sup>G. S. Oehrlein, K. K. Chan, M. A. Jaso, and G. W. Rubloff, *J. Vac. Sci. Technol. A* **7**, 1030 (1989).
- <sup>151</sup>K. V. Guinn and V. M. Donnelly, *J. Appl. Phys.* **75**, 2227 (1994).
- <sup>152</sup>K. V. Guinn, C. C. Cheng, and V. M. Donnelly, *J. Vac. Sci. Technol. B* **13**, 214 (1995).
- <sup>153</sup>O. Joubert, P. Czuprynski, F. H. Bell, P. Berruyer, and R. Blanc, *J. Vac. Sci. Technol. B* **15**, 629 (1997).
- <sup>154</sup>F. H. Bell and O. Joubert, *J. Vac. Sci. Technol. B* **15**, 88 (1997).
- <sup>155</sup>J. W. Coburn and H. F. Winters, *J. Appl. Phys.* **50**, 3189 (1979).
- <sup>156</sup>S. A. Vitale, H. Chae, and H. H. Sawin, *J. Vac. Sci. Technol. A* **19**, 2197 (2001).
- <sup>157</sup>Z. H. Walker and E. A. Ogryzlo, *J. Appl. Phys.* **69**, 548 (1991).
- <sup>158</sup>Z. H. Walker and E. A. Ogryzlo, *J. Appl. Phys.* **69**, 2635 (1991).
- <sup>159</sup>H. F. Winters and D. Haarer, *Phys. Rev. B* **36**, 6613 (1987).
- <sup>160</sup>J. A. Levinson, E. S. G. Shaqfeh, M. Balooch, and A. V. Hamza, *J. Vac. Sci. Technol. A* **15**, 1902 (1997).
- <sup>161</sup>C. Steinbruechel, *Appl. Phys. Lett.* **55**, 1960 (1989).
- <sup>162</sup>J. P. Chang, J. C. Arnold, G. C. H. Zau, H.-S. Shin, and H. H. Sawin, *J. Vac. Sci. Technol. A* **15**, 1853 (1997).
- <sup>163</sup>H. C. Flaum, D. J. D. Sullivan, and A. C. Kummel, *J. Phys. Chem.* **98**, 1719 (1994).
- <sup>164</sup>J. P. Chang and H. H. Sawin, *J. Vac. Sci. Technol. A* **15**, 610 (1997).
- <sup>165</sup>W. Jin, S. A. Vitale, and H. H. Sawin, *J. Vac. Sci. Technol. A* **20**, 2106 (2002).
- <sup>166</sup>M. Balooch, M. Moalem, W.-E. Wang, and A. V. Hamza, *J. Vac. Sci. Technol. A* **14**, 229 (1996).
- <sup>167</sup>H. Shin, W. Zhu, V. M. Donnelly, and D. J. Economou, *J. Vac. Sci. Technol. A* **30**, 021306 (2012).
- <sup>168</sup>M. A. Vyvoda, H. Lee, M. V. Malyshev, F. P. Klemens, M. Cerullo, V. M. Donnelly, D. B. Graves, A. Kornblit, and J. T. C. Lee, *J. Vac. Sci. Technol. A* **16**, 3247 (1998).
- <sup>169</sup>M. A. Vyvoda, M. Li, D. B. Graves, H. Lee, M. V. Malyshev, F. P. Klemens, J. T. C. Lee, and V. M. Donnelly, *J. Vac. Sci. Technol. B* **18**, 820 (2000).
- <sup>170</sup>B. A. Helmer and D. B. Graves, *J. Vac. Sci. Technol. A* **16**, 3502 (1998).
- <sup>171</sup>D. B. Graves and P. Braut, *J. Phys. D: Appl. Phys.* **42**, 194011 (2009).
- <sup>172</sup>T. D. Durbin, W. C. Simpson, V. Chakarian, D. K. Shuh, P. R. Varekamp, C. W. Lo, and J. A. Yarmoff, *Surf. Sci.* **316**, 257 (1994).
- <sup>173</sup>N. Layadi, V. M. Donnelly, and J. T. C. Lee, *J. Appl. Phys.* **81**, 6738 (1997).
- <sup>174</sup>J. W. Coburn, *J. Vac. Sci. Technol. A* **12**, 1417 (1994).
- <sup>175</sup>R. A. Barker, T. M. Mayer, and W. C. Pearson, *J. Vac. Sci. Technol. B* **1**, 37 (1983).
- <sup>176</sup>E. L. Barish, D. J. Vitkavage, and T. M. Mayer, *J. Appl. Phys.* **57**, 1336 (1985).
- <sup>177</sup>M. E. Barone, T. O. Robinson, and D. B. Graves, *IEEE Trans. Plasma Sci.* **24**, 77 (1996).
- <sup>178</sup>C. C. Cheng, K. V. Guinn, and V. M. Donnelly, *J. Vac. Sci. Technol. B* **14**, 85 (1996).
- <sup>179</sup>L. Desvoivres, L. Vallier, and O. Joubert, *J. Vac. Sci. Technol. B* **19**, 420 (2001).
- <sup>180</sup>Silicon nitride can be either stoichiometric Si<sub>3</sub>N<sub>4</sub> or either silicon or nitrogen rich, depending on requirements. In case of plasma-enhanced deposition, hydrogen may be incorporated in the film as well. Unless otherwise specified, SiN refers to any of these materials.
- <sup>181</sup>J. W. Butterbaugh, D. C. Gray, and H. H. Sawin, *J. Vac. Sci. Technol. B* **9**, 1461 (1991).
- <sup>182</sup>J. W. Coburn, *J. Appl. Phys.* **50**, 5210 (1979).
- <sup>183</sup>D. C. Gray, I. Tepermeister, and H. H. Sawin, *J. Vac. Sci. Technol. B* **11**, 1243 (1993).
- <sup>184</sup>T. E. F. M. Standaert, C. Hedlund, E. A. Joseph, G. S. Oehrlein, and T. J. Dalton, *J. Vac. Sci. Technol. A* **22**, 53 (2004).
- <sup>185</sup>G. S. Oehrlein, *Surf. Sci.* **386**, 222 (1997).
- <sup>186</sup>M. Schaepkens and G. S. Oehrlein, *J. Electrochem. Soc.* **148**, C211 (2001).
- <sup>187</sup>A. Sankaran and M. J. Kushner, *Appl. Phys. Lett.* **82**, 1824 (2003).
- <sup>188</sup>D. J. Economou and R. C. Alkire, *J. Electrochem. Soc.* **135**, 941 (1988).
- <sup>189</sup>S. Murakawa and J. P. McVittie, *Jpn. J. Appl. Phys., Part 1* **33**, 2184 (1994).
- <sup>190</sup>S. Murakawa and J. P. McVittie, *Jpn. J. Appl. Phys., Part 1* **33**, 4446 (1994).
- <sup>191</sup>J. I. Ullacia and J. P. McVittie, *J. Appl. Phys.* **65**, 1484 (1989).
- <sup>192</sup>K. Hashimoto, *Jpn. J. Appl. Phys., Part 1* **32**, 6109 (1993).
- <sup>193</sup>H. Ootera, T. Oomori, M. Tuda, and K. Namba, *Jpn. J. Appl. Phys., Part 1* **33**, 4276 (1994).
- <sup>194</sup>S. Sakamori, T. Maruyama, N. Fujiwara, and H. Miyatake, *Jpn. J. Appl. Phys., Part 1* **36**, 2521 (1997).
- <sup>195</sup>K. K. Chi, H. S. Shin, W. J. Yoo, C. O. Jung, Y. B. Koh, and M. Y. Lee, *Jpn. J. Appl. Phys., Part 1* **35**, 2440 (1996).
- <sup>196</sup>K. Arita and T. Asano, *Jpn. J. Appl. Phys., Part 1* **35**, 6534 (1996).
- <sup>197</sup>S. Ogino, N. Fujiwara, H. Miyatake, and M. Yoneda, *Jpn. J. Appl. Phys., Part 1* **35**, 2445 (1996).
- <sup>198</sup>T. Kamata and H. Arimoto, *J. Appl. Phys.* **80**, 2637 (1996).
- <sup>199</sup>G. S. Hwang and K. P. Giapis, *J. Vac. Sci. Technol. B* **15**, 70 (1997).
- <sup>200</sup>K. P. Giapis and G. S. Hwang, *Jpn. J. Appl. Phys., Part 1* **37**, 2281 (1998).



- <sup>201</sup>J. Matsui, N. Nakano, Z. L. Petrović, and T. Makabe, *Appl. Phys. Lett.* **78**, 883 (2001).
- <sup>202</sup>M. Wang and M. J. Kushner, *J. Appl. Phys.* **107**, 023309 (2010).
- <sup>203</sup>N. Possème, T. Chevolleau, O. Joubert, L. Vallier, and P. Mangiagalli, *J. Vac. Sci. Technol. B* **21**, 2432 (2003).
- <sup>204</sup>D. Eon, V. Raballand, G. Cartry, and C. Cardinaud, *J. Phys. D: Appl. Phys.* **40**, 3951 (2007).
- <sup>205</sup>T. E. F. M. Standaert, P. J. Matsuo, S. D. Allen, G. S. Oehrlein, and T. J. Dalton, *J. Vac. Sci. Technol. A* **17**, 741 (1999).
- <sup>206</sup>T. E. F. M. Standaert, E. A. Joseph, G. S. Oehrlein, A. Jain, W. N. Gill, J. P. C. Wayner, and J. L. Plawsky, *J. Vac. Sci. Technol. A* **18**, 2742 (2000).
- <sup>207</sup>A. Sankaran and M. J. Kushner, *J. Appl. Phys.* **97**, 023307 (2005).
- <sup>208</sup>V. M. Donnelly, F. P. Klemens, T. W. Sorsch, G. L. Timp, and F. H. Baumann, *Appl. Phys. Lett.* **74**, 1260 (1999).
- <sup>209</sup>D. L. Flamm, in *Plasma Etching—An Introduction*, edited by D. M. Manos and D. L. Flamm (Academic, New York, 1989), pp. 91–183.
- <sup>210</sup>C. J. Mogab, in *VLSI Technology*, 1st ed., edited by S. M. Sze (McGraw-Hill, New York, 1983), pp. 303–345.
- <sup>211</sup>C. J. Mogab, *J. Electrochem. Soc.* **124**, 1262 (1977).
- <sup>212</sup>D. L. Flamm, D. N. K. Wang, and D. Maydan, *J. Electrochem. Soc.* **129**, 2755 (1982).
- <sup>213</sup>O. Wada, *J. Electrochem. Soc.* **131**, 2373 (1984).
- <sup>214</sup>A. Y. Feldblum, C. R. Nijander, W. P. Townsend, and C. M. Mayer-Costa, *Proc. SPIE* **1544**, 200 (1991).
- <sup>215</sup>R. A. Gottscho, C. W. Jurgensen, and D. J. Vitkavage, *J. Vac. Sci. Technol. B* **10**, 2133 (1992).
- <sup>216</sup>O. Joubert, G. S. Oehrlein, and M. Surendra, *J. Vac. Sci. Technol. A* **12**, 665 (1994).
- <sup>217</sup>D. J. Vitkavage, A. Kornblit, S. C. McNevin, D. P. Favreau, and R. S. Nicholas, in *Proceedings of the Tegal Plasma Seminar* (Redwood City, CA, 1991), late submission, included in the proceedings.
- <sup>218</sup>H. L. Bay and J. Bohdanský, *Appl. Phys.* **19**, 421 (1979).
- <sup>219</sup>Y. Yamamura, Y. Itikawa, and N. Itoh, Nagoya University Institute of Plasma Physics Report IPPJ-AM-26 (1983).
- <sup>220</sup>M. R. Nakles, M.S. thesis (Virginia Polytechnic Institute and State University, 2004).
- <sup>221</sup>J. M. E. Harper, in *Plasma Etching—An Introduction*, edited by D. M. Manos and D. L. Flamm (Academic, New York, 1983), pp. 406–423.
- <sup>222</sup>A. Kornblit, M. J. Grieco, D. W. Peters, and T. E. saunders, *Proc. SPIE* **0775**, 320 (1987).
- <sup>223</sup>M. Vyvoda, H. Lee, M. V. Malyshev, F. P. Klemens, M. Cerullo, V. M. Donnelly, D. B. Graves, and A. K. J. T. C. Lee, *J. Vac. Sci. Technol. A* **16**, 3247 (1998).
- <sup>224</sup>K. H. A. Bogart, F. P. Klemens, M. V. Malyshev, J. I. Colonell, V. M. Donnelly, J. T. C. Lee, and J. M. Lane, *J. Vac. Sci. Technol. A* **18**, 197 (2000).
- <sup>225</sup>M. A. Vyvoda, H. Lee, M. V. Malyshev, F. P. Klemens, M. Cerullo, V. M. Donnelly, D. B. Graves, A. Kornblit, and J. T. C. Lee, in *AVS 44th International Symposium* (American Vacuum Society, San Jose, CA, 1997).
- <sup>226</sup>K. H. A. Bogart, F. P. Klemens, J. Lane, M. V. Malyshev, V. M. Donnelly, A. Kornblit, and J. T. C. Lee, in *AVS 45th International Symposium* (American Vacuum Society, Baltimore, MD, 1998).
- <sup>227</sup>N. Selamoglu, C. N. Bredbenner, T. A. Giniecki, and H. J. Stocker, *J. Vac. Sci. Technol. B* **9**, 2530 (1991).
- <sup>228</sup>P. Werbaneth, Z. Hasan, P. Rajora, and M. Rousey-Seidel, in *International Conference on Compound Semiconductor Manufacturing Technology* (CS MANTECH, 1999).
- <sup>229</sup>M. McNie *et al.*, *Proc. SPIE* **4979**, 34 (2003).
- <sup>230</sup>N. A. Ciampa, J. I. Colonell, A. Kornblit and J. T. C. Lee, in *AVS 43rd National Symposium* (American Vacuum Society, Philadelphia, PA, 1996).
- <sup>231</sup>C. Chu and T. A. Letson, US patent 7,208,399 (24 Apr. 2007); also filed with the World International Property Organization, 7 Dec. 1999 and published as WO 00/34984, 15 June 2000).
- <sup>232</sup>C. J. D. Craigie, T. Sheehan, V. N. Johnson, S. L. Burkett, A. J. Moll, and W. B. Knowlton, *J. Vac. Sci. Technol. B* **20**, 2229 (2002).
- <sup>233</sup>R. J. Shul, C. G. Willison, and L. Zhang, *Proc. SPIE* **3511**, 252 (1998).
- <sup>234</sup>R. J. Shul and J. G. Fleming, in *Handbook of Advanced Plasma Processing Techniques*, edited by R. J. Shul and S. J. Pearton (Springer, New York, 2000), pp. 419–458.
- <sup>235</sup>J. D. Chinn, I. Adesida, and E. D. Wolf, *J. Vac. sci. Technol. B* **1**, 1028 (1983).
- <sup>236</sup>Freon® is DuPont's trademark for fluorinated or partially fluorinated hydrocarbons, used mainly for refrigeration purposes (the electronic-grade equivalent is marketed under the trademark Zyrone®). It is commonly used in the literature even though many of these substances are not manufactured by DuPont. The Freon (or Zyrone) numbering scheme follows what is known as the 'DuPont 90 Rule': If the number 90 is added to the Freon number, a three digit number is obtained; the first second and the third digits correspond to the number of carbon, hydrogen and fluorine atoms, respectively. Thus, adding the number 90 to 23 (Freon 23) will yield 113, corresponding to CHF<sub>3</sub>. If the number of bonds is not satisfied by the above procedure, the missing atoms are Cl, thus Freon 11 will have one carbon, one fluorine, and three chlorine atoms (CFC1<sub>3</sub>). If bromine atoms are included in the molecule, the suffix B is added, followed by the number of the bromine atoms (e.g., Freon 12B1—CBrClF<sub>2</sub>). Source: Michael Mocella (DuPont).
- <sup>237</sup>L. M. Ephrath and E. J. Petrillo, *J. Electrochem. Soc.* **129**, 2282 (1982).
- <sup>238</sup>D. C. Marra and E. S. Aydil, *J. Vac. Sci. Technol. A* **15**, 2508 (1997).
- <sup>239</sup>S. J. Fonash, *J. Electrochem. Soc.* **137**, 3885 (1990).
- <sup>240</sup>J. M. Heddleson, M. W. Horn, S. J. Fonash, and D. C. Nguyen, *J. Vac. Sci. Technol. B* **6**, 280 (1988).
- <sup>241</sup>X. C. Mu, S. J. Fonash, A. Rohatgi, and J. Rieger, *Appl. Phys. Lett.* **48**, 1147 (1986).
- <sup>242</sup>X. C. Mu, S. J. Fonash, and R. Singh, *Appl. Phys. Lett.* **49**, 67 (1986).
- <sup>243</sup>G. S. Oehrlein, *J. Appl. Phys.* **59**, 3053 (1986).
- <sup>244</sup>G. S. Oehrlein, R. M. Tromp, Y. H. Lee, and E. J. Petrillo, *Appl. Phys. Lett.* **45**, 420 (1984).
- <sup>245</sup>J. P. Simko, G. S. Oehrlein, and T. M. Mayer, *J. Electrochem. Soc.* **138**, 277 (1991).
- <sup>246</sup>H. Norström, H.-O. Blom, M. Ostling, A. N. Larsen, J. Keinonen, and S. Berg, *J. Vac. Sci. Technol. B* **9**, 34 (1991).
- <sup>247</sup>R. G. Frieser, F. J. Montillo, N. B. Zingerman, W. K. Chu, and S. R. Mader, *J. Electrochem. Soc.* **130**, 2237 (1983).
- <sup>248</sup>M. Yamada, Y. Ito, K. Inazawa, A. Toure, K. Hinata, and H. Sakima, US patent 6,159,862 (12 Dec. 2000).
- <sup>249</sup>T. Yanagida, US patent 5,338,399 (16 Aug. 1994).
- <sup>250</sup>P. Forster *et al.*, in *Climate Change 2007: The Physical Science Basis. Contribution of Working Group I to the Fourth Assessment Report of the Intergovernmental Panel on Climate Change (Chapter 2: Changes in Atmospheric Constituents and in Radiative Forcing)*, edited by S. Solomon, D. Qin, M. Manning, Z. Chen, M. Marquis, K. B. Averyt, M. Tignor, and H. L. Miller (Cambridge University, Cambridge, England, 2007), pp. 212–213.
- <sup>251</sup>B. Ji, S. Motika, P. Badowski, S. Dheandhanoo, J. R. Stets, and E. J. Karwacki, *Solid State Technol.* **48**, 45 (2005).
- <sup>252</sup>J. K. Olthoff and K. E. Greenberg, *J. Res. Natl. Inst. Stand. Technol.* **100**, 327 (1995).
- <sup>253</sup>C. J. Radens and C. A. Fairchick, US patent 5,928,967 (27 July 1999).
- <sup>254</sup>H. J. Stocker, US patent 4,484,979 (27 November 1984).
- <sup>255</sup>C. Reyes-Betanzo, S. A. Moshkalyov, J. W. Swart, and A. C. S. Ramos, *J. Vac. Soc. Technol. A* **21**, 461 (2003).
- <sup>256</sup>S. Lee, J. Oh, K. Lee, and H. Sohn, *J. Vac. Sci. Technol. B* **28**, 131 (2010).
- <sup>257</sup>S. Kadamura, US patent 4,654,114 (31 Mar. 1987).
- <sup>258</sup>D. Thomas, Y. Song, and K. Powell, *Solid State Technol.* **44**, 107 (2001).
- <sup>259</sup>S. P. Murarka, *Silicides for VLSI Applications* (Academic, New York, 1983).
- <sup>260</sup>J. S. Deslauriers and H. J. Levinstein, US patent 4,472,237 (18 Sept. 1984).
- <sup>261</sup>G. K. Herb, in *MRS Proceedings* (Material Research Society, 1986), Vol. 68, p. 3.
- <sup>262</sup>D. S. Fischl, G. W. Rodrigues, and D. W. Hess, *J. Electrochem. Soc.* **135**, 2016 (1988).
- <sup>263</sup>E. Kobeda, N. J. Mazzeo, J. P. Gambino, H. Ng, G. L. Patton, J. D. Warnock, S. Basavaiah, J. F. White, and J. D. Cressler, *J. Electrochem. Soc.* **140**, 3007 (1993).
- <sup>264</sup>H. Nakata, H. Nishioka, and H. Abe, *J. Vac. Sci. Technol.* **17**, 1351 (1980).
- <sup>265</sup>A. Kornblit, J. J. DeMarco, J. Garofalo, D. A. Mixon, A. E. Novembre, S. Vaidya, and T. Kook, *J. Vac. Sci. Technol. B* **13**, 2944 (1995).
- <sup>266</sup>R. Ditzio, P. Werbaneth, and J.-G. Zhu, *Semicond. Manufact. Mag.* **5**, 90 (2004).
- <sup>267</sup>R. M. Ranade, S. S. Ang, and W. D. Brown, *J. Electrochem Soc.* **140**, 3676 (1993).

- <sup>268</sup>C. Zarowin, in *Proceedings of the 4th International Conference on Plasma Chemistry* (1979), 56 pp.
- <sup>269</sup>C. Zarowin, *Thin Solid Films* **85**, 33 (1981).
- <sup>270</sup>F. T. Aldridge, *J. Electrochem. Soc.* **142**, 1563 (1995).
- <sup>271</sup>C. P. Chang *et al.*, in *IEDM Technical Digest* (Washington, D.C., 1997), p. 661.
- <sup>272</sup>C.-K. Yeon and H.-J. You, *J. Vac. Sci. Technol. A* **16**, 1502 (1998).
- <sup>273</sup>S. C. McNevin, *J. Vac. Sci. Technol. B* **8**, 1185 (1990).
- <sup>274</sup>F. P. Klemens *et al.*, in *The 192nd Meeting of the Electrochemical Society and the 48th Annual Meeting of the International Society of Electrochemistry* (The Electrochemical Society, Paris, France, 1997), Electrochemical Society Proceedings, Vols. 97–30, p. 85.
- <sup>275</sup>L. Manchanda *et al.*, in *IEDM Technical Digest* (San Francisco, CA, 2000), p. 23.
- <sup>276</sup>C. Auth *et al.*, *Intel Technol. J.* **12**, 77 (2008).
- <sup>277</sup>O. Joubert *et al.*, in *AVS 53rd International Symposium* (American Vacuum Society, San Francisco, CA, 2006), p. 10.
- <sup>278</sup>K. Pelhos, V. M. Donnelly, A. Kornblit, M. L. Green, R. B. V. Dover, L. Manchanda, Y. Hu, M. Morris, and E. Bower, *J. Vac. Sci. Technol. A* **19**, 1361 (2001).
- <sup>279</sup>L. Sha and J. P. Chang, in *AVS 49th International Symposium* (American Vacuum Society, Denver, CO, 2002), p. 31.
- <sup>280</sup>J. T. C. Lee *et al.*, in *25th International Conference on Phenomena in Ionized Gases* (International Union of Pure and Applied Physics, Nagoya, Japan, July 18, 2001), Workshop I (1).
- <sup>281</sup>M. Niwa, in *7th Annual SEMATECH Symposium*, (SEMATECH, Tokyo, Japan, 2011).
- <sup>282</sup>M. Matsui, T. Tatsumi, and M. Sekine, *Plasma Sources Sci. Technol.* **11**, A202 (2002).
- <sup>283</sup>J. Givens, S. Geissler, J. Lee, O. Cain, J. Marks, S. Geisler, and C. Cunningham, *J. Vac. Sci. Technol. B* **12**, 427 (1994).
- <sup>284</sup>J. Kim, C. W. Chu, C. J. Kang, W. S. Han, and J. T. Moon, *J. Vac. Sci. Technol. B* **20**, 2065 (2002).
- <sup>285</sup>J. P. Roland, N. E. Hendrickson, D. D. Kessler, J. Donald E. Novy, and D. W. Quint, *Hewlett Packard J.* **34**, 30 (1983).
- <sup>286</sup>D. B. Fraser, in *VLSI Technology*, 1st ed., edited by S. M. Sze (McGraw-Hill, New York, 1983), pp. 369–372.
- <sup>287</sup>H. J. Levinstein and D. N. Wang, US patent 4,256,534 (17 Mar. 1981).
- <sup>288</sup>D. A. Danner, M. Dalvie, and D. W. Hess, *J. Electrochem. Soc.* **134**, 669 (1987).
- <sup>289</sup>A. L. Keaton and D. W. Hess, *J. Vac. Sci. Technol. A* **3**, 962 (1985).
- <sup>290</sup>S. I. J. Ingrey, H. J. Nentwich, and R. G. Poulsen, US patent 4,030,967 (21 June 1977).
- <sup>291</sup>W. R. Harshbarger, H. J. Levinstein, C. J. Mogab, and R. A. Porter, US patent 4,208,241 (17 June 1980).
- <sup>292</sup>P. Czuprynski, O. Joubert, L. Vallier, M. Puttock, and M. Heitzmann, *J. Vac. Sci. Technol. B* **16**, 147 (1998).
- <sup>293</sup>T. Arikado, M. Sekine, H. Okano, and Y. Horiike, in *International Electron Device Meeting* (IEEE, Los Angeles, CA, 1986), pp. 54–57.
- <sup>294</sup>G. Cameron and A. Chambers, *Semicond. Int.* **12**, 142 (1989).
- <sup>295</sup>P. Czuprynski, O. Joubert, M. Heitzmann, D. Louis, C. Vizioz, and E. Lajoinie, *J. Vac. Sci. Technol. B* **15**, 1000 (1997).
- <sup>296</sup>R. H. Havemann and J. A. Hutchby, *Proc. IEEE* **89**, 586 (2001).
- <sup>297</sup>J. Kriz, C. Angelkort, M. Czekalla, S. Huth, D. Meinhold, A. Pohl, S. Schulte, A. Thamm, and S. Wallace, *Microelectron. Eng.* **85**, 2128 (2008).
- <sup>298</sup>Metalwork, *Encyclopædia Britannica Ultimate Reference Suite* (Encyclopædia Britannica, Chicago, 2013).
- <sup>299</sup>D. Moore, R. Carter, H. Cui, P. Burke, P. McGrath, S. Q. Gu, D. Gidley, and H. Peng, *J. Vac. Sci. Technol. B* **23**, 332 (2005).
- <sup>300</sup>K. Takeda, Y. Miyawaki, S. Takashima, M. Fukasawa, K. Oshima, K. Nagahata, T. Tatsumi, and M. Hori, *J. Appl. Phys.* **109**, 033303 (2011).
- <sup>301</sup>C. Labelle *et al.*, in *AVS 59th National Symposium* (American Vacuum Society Tampa, FL, 2012), p. 148.
- <sup>302</sup>C. B. Labelle *et al.*, in *Proc. SPIE 8328: Advanced Etch Technology for Nanopatterning* (SPIE, 2012), paper 83280C.
- <sup>303</sup>*International Technical Roadmap for Semiconductors (ITRS). Section: Interconnect* (2011), 27 pp.
- <sup>304</sup>H. Cui, S. J. Kirk, and D. Maloney, in *IEEE/SEMI Advanced Semiconductor Manufacturing Conference* (Stresa, Italy, June 2007).
- <sup>305</sup>D. Hisamoto *et al.*, *IEEE Trans. Electron Devices* **47**, 2320 (2000).
- <sup>306</sup>X. Huang *et al.*, *IEEE Trans. Electron Devices* **48**, 880 (2001).
- <sup>307</sup>X. Huang *et al.*, in *IEDM Technical Digest* (IEEE, Washington DC, 1999), pp. 67–70.
- <sup>308</sup>C. Auth *et al.*, in *2012 Symposium on VLSI Technology Digest of Technical Papers* (2012), pp. 131–132.
- <sup>309</sup>H. Mendez, D. M. Fried, S. B. Samavedam, Thomas Hoffmann, and B.-Y. Nguyen, *Solid State Technol.* **52**, 10 (2009).
- <sup>310</sup>C. Auth, in *Custom Integrated Circuits Conference (CICC)* (IEEE, San Jose, CA, 2012), pp. 1–6.
- <sup>311</sup>K. J. Kanarik, G. Kamarthy, and R. A. Gottscho, *Solid State Technol.* **55**, 15 (2012).
- <sup>312</sup>P. L. Jones and C. B. Labelle, in *Proc. of SPIE 8328: Advanced Etch Technology for Nanopatterning* (SPIE, 2012), paper 8328-12.
- <sup>313</sup>K. J. Kuhn, *IEEE Trans. Electron Devices* **59**, 1813 (2012).
- <sup>314</sup>K. J. Kuhn *et al.*, in *IEDM Technical Digest* (IEEE, San Francisco, CA, 2012) pp. 8.1.1–8.1.4.
- <sup>315</sup>X. Mellhaoui, R. Dussart, A. Basillais, T. Tillocher, P. Lefaucheux, and P. Ranson, in *AVS 50th International Symposium* (Baltimore, MD, 2003), 145 pp.
- <sup>316</sup>T. Tillocher, A. Basillais, X. Mellhaoui, P. Lefaucheux, M. Boufnichel, R. Dussart, and P. Ranson, in *AVS 50th National Symposium* (Baltimore, MD, 2003), pp. 35.
- <sup>317</sup>X. Mellhaoui, R. Dussart, T. Tillocher, P. Lefaucheux, P. Ranson, M. Boufnichel, and L. J. Overzet, *J. Appl. Phys.* **98**, 104901 (2005).
- <sup>318</sup>F. Laermer and A. Schilp, US patent 5,501,893 (26 March 1996).
- <sup>319</sup>C. B. Labelle, V. M. Donnelly, G. R. Bogart, R. L. Opila, and A. Kornblit, *J. Vac. Sci. Technol. A* **22**, 2500 (2004).
- <sup>320</sup>A. Kornblit *et al.*, in *Proceedings of the International Symposium on Microfabricated Systems and MEMS VII*, edited by J. L. Davidson, P. J. Hesketh, D. Misra, and S. Shoji (Electrochemical Society Honolulu, HI, 2004), pp. 11–25.
- <sup>321</sup>G. R. Bogart *et al.*, *Proc. SPIE* **3676**, 171 (1999).
- <sup>322</sup>S.-B. Wang and A. E. Wendt, *J. Appl. Phys.* **88**, 643 (2000).
- <sup>323</sup>M. C. M. v. d. Sanden, M. A. Blauw, F. Roozeboom, and W. M. M. Kessels, in *AVS 54th International Symposium* (Seattle, WA, 2007), 19 pp.
- <sup>324</sup>H. T. Soh, C. P. Yue, A. McCarthy, Changsup Ryu, T. H. Lee, S. S. Wong, and C. F. Quate, *Jpn. J. Appl. Phys.* **38**, 2393 (1999).
- <sup>325</sup>F. Pardo *et al.*, in *Hilton Head Conference* (2006).
- <sup>326</sup>B. N. Engel, N. D. Rizzo, J. Janesky, J. M. Slaughter, R. Dave, Mark DeHerrera, M. Durlam, and S. Tehrani, *IEEE Trans. Nanotechnol.* **1**, 32 (2002).
- <sup>327</sup>W. Shen, D. Mazumdar, X. Zou, X. Liu, B. D. Schrag, and G. Xiao, *Appl. Phys. Lett.* **88**, 182508 (2006).
- <sup>328</sup>K. B. Jung, E. S. Lambers, J. R. Childress, S. J. Pearton, M. Jensen, and J. A. T. Hurst, *Appl. Phys. Lett.* **71**, 1255 (1997).
- <sup>329</sup>K. B. Jung, E. S. Lambers, J. R. Childress, S. J. Pearton, M. Jensen, and J. A. T. Hurst, *J. Vac. Sci. Technol. A* **16**, 1697 (1998).
- <sup>330</sup>H. Cho, K. P. Lee, Y. B. Hahn, E. S. Lambers, and S. J. Pearton, *J. Vac. Sci. Technol. A* **18**, 1273 (2000).
- <sup>331</sup>I. Nakatani, *IEEE Trans. Magn.* **32**, 4448 (1996).
- <sup>332</sup>K. B. Jung, J. Hong, a. H. Cho, S. Onishi, D. Johnson, Y. D. Park, J. R. Childress, and S. J. Pearton, *J. Vac. Sci. Technol. A* **17**, 535 (1999).
- <sup>333</sup>K. B. Jung, a. J. Hong, H. Cho, S. Onishi, D. Johnson, Y. D. Park, J. R. Childress, and S. J. Pearton, *J. Electrochem. Soc.* **146**, 2163 (1999).
- <sup>334</sup>R. Blumenthal and A. S. Orland, in *AVS 49th International Symposium* (Denver, CO, 2002), 119 pp.
- <sup>335</sup>T. Abe, Y. G. Hong, and M. Esashi, *J. Vac. Sci. Technol. B* **21**, 2159 (2003).
- <sup>336</sup>N. Matsui, K. Mashimo, A. Egami, A. Konishi, O. Okada, and T. Tsukada, *Vacuum* **66**, 479 (2002).
- <sup>337</sup>J. L. Gaddis, *The Landscape of History: How Historians Map the Past* (Oxford University, New York, 2002).
- <sup>338</sup>Bohr used this quote when asked about the future of quantum physics, but he may have been quoting someone else. Similar quotes are attributed to Samuel Goldwyn and Yogi Berra. See discussion in [http://www.economist.com/blogs/theinbox/2007/07/the\\_perils\\_of\\_prediction\\_june](http://www.economist.com/blogs/theinbox/2007/07/the_perils_of_prediction_june)
- <sup>339</sup>“Semiconductor Industry Post Near-Record Sales Total in 2012,” Semiconductor Industry Association (4 February 2013).
- <sup>340</sup>*International Technical Roadmap for Semiconductors (ITRS)*.
- <sup>341</sup>“Front end processes” in *International Technical Roadmap for Semiconductors* (ITRS, 2011).
- <sup>342</sup>“Emerging research materials” in *International Technical Roadmap for Semiconductors* (ITRS, 2011).
- <sup>343</sup>“Emerging research devices” in *International Technical Roadmap for Semiconductors* (ITRS, 2011).
- <sup>344</sup>“Process integration, devices, and structures” in *International Technical Roadmap for Semiconductors* (ITRS, 2011).

- <sup>345</sup>“Interconnect” in *International Technical Roadmap for Semiconductors* (ITRS, 2011).
- <sup>346</sup>“Lithography” in *International Technical Roadmap for Semiconductors* (ITRS, 2011).
- <sup>347</sup>R. A. Cirelli, O. Nalamasu, S. Pau, and G. P. Watson, US patent 6,218,057 (17 Apr. 2001).
- <sup>348</sup>S. Pau, O. Nalamasu, R. Cirelli, J. Frackoviak, A. Timko, P. Watson, F. Klemens, and G. Timp, *J. Vac. Sci. Technol. B* **18**, 317 (2000).
- <sup>349</sup>Y. Chen, P. Xu, Y. Chen, L. Miao, X. Xu, C. Bencher, and C. Ngai, in *International Symposium on Lithography Extensions* (Kobe, Japan, 2010).
- <sup>350</sup>B. Mebarki, in *2010 International Symposium on Lithography Extensions* (Kobe, Japan, 2010).
- <sup>351</sup>C. Bencher, Y. Chen, H. Dai, W. Montgomery, and L. Huli, *Proc. SPIE* **6924**, 69244E (2008).
- <sup>352</sup>D. Medeiros, in *6th International Symposium on Immersion Lithography Extensions* (Prague, 2009).
- <sup>353</sup>E. Kinsbron, W. E. Willenbrock, and H. J. Levinstein, in *ECS Fall Meeting Extended Abstracts* (Detroit, MI, 1982), Vol. 82-2, 243 pp.
- <sup>354</sup>E. Kinsbron and W. T. Lynch, US patent 4,432,132 (21 February 1984).
- <sup>355</sup>D. S. Y. Hsu, *Appl. Phys. Lett.* **59**, 2193 (1991).
- <sup>356</sup>W.-Y. Jung *et al.*, *Proc. SPIE* **6520**, 65201C (2007).
- <sup>357</sup>B. Mebarki *et al.*, *Proc. SPIE* **7973**, 79730G (2011).
- <sup>358</sup>C. Bencher *et al.*, *Proc. SPIE* **7973**, 79730K (2011).
- <sup>359</sup>Chris A. Mack, *Field Guide to Optical Lithography* (SPIE Press, Bellingham, WA, 2006).
- <sup>360</sup>Chris Mack, *Fundamental Principles of Optical Lithography* (Wiley, Chichester, England, 2007).
- <sup>361</sup>G. S. Oehrlein, R. J. Phaneuf, and D. B. Graves, *J. Vac. Sci. Technol. B* **29**, 010801 (2011).
- <sup>362</sup>S. Xiong, J. Bokor, Q. Xiang, P. Fisher, I. Dudley, and P. Rao, *Proc. SPIE* **4689**, 733 (2002).
- <sup>363</sup>W. H. Yan, W. Moreau, R. Wise, and Y. Chui, in *AVS 46th International Symposium* (Seattle, WA, 1999).
- <sup>364</sup>S. Halle, W. H. Yan, W. Moreau, J. Wittmann, and A. Gutmann, in *AVS 46th International Symposium* (Seattle, WA, 1999).
- <sup>365</sup>H. L. Maynard and W. W. Tai, “Striation reduction in oxide etching” (unpublished).
- <sup>366</sup>M. Nault, T. Weidman, D. Sugiarto, D. Mui, C. Lee, and J. Yang, *J. Vac. Sci. Technol. B* **16**, 3730 (1998).
- <sup>367</sup>J. Stowers and D. A. Keszler, *Microelectron. Eng.* **86**, 730 (2009).
- <sup>368</sup>B. Ozpineci and L. Tolbert, “Silicon carbide: Smaller, faster, tougher” *IEEE Spectrum* (in press).
- <sup>369</sup>F. Schwierz, *Nature Nanotechnol.* **5**, 487 (2010).
- <sup>370</sup>T. Seo, T. Yoshino, Y. Cho, N. Hata, and T. Kikkawa, *Jpn. J. Appl. Phys.* **46**, 5742 (2007).
- <sup>371</sup>P.-I. Wang, Z. Wu, T.-M. Lun and L. V. Interrante, *J. Electrochem. Soc.* **153**, G267 (2006).
- <sup>372</sup>A. Itoh, A. Inokuchi, S. Yasuda, A. Teramoto, T. Goto, M. Hirayama, and T. Ohmi, *Jpn. J. Appl. Phys.* **47**, 2515 (2008).
- <sup>373</sup>H. J. Cho *et al.*, in *Proceedings of the 36th European Solid-State Device Research Conference*, edited by M. D. Adrian M. Ionescu, and Yusuf Leblebici (Montreux, Switzerland, 2006), 146 pp.
- <sup>374</sup>D.-S. Kil *et al.*, in *2004 Symposium on VLSI Technology Digest of Technical Papers* (2004), pp. 126–127.
- <sup>375</sup>D.-S. Kil *et al.*, in *2006 Symposium on VLSI Technology Digest of Technical Papers* (Honolulu, HI, 2006), pp. 38–39.
- <sup>376</sup>C. B. Kaynak, Dr.-Ing Thesis, Technical University of Berlin, 2013.
- <sup>377</sup>*Micron Technology Phase Change Module Flyer* (15 Oct. 2012).
- <sup>378</sup>I. S. Kim *et al.*, in *2010 Symposium on VLSI Technology* (2010), pp. 203–204.
- <sup>379</sup>S.-W. Chung *et al.*, in *2006 Symposium on VLSI Technology Digest of Technical Papers* (2006), pp. 32–33.
- <sup>380</sup>J. Y. Kim *et al.*, *2003 Symposium on VLSI Technology Digest of Technical Papers* (2003), pp. 11–12.
- <sup>381</sup>M. A. Siddiqi, *Dynamic RAM: Technology Advancements* (CRC, Boca Raton, FL, 2012).
- <sup>382</sup>B. El-Kareh, G. B. Bronner, and S. E. Schuster, *Solid State Technol.* **40**, 89 (1997).
- <sup>383</sup>M. Koyanagi, in *IEEE SSCS News* (Winter 2008), pp. 37–41.
- <sup>384</sup>K. W. Lee, T. Nakamura, T. Ono, Y. Yamada, T. Mizukusa, H. Hashimoto, K. T. Park, H. Kurino and M. Koyanagi, in *IEDM Technical Digest* (San Francisco, CA), pp. 165–168.
- <sup>385</sup>T. Fukushima, Y. Yamada, H. Kikuchi, and M. Koyanagi, in *IEDM Technical Digest* (Washington DC, 2005), pp. 359–362.
- <sup>386</sup>B. Shieh, K. C. Saraswat, J. P. McVittie, S. List, S. Nag, M. Islamraja, and R. H. Havemann, *Electron Devices Lett.* **19**, 16 (1998).
- <sup>387</sup>L. G. Gosset *et al.*, *Microelectron. Eng.* **82**, 321 (2005).
- <sup>388</sup>R. J. O. M. Hoofman, G. J. A. M. Verheijden, J. Michelon, F. Iacopi, Y. Travalay, M. R. Baklanov, Z. Tökei, and G. P. Beyer, *Microelectron. Eng.* **80**, 337 (2005).
- <sup>389</sup>R. Hoofman, R. Daamen, J. Micheton, and V. Nguyenhoang, *Solid State Technol.* **49**, 55 (2006).
- <sup>390</sup>R. H. Havemann and Shin-puu Jeng, US patent 5,461,003 (24 Oct. 1995).
- <sup>391</sup>M. B. Anand, M. Yamada, and H. Shibata, *IEEE Trans. Electron Devices* **44**, 1965 (1997).
- <sup>392</sup>C.-H. Chen, Y.-K. Fang, C.-S. Lin, C.-W. Yang, and J.-C. Hsieh, *Solid-State Electron.* **45**, 199 (2001).
- <sup>393</sup>P. A. Kohl, D. M. Bhusari, M. Wedlake, C. Case, F. P. Klemens, J. Miner, B.-C. Lee, R. J. Gutmann, and R. Shick, *IEEE Electron Devices Lett.* **21**, 557 (2000).
- <sup>394</sup>K. Chan and K. K. Gleason, *J. Electrochem. Soc.* **153**, C223 (2006).
- <sup>395</sup>L. H. Lee and K. K. Gleason, *J. Electrochem. Soc.* **155**, G78 (2008).
- <sup>396</sup>R. P. Feynman, *Int. J. Theor. Phys.* **21**, 467 (1982).
- <sup>397</sup>A. Ekert, *AIP Conf. Proc.* **323**, 450 (1994).
- <sup>398</sup>S. R. Das, *IEEE Spectrum* **48**, 18 (2011).
- <sup>399</sup>B. E. Kane, *Nature* **393**, 133 (1998).
- <sup>400</sup>J. J. Pla, K. Y. Tan, J. P. Dehollain, W. H. Lim1, J. J. L. Morton, F. A. Zwanenburg, D. N. Jamieson, A. S. Dzurak, and A. Morello, *Nature* **496**, 334 (2013).
- <sup>401</sup>G. D. Sanders, K. W. Kim, and W. C. Holton, *Phys. Rev. A* **60**, 4146 (1999).
- <sup>402</sup>G. D. Sanders, K. W. Kim, and W. C. Holton, *Phys. Rev. B* **61**, 7526 (2000).
- <sup>403</sup>M. R. Sakr, H. W. Jiang, E. Yablonovitch, and E. T. Croke, *Appl. Phys. Lett.* **87**, 223104 (2005).
- <sup>404</sup>D. F. V. James, *Appl. Phys. B* **66**, 181 (1998).
- <sup>405</sup>S. Pau, C. S. Pai, Y. L. Low, J. Moxom, P. T. A. Reilly, W. B. Whitten, and J. M. Ramsey, *Phys. Rev. Lett.* **96**, 120801 (2006).
- <sup>406</sup>H. Häffner, C. F. Roosa, and R. Blatt, *Phys. Rep.* **469**, 155 (2008).
- <sup>407</sup>L.-M. Duan and C. Monroe, *Rev. Mod. Phys.* **82**, 1209 (2010).
- <sup>408</sup>D. J. Wineland and D. Leibfried, *Laser Phys. Lett.* **8**, 175 (2011).
- <sup>409</sup>S. C. Doret *et al.*, *New J. Phys.* **14**, 073012 (2012).
- <sup>410</sup>K. Wright *et al.*, *New J. Phys.* **15**, 033004 (2013).
- <sup>411</sup>F. Roozboom *et al.*, in *Handbook of 3D Integration, Volume 1 - Technology and Applications of 3D Integrated Circuits*, edited by P. Garrou, C. Bower, and P. Ramm (John Wiley, U.S., 2011), Vol. 1 - Technology and Applications of 3D Integrated Circuits, pp. 66–67.
- <sup>412</sup>E. Pargon, M. Martin, K. Menguelti, L. Azarnouche, J. Foucher, and O. Joubert, *Appl. Phys. Lett.* **94**, 103111 (2009).
- <sup>413</sup>L. J. Overzet, J. T. Verdeyen, R. M. Roth, and F. F. Carasco, presented at the Material Research Society Symposium, Pittsburgh, PA, 1987 (unpublished).
- <sup>414</sup>Y. Watanabe, M. Shiratani, Y. Kubo, I. Ogawa, and S. Ogi, *Appl. Phys. Lett.* **53**, 1263 (1988).
- <sup>415</sup>S. Samukawa and S. Furuoya, *Appl. Phys. Lett.* **63**, 2044 (1993).
- <sup>416</sup>K. Hashimoto, *Jpn. J. Appl. Phys.* **33**, 6013 (1994).
- <sup>417</sup>S. Samukawa and K. Terada, *J. Vac. Sci. Technol. B* **12**, 3300 (1994).
- <sup>418</sup>H. Sugai, K. Nakamura, Y. Hikosaka, and M. Nakamura, *J. Vac. Sci. Technol. A* **13**, 887 (1995).
- <sup>419</sup>T. Mieno and S. Samukawa, *Jpn. J. Appl. Phys.* **34**, L1079 (1995).
- <sup>420</sup>S. Samukawa and T. Tsukada, *Appl. Phys. Lett.* **69**, 1056 (1996).
- <sup>421</sup>M. A. Lieberman and S. Ashida, *Plasma Sources Sci. Technol.* **5**, 145 (1996).
- <sup>422</sup>T. H. Ahn, K. Nakamura, and H. Sugai, *Plasma Sources Sci. Technol.* **5**, 139 (1996).
- <sup>423</sup>G. A. Heibner and C. B. Fleddermann, *J. Appl. Phys.* **82**, 2814 (1997).
- <sup>424</sup>D. P. Lymberopoulos, V. I. Kolobov, and D. J. Economou, *J. Vac. Sci. Technol. A* **16**, 564 (1998).
- <sup>425</sup>M. V. Malyshev, V. M. Donnelly, J. I. Colonell, and S. Samukawa, *J. Appl. Phys.* **86**, 4813 (1999).
- <sup>426</sup>M. Malyshev and V. M. Donnelly, *Plasma Sources Sci. Technol.* **9**, 353 (2000).
- <sup>427</sup>S. Samukawa, K. Noguchi, J. I. Colonell, K. H. A. Bogart, M. V. Malyshev, and V. M. Donnelly, *J. Vac. Sci. Technol. B* **18**, 834 (2000).
- <sup>428</sup>P. Subramonium and M. J. Kushner, *Appl. Phys. Lett.* **79**, 2145 (2001).



- <sup>429</sup>P. Subramonium and M. J. Kushner, *J. Vac. Sci. Technol. A* **20**, 313 (2002).
- <sup>430</sup>D. J. Economou, *Appl. Surf. Sci.* **253**, 6672 (2007).
- <sup>431</sup>H. Shin, W. Zhu, D. J. Economou, and V. M. Donnelly, *J. Vac. Sci. Technol. A* **30**, 031304 (2012).
- <sup>432</sup>S. K. Kanakasabapathy, L. J. Overzet, V. Midha, and D. J. Economou, *Appl. Phys. Lett.* **78**, 22 (2001).
- <sup>433</sup>L. Xu, D. J. Economou, V. M. Donnelly, and P. Ruchhoeft, *Appl. Phys. Lett.* **87**, 041502 (2005).
- <sup>434</sup>H. Shin, W. Zhu, L. Xu, V. M. Donnelly, and D. J. Economou, *Plasma Sources Sci. Technol.* **20**, 055001 (2011).
- <sup>435</sup>S. Banna *et al.*, *IEEE Trans. Plasma Sci.* **37**, 1730 (2009).
- <sup>436</sup>P. Diomed, D. J. Economou, and V. M. Donnelly, *J. Appl. Phys.* **109**, 083302 (2011).
- <sup>437</sup>L. Chen and Q. Yang, presented at the Electrochemical Society Symposium, Los Angeles, CA, 1996 (unpublished).
- <sup>438</sup>M. J. Goeckner, T. K. Bennett, and S. A. Cohen, *Appl. Phys. Lett.* **71**, 980 (1997).
- <sup>439</sup>K. P. Giapis, T. A. Moore, and T. K. Minton, *J. Vac. Sci. Technol. A* **13**, 959 (1995).
- <sup>440</sup>S. Samukawa, *Jpn. J. Appl. Phys.* **45**, 2395 (2006).
- <sup>441</sup>D. J. Economou, *J. Phys. D: Appl. Phys.* **41**, 024001 (2008).
- <sup>442</sup>S. Panda, D. J. Economou, and L. Chen, *J. Vac. Sci. Technol. A* **19**, 398 (2001).
- <sup>443</sup>A. Ranjan, V. M. Donnelly, and D. J. Economou, *J. Vac. Sci. Technol. A* **24**, 1839 (2006).
- <sup>444</sup>Y. Tamural *et al.*, Presented at the 12th IEEE International Conference on Nanotechnology (IEEE-NANO), The International Conference Centre Birmingham, Birmingham, United Kingdom, 2012 (unpublished).
- <sup>445</sup>T. Meguro, M. Hamagaki, S. Modaressi, T. Hara, Y. Aoyagi, M. Ishii, and Y. Yamamoto, *Appl. Phys. Lett.* **56**, 1552 (1990).
- <sup>446</sup>H. Sasaue, S. Iseda, K. Asami, J. Yamamoto, M. Hirose, and Y. Horiike, *Jpn. J. Appl. Phys.* **29**, 2648 (1990).
- <sup>447</sup>S. D. Athavale and D. J. Economou, *J. Vac. Sci. Technol. B* **14**, 3702 (1996).
- <sup>448</sup>S. D. Athavale and D. J. Economou, *J. Vac. Sci. Technol. A* **13**, 966 (1995).
- <sup>449</sup>S. D. Park, C. K. Oh, J. W. Bae, G. Y. Yeom, T. W. Kim, J. I. Song, and J. H. Jang, *Appl. Phys. Lett.* **89**, 043109 (2006).
- <sup>450</sup>V. M. Donnelly and D. J. Economou, "Atomic Layer Etching with Pulsed Plasmas," Provisional Patent Application No. 61/286,572, 15 December 2009.
- <sup>451</sup>V. M. Donnelly and D. J. Economou, "Atomic Layer Etching with Pulsed Plasmas," Provisional International Patent Application No. PCT/US/2010/060251, 14 December 2010.
- <sup>452</sup>F. Schwierz, *Nature Nanotechnol.* **5**, 487 (2010).
- <sup>453</sup>H. Song, M. A. Reed, and T. Lee, *Adv. Mater.* **23**, 1583 (2011).
- <sup>454</sup>A. D. Franklin, M. Luisier, S.-J. Han, G. Tulevski, C. M. Breslin, L. Gignac, M. S. Lundstrom, and W. Haensch, *Nano Lett.* **12**, 758 (2012).

- <sup>455</sup>M. Fuechsle, J. A. Miwa, S. Mahapatra, H. Ryu, S. Lee, O. Warschkow, L. C. L. Hollenberg, G. Klimeck, and M. Y. Simmons, *Nature Nanotechnol.* **7**, 242 (2012).

- <sup>456</sup>M. V. Malyshev, V. M. Donnelly, A. Kornblit, and N. A. Ciampa, *J. Appl. Phys.* **84**, 137 (1998).



**Vincent M. Donnelly** is a John and Rebecca Moores Professor and Graduate Program Director in the Department of Chemical and Biomolecular Engineering at the University of Houston. Prior to 2002, he was a Distinguished Member of Technical Staff at Bell Laboratories, in Murray Hill, New Jersey. He received a B.A. degree in Chemistry from LaSalle University, a Ph.D. degree in Physical Chemistry from the University of Pittsburgh, and was a NRC post-doc at the Naval Research Lab. His research

includes experimental studies of plasmas and plasma etching, plasma-surface interactions, control of ion and energy distributions in plasmas, new nanopatterning methods, and atmospheric pressure microdischarges. He is a Fellow of the American Vacuum Society and a recipient of the AVS Plasma Science and Technology Division Plasma Prize. In 2011, he received the AVS John Thornton Memorial Award and Lecture.



**Avinoam (Avi) Kornblit** is a consultant in silicon processing, based in New Jersey. Until his retirement in April, 2008, he was a Technical Manager both at Bell Labs and the New Jersey Nanotechnology Consortium, a wholly owned subsidiary of Lucent Technologies (later Alcatel-Lucent). He received his B.Sc. degree in Mathematics and Physics from the Hebrew University in Jerusalem in 1967 and a Ph. D. degree in Mechanics and Material Science from Rutgers University in NJ in 1981. He joined

Bell Telephone Laboratories in 1970, working initially in the Condensed Matter Physics department. Since 1981 he is involved in silicon processing, focusing primarily on plasma processes for the fabrication of silicon ICs. He was the Technical Manager of the Plasma Processing Group and later the Nano-patterning Group at Bell Labs at Murray Hill, NJ. He was responsible for plasma processing development and characterization in multiple Bell Labs locations and worked closely with manufacturing engineers in implementing etching processes in AT&T's (later Lucent Technologies) IC manufacturing facilities worldwide. He has published over 200 articles and holds 20 patents. He is a member of the American Vacuum Society and the IEEE.